UNIVERSITY OF CALIFORNIA

Santa Barbara

CONTROLS ON THE MORPHOLOGY AND INTERNAL ARCHITECTURE OF SHELF HYPERPYCNITES: INSIGHTS FROM THE SANTA BARBARA SHELF, FLUME EXPERIMENTS, AND THE ANCIENT ROCK RECORD

A dissertation submitted in partial satisfaction of the

requirements for the degree

DOCTOR OF PHILOSOPHY

in Geological Sciences

BY

LINN-ELISABETH STEEL

Committee in charge:

Professor Alexander Simms, Chair

Professor Douglas Burbank

Professor Eckart Meiburg

September 2017

The dissertation of Linn-Elisabeth Steel is approved.

_____

Douglas Burbank

_____

Eckart Meiburg

_____

Alexander Simms, Committee Chair

July 2017

ACKNOWLEDGMENTS

My time in graduate school has been shaped by many people: mentors, friends, role models, those providing emotional support, and those providing financial support. I would like to start by thanking my advisor, Alex Simms. Thank you for always having an open door, for answering my endless questions, for pushing me to have high expectations, for being kind and supportive, especially during times when perhaps I didn't believe in myself, and for not laughing at me when I got sea-sick in a kayak on a windless lagoon. I truly appreciate the time you dedicate to helping your students, editing papers, and listening to practice talks. You have shown me what it looks like to be both a great scientist and a great mentor.

Thank you to my fellow graduate students and friends. Without you, I'm not sure I would have survived graduate school. To Mary Kate Fidler and Sophie Briggs: you were always there when I needed you the most and I feel so lucky to call you my friends and my housemates. Thank you for hugging me on my bad days and for celebrating with me on my good days. To the rest of the Ravenscroft crew: Alex Wrobel, Diane Seely, Joshua Garber, Drake Hebert, Will Junkin, and Tyson McKinney, thank you for the pig roasts, breakfasts at Domingo's, and for always being ready to have fun. Thank you to my fellow lab mates, including Lauren Simkins, Laura Reynolds, Daniel Livsey, Julie Zurbuchen, Zack Nelson, Baird King, Michael Bentz, and John Rice. I am so grateful for your help in collecting data, editing my writing, listening to talks, and for our many fruitful discussions. Thank you to Carlye Peterson, Daniel Luna, Gina Lee, Jason Womer, and Katie Markovich for your friendship and support.

A special thank you to Laura Reynolds. We have been through so much together and I can't imagine these years of graduate school without you by my side. It's hard to believe how much we've grown as scientists since that first time in the field in Texas, and I'm proud to call you my colleague, my friend, and my moral compass. Thank you to Elisa Medri, who served as an excellent field assistant and translator for our work in Argentina, and to Olivia Nicholson for running endless grain-size samples for me.

Thank you to all of the faculty and staff of the Earth Science department for your support and for making my experience at UCSB overwhelmingly positive. To Kate Lima, thank you for always listening, for your endless enthusiasm and positivity, and for being a friend. Thanks to Tim Cuellar for letting me be part of the Earth Science motorcycle gang and for always making our field trips run smoothly. Thank you to Susannah Porter and Lorraine Lisiecki for serving as strong role models and mentors. Thank you to those who have served on my committees: Doug Burbank, Dave Valentine, Eckart Meiburg, Jonathan Warrick, and Stan Awramik. Your feedback and questions consistently improved the quality of my work. Thank you to my various sources of financial support, which includes the Petroleum Research Fund, GSA and AAPG research grants, and departmental fellowships and awards.

Finally, thank you to my family for being a constant source of support and inspiration. To my brothers, Alastair and Jan-Erik, you've always been my role models in more ways than you know and I thank you for that. Thank you to my mother for always being sympathetic, for encouraging me to continue, and for teaching me to be strong. And last but not least, thank you to my father, who is the reason I'm a geologist at all. If I can be even a fraction of the modest, kind, and hard-working geologist that you are I will be lucky.

VITA OF LINN-ELISABETH STEEL

JULY 2017

EDUCATION

Bachelors of Science in Geology, University of Texas at Austin, May 2012

Doctor of Philosophy in Geological Sciences, University of California Santa Barbara, September 2017 (expected)

PROFESSIONAL EMPLOYMENT

2010 – 2012: Research Assistant, University of Texas at Austin

2013: Geology Intern, Aera Energy, Bakersfield, CA

2015: Geology Intern, California Resources Corporation, Bakersfield, CA

2012 – 2017: Teaching Assistant, University of California Santa Barbara

2016 – 2017: Teaching Associate, University of California, Santa Barbara

2016: Summer Teaching Institute for Associates, University of California, Santa Barbara

PUBLICATIONS

Steel, E., Simms, A.R., Steel, R., Delivery of sand to the continental shelf by hyperpycnal currents: an example from the Jurassic Lajas formation, Neuquén Basin, Argentina: *in review*

Rice, J.A., Simms, A.R., Buzas-Stephens, P., **Steel, E.**, Yokohama, Y., and Halihan, T., Deltaic responses to climate change: the Holocene history of the Nueces Bayhead Delta: *in review*

Schwalbach, J. R., Holloway, J.W., **Steel, E.**, and Coldewey, R., Pliocene Repetto Formation Turbidites, Ventura Avenue Field, Ventura, California: Linking Reservoir Properties, Lithofacies, and Stratigraphic Elements: *accepted, SEPM/PS-SEPM From the Mountains to the Abyss: The California Borderland as an Archive of Southern California Geologic Evolution*

Steel, E., Buttles, J., Simms, A., Mohrig, D., and Meiburg, E., 2017, The role of buoyancy reversal in turbidite deposition and submarine fan geometry: Geology, v. 45, no. 1, p. 35-38.

Steel, E., Simms, A., Warrick, J., and Yokoyama, Y., 2016, Highstand shelf fans: the role of buoyancy reversal in the deposition of a new type of shelf sand body: GSA Bulletin, v. 128, no. 11-12, p. 1717-1724.

Warrick, J.A., Simms, A.R., Ritchie, A., **Steel, E.,** Dartnell, P., Conrad, J.E., and Finlayson, D.P., 2013, Hyperpycnal plume-derived fans in the Santa Barbara Channel, California: Geophysical Research Letters, v. 40, p. 1-6.

Kim, W., Connell, S.D., **Steel, E.,** Smith, G.A., and Paola, C., 2011, Mass balance control on the interaction of axial and transverse channel systems: Geology, v.39, p. 611-614.

HONORS AND AWARDS

2017 UCSB Earth Science Dept. G.K. Gilbert Award (best student seminar)

2016 Alumni Graduate Award for Research Excellence (UCSB)

2015 Global Travel Field Award (UCSB)

2015 Wendell Phillips Woodring Memorial Graduate Fellowship (UCSB)

2014 GSA Graduate Student Research Grant

2014 AAPG Foundation Grants-in-Aid

2014 Coast Geological Society Scholarship

2013 Graduate Student Opportunity Grant (UCSB)

2012 Valedictorian for Jackson School of Geosciences Class of 2012

2012 Estwing Hammer Award for Field Geology (University of Texas)

2011 Undergraduate Research Fellowship (University of Texas)

2008 – 2012 Member of National Society of Collegiate Scholars

2008 – 2012 University Honors, University of Texas at Austin

FIELDS OF STUDY

Major Field: Sediment Gravity Flows

Study of hyperpycnal shelf fans in the Santa Barbara Channel, Southern California, with Dr. Alexander Simms and Dr. Jonathan Warrick

Study of buoyancy reversal in experimental turbidity currents, with Dr. Alexander Simms, Dr. David Mohrig, and Dr. James Buttles

Study of Jurassic hyperpycnites on the continental shelf of the Neuquén Basin, Southwestern Argentina, with Dr. Alexander Simms and Dr. Ronald Steel

ABSTRACT

CONTROLS ON THE MORPHOLOGY AND INTERNAL ARCHITECTURE OF SHELF HYPERPYCNITES: INSIGHTS FROM THE SANTA BARBARA SHELF, FLUME EXPERIMENTS, AND THE ANCIENT ROCK RECORD

BY

LINN-ELISABETH STEEL

Although sea-level highstands are typically associated with sediment-starved continental shelves, high sea level does not hinder major river floods. Hyperpycnal currents are turbidity currents generated by plunging of sediment-laden rivers at the fluvial-marine interface, and they allow for cross-shelf transport of suspended sand beyond the high-energy coastline. Hyperpycnal currents are an important mechanism operating within source-to-sink systems as they can form a link between terrestrial and marine environments during sea-level highstands. Because hyperpycnal currents are typically only generated during extreme river floods, their deposits may serve as paleoflood archives. Hyperpycnites also have the potential to serve as high quality hydrocarbon reservoirs; however, a broader understanding of where hyperpycnal currents are most likely to deposit significant volumes of sand and the morphology of those deposits is necessary for accurate reservoir modeling. The studies included here present results

from field studies of Holocene fans on the continental shelf of Southern California and Jurassic hyperpycnites in the Neuquén Basin of Argentina, in combination with three-dimensional flume experiments, to demonstrate that hyperpycnal currents are capable of depositing well-sorted sand bodies on the continental shelf, and that their deposits may differ from "classic" sediment gravity flow deposits due to the effects of freshwater within the currents.

River-derived hyperpycnal currents and turbidity currents initiated in relatively shallow water that travel into deeper and colder water commonly contain interstitial fluid less dense than the surrounding ambient water. These currents are initially ground-hugging due to high suspended sediment concentrations. However, as sediment settles from suspension, bulk current density will decrease and may become less dense than the surrounding ambient water, at which point the current becomes buoyant and rises from the basin floor. This process of buoyancy reversal, or lofting, affects both the internal architecture of turbidites and their overall morphology. Cores collected from shelf hyperpycnites in the Santa Barbara Channel provide grain-size trends, radiocarbon dates, and overall stratigraphic architecture of lofted-current deposits (Chapter 2). The hyperpycnal currents deposited slightly graded, structureless fine- to medium-grained sand beds. These beds became well-sorted through the stripping of fine-grained material in suspension at the point of lift-off.

Lofting not only affects sorting within hyperpycnites, but also changes the lateral spreading rates of turbidity currents and therefore affects deposit morphology. Flume experiments show that lofting currents are width-limited and generate narrower, more elongate deposits than ground-hugging currents (Chapter 3). Factors such as steeper basin floor gradients and higher suspended-sediment concentrations push the lofting point farther basinward and ultimately result in wider deposits. Most importantly, the use of a 3-dimensional

experimental tank allows for the first detailed analysis of the lofting process and its effects on length-to-width ratios of turbidite lobes.

Discoveries of modern shelf hyperpycnites and experimental work describing turbidity currents with light interstitial fluid provide a valuable framework for understanding and recognizing shelf hyperpycnites in the rock record. We compare our experimental results and findings from the Santa Barbara Channel with hyperpycnites of the Mid-Jurassic Lajas Formation of the Neuquén Basin, Western Argentina (Chapter 4). Hyperpycnites of the Jurassic Lajas Formation are characterized by dm thick beds of well-sorted medium-grained sandstones with parallel laminations. These beds are encased by organic-rich, thinly laminated sandstone and siltstone. These deposits represent obliquely-migrating sand lobes deposited on the continental shelf and were likely fed by small rivers. Recognition of shelf hyperpycnites in the Lajas Formation of the Neuquén Basin allows for a broader understanding of shelf processes and adds to the developing hyperpycnite facies models. Overall, recognizing and understanding the geometry and internal architecture of shelf hyperpycnites will improve understanding of sediment transfer from rivers to deeper water, paleoenvironmental interpretations of gravity-flow deposits, and has implications for modeling potentially high-quality hydrocarbon reservoirs.

TABLE OF CONTENTS

LIST OF FIGURES

LIST OF TABLES

CHAPTER 1

INTRODUCTION

The fate of river-derived sediment in an ocean or lake basin is highly dependent on the bulk density of the river effluent and the density of the marine or lake water. Commonly, the combination of fresh river water and suspended sediment is less dense than the ambient water into which it is draining, and the river effluent overrides the ambient water as a hypopycnal plume (Bates, 1953). However, high suspended sediment concentrations can result in the generation of hyperpycnal currents, in which freshwater and suspended sediment travel across the sea-floor as a sediment gravity flow (Bates, 1953). Sediment concentrations necessary to induce plunging of fluvial outflow and the subsequent formation of hyperpycnal currents vary based on local ambient water density, but in marine basins typically range from ~35 to 45 kg/m^{-3} (Mulder and Syvitski, 1995). Initially, hyperpycnal currents were not widely accepted as significant processes operating on marine continental shelves because of the high suspended sediment concentrations needed for freshwater to overcome the density of salt water. However, Mulder and Syvitski (1995) found that out of 150 world rivers surveyed, 66% were capable of exceeding the sediment concentrations necessary to induce hyperpycnal currents. Small, mountainous rivers were found to be more likely to exceed this threshold because large rivers retain much of their sediment within their floodplains (Milliman and Syvitski, 1992; Mulder and Syvitski, 1995). Further work suggests that hyperpycnal currents may be even more common due to mixing within estuaries (Felix et al., 2006) and due to the generation of

hyperpycnal flow from convective instability within a hypopycnal plume (Parsons et al., 2001). Many studies promote hyperpycnal currents as important mechanisms for cross-shelf transfer of sediment (e.g. Normark and Piper, 1991; Myrow et al., 2002; Mulder et al., 2003; Wright and Friedrichs, 2006; Warrick et al., 2008), and ancient hyperpycnal currents have been interpreted in the rock record (Plink-Bjorklund and Steel, 2004; Pattison, 2005). However, limited evidence of hyperpycnal deposits on modern continental shelves exists (Warrick et al., 2013). Modern shelves are an excellent starting point for understanding and interpreting hyperpycnal deposits in the rock record, and Holocene deposits on the shelf of the Santa Barbara Channel, Southern California provide a unique opportunity to refine hyperpycnite facies models that currently lack Quaternary examples (Chapter 2).

Hyperpycnal currents are distinct from other types of turbidity currents, such as those triggered by earthquakes or by the intersection of littoral cells with submarine canyons. One key difference arises from the fresh interstitial water within hyperpycnal currents, which alters the evolution of the flow and the dispersal of sediment. Hyperpycnal currents traveling through marine basins may undergo buoyancy reversal, or lofting, in which deposition of suspended sediment causes the current to become less dense than the surrounding ambient water and to lift off from the basin floor (Sparks et al., 1993). Lighter constituents in the flow, such as fine-grained sediment and organic debris, travel vertically with the lofting plume; however, sand-sized or larger sediment remains behind on the seabed (Pritchard and Gladstone, 2009; Zavala et al., 2011). The resulting deposit is likely to have a well-sorted basal sand deposited by the bed-attached flow, with a mantle of fine-grained, organic rich sediment that settled from the lofted plume (Walker and McBroome, 1983; Pritchard and Gladstone, 2009). Experimental work by Gladstone and Pritchard (2010) suggests that lofting also produces deposits with an

abrupt frontal termination as the sediment is rapidly deposited at the lofting point. Existing studies on lofting currents focus on streamwise (1-dimensional) variations in flow evolution and deposit characteristics and are conducted in narrow flume tanks. However, no studies explore the effects of lofting on lateral flow expansion and the three-dimensional deposit morphology (Chapter 3).

Work on Holocene deposits in the Santa Barbara Channel (Chapter 2) and analog flume experiments (Chapter 3), provide a framework for understanding and interpreting hyperpycnites preserved in the rock record (Chapter 4). Additionally, the recent development of a genetic facies model for hyperpycnites allows for improved identification and classification of hyperpycnites (Zavala et al., 2011). This facies model breaks deposits into those formed by bed load, suspended load, and lofting processes. Although hyperpycnites are becoming increasingly recognized in the rock record (Plink-Bjorklund and Steel, 2004; Pattison, 2005; Zavala et al., 2006; Myrow et al., 2008; Soyinka and Slatt, 2008), the facies model proposed by Zavala et al. (2011) remains in its early stages and a broader range of examples is required in order to confirm and refine the model. The Neuquén Basin of Southwestern Argentina contains Jurassic shelf sand bodies that are interpreted as hyperpycnites (Chapter 4). These deposits display many similarities to previously recognized hyperpycnites (Zavala et al., 2006; Zavala et al., 2011; Mutti et al., 2003; Plink-Bjorklund and Steel, 2004) and are characterized by well-sorted, medium-grained sandstones containing extensive parallel laminations (Facies S2 of Zavala et al., 2011). These sandstones are encased by thinly laminated siltstone and fine-grained sandstone with abundant terrestrial organic debris (facies L of Zavala et al., 2011).

The studies discussed here approach the question of how hyperpycnal currents deposit their sediment and what controls the internal architecture and overall morphology of hyperpycnites by taking a three-part approach of studying Holocene hyperpycnites, experimental hyperpycnal currents, and ancient hyperpycnites in the rock record. Chapter one is an introduction to the topics and research discussed in the following chapters. Chapter two focuses on Holocene deposits from the Santa Barbara Channel, which provide a nice starting point for understanding hyperpycnal systems because the geologic context is relatively well understood. Chapter three is focused on the ways in which interstitial fluid density can alter the dynamics and evolution of hyperpycnal currents, and in particular the ways in which buoyancy reversal affects length-to-width ratios of hyperpycnites. In Chapter four, Jurassic hyperpycnites deposited on the continental shelf of the Neuquén basin of Argentina are described in detail and placed into the context of previously described sand bodies. Finally, Chapter 5 provides concluding remarks regarding the recognition of hyperpycnites in the rock record and discusses hyperpycnal shelf sand bodies in a larger framework of source-to-sink systems.

REFERENCES CITED

Bates, C.C., 1953, Rational theory of delta formation: American Association of Petroleum Geologists Bulletin, v. 27, p. 2119-2216.

Felix, M., Peakall, J. and McCaffrey, W.D., 2006, Relative importance of processes that govern the generation of particulate hyperpycnal flows: Journal of Sedimentary Research, v. 76, p. 382-387.

Gladstone, C., and Pritchard, D., 2010, Patterns of deposition from experimental turbidity currents with reversing buoyancy: Sedimentology, v. 57, no. 1, p. 53-84.

Milliman, J.D., and Syvitski, J.P.M, 1992, Geomorphic/tectonic control of sediment discharge to the ocean: Importance of small mountainous rivers: The Journal of Geology, v. 100, p. 525-544.

Mulder, T., and Syvitski, J.P., 1995, Turbidity currents generated at river mouths during exceptional discharges to the world oceans: The Journal of Geology, v. 103, p. 285-299.

Mulder, T., Syvitski, J.P.M., Migeon, S., Faugeres, J.C., Savoye, B., 2003, Marine hyperpycnal flows: initiation, behavior and related deposits. A review: Marine and Petroleum Geology, v. 20, p. 861-882.

Mutti, E., Tinterri, R., Benevelli, G., di Biase, D., and Cavanna, G., 2003, Deltaic, mixed and turbidite sedimentation of ancient foreland basins: Marine and Petroleum Geology, v. 20, p. 733-755.

Myrow, P.M., Fischer, W., and Goodge, J.W., 2002, Wave modified turbidites: combined-flow shoreline and shelf deposits, Cambrian, Central Transantarctic Mountains: Journal of Sedimentary Research, v. 72, p. 641-656.

Myrow, P.M., Lukens, C., Lamb, M.P., Houck, K., and Strauss, J., 2008, Dynamics of a transgressive prodeltaic system: Implications for geography and climate with a Pennsylvanian intracratonic basin: Journal of Sedimentary Research, v. 78, p. 512-528.

Normark, W. R., and Piper, D. J. W., 1991, Initiation processes and flow evolution of turbidity currents: Implications for the depositional record: Shoreline to Abyss: SEPM Special Publication, v. 46, p. 207-230.

Parsons, J.D., Bush, J.W.M., and Syvitski, J.P.M, 2001, Hyperpycnal plume formation from riverine outflow with small sediment concentrations: Sedimentology, v. 48, p. 465-478.

Pattison, S.A.J., 2005, Storm-influenced prodelta turbidite complex in the lower Kenilworth Member at Hatch Mesa, Book Cliffs, Utah, U.S.A.: Implications for shallow marine facies models: Journal of Sedimentary Research, v. 75, no. 3, p. 420-439.

Plink-Bjorklund, P. and Steel, R.J., 2004, Initiation of turbidity currents: outcrop evidence for Eocene hyperpycnal-flow turbidites: Sedimentary Geology, v. 165, p. 29-52.

Pritchard, D., and Gladstone, C., 2009, Reversing buoyancy in turbidity currents: Developing a hypothesis for flow transformation and for deposit facies and architecture: Marine and Petroleum Geology, v. 26, p. 1997–2010.

Soyinka, O., and Slatt, R.M., 2008, Identification and micro-stratigraphy of hyperpycnites and turbidites in Cretaceous Lewis Shale, Wyoming: Sedimentology, v. 55, p. 1117-1133.

Sparks, R.S.J., Bonnecaze, R.T., Huppert, H.E., Lister, J.R., Hallworth, M.A., Mader, H., and Phillips, J., 1993, Sediment-laden gravity currents with reversing buoyancy: Earth and Planetary Science Letters, v. 114, p. 243–257.

Walker, G. P., and McBroome, L. A., 1983, Mount St. Helens 1980 and Mount Pelée 1902—flow or surge?: Geology, v. 11, no. 10, p. 571-574.

Warrick, J.A., Xu, J., Noble, M.A., and Lee, H.J., 2008, Rapid formation of hyperpycnal sediment gravity currents offshore of a semi-arid California river: Continental Shelf Research, v. 28, p. 991-1009.

Warrick, J.A., Simms, A.R., Ritchie, A., Steel, E., Dartnell, P., Conrad, J.E., and Finlayson, D.P., 2013, Hyperpycnal plume-derived fans in the Santa Barbara Channel, California: Geophysical Research Letters, v. 40, p. 2081–2086.

Wright, L.D., and Friedrichs, C.T., 2006, Gravity-driven sediment transport on continental shelves: a status report: Continental Shelf Research, v. 26, p. 2092-2107.

Zavala, C., Ponce, J. J., Arcuri, M., Drittanti, D., Freije, H., and Asensio, M., 2006, Ancient lacustrine hyperpycnites: A depositional model from a case study in the Rayoso Formation (Cretaceous) of west-central Argentina: Journal of Sedimentary Research, v. 76, no. 1, p. 41-59.

Zavala, C., Arcuri, M., Di Meglio, M., Diaz, H.G., and Contreras, C., 2011, A genetic facies tract for the analysis of sustained hyperpycnal flow deposits: in Slatt, R.M., and Zavala, C., eds., Sediment transfer from shelf to deep water – revisiting the delivery system: AAPG Studies in Geology 61, p. 31-51

CHAPTER 2

HIGHSTAND SHELF FANS: THE ROLE OF BUOYANCY REVERSAL IN THE DEPOSITION OF A NEW TYPE OF SHELF SAND BODY

2.1 INTRODUCTION

Documenting the survival of river-derived sediment beyond the high-energy coastal fence is critical to understanding source-to-sink connections through geologic time. The continental shelf is thought to be starved of sediment during sea-level highstands, with the majority of sand trapped at the coast (Posamentier and Allen, 1999). However, recently mapped Holocene fans on the shelf of the Santa Barbara Channel (SBC) suggest that deposition of sediment lobes on the continental shelf may not be restricted to falling-stage or lowstand systems tracts (Warrick et al., 2013).

The fate of sediment discharged by coastal rivers depends heavily on the interactions between ambient water density (ρ_a), bulk flow density (ρ_b), and interstitial fluid density (ρ_i). If high suspended-sediment concentrations cause ρ_b to exceed ρ_a, flows with light interstitial fluid can travel as bottom-hugging currents known as hyperpycnal flows and escape reworking by coastal littoral cells (Normark and Piper, 1991; Mulder and Syvitski, 1995; Felix et al., 2006).

A version of this chapter is published as a paper in GSA Bulletin under the citation: Steel, E., Simms, A.R., Warrick, J., and Yokoyama, Y., 2016, Highstand shelf fans: The role of buoyancy reversal in the deposition of a new type of shelf sand body: Geological Society of America Bulletin, v. 128, no. 11-12, p. 1717-1724. doi:10.1130/B31438.1.

Despite modern observations of hyperpycnal discharge (Wright et al., 1986; Milliman et al., 2007) and identification of hyperpycnites in outcrop (Myrow et al., 2002; Plink-Bjorklund and Steel, 2004; Zavala et al., 2006; Lamb et al., 2008; Olariu et al., 2010) hyperpycnites that have survived on the continental shelf for more than a few years have yet to be identified and sampled.

The mountainous rivers draining the Transverse Ranges of southern California, when in flood, are known to exceed the suspended sediment threshold of 40 g/L usually necessary for direct hyperpycnal plunging at the fluvial-marine interface (Warrick and Mertes, 2009). The location and geometry of the recently mapped lobes on the SBC shelf suggests that they were deposited by hyperpycnal flows (Warrick et al., 2013). In this study, we test this hypothesis by investigating fan stratigraphic architecture using cores, grain-size trends, and radiocarbon (^{14}C) ages. Our new observations of these recent sediment gravity flow deposits provide valuable new insights for interpreting marine sediment and understanding sequence stratigraphic models.

2.1.1. BUOYANCY REVERSAL IN HYPERPYCNAL FLOWS

The fate of hyperpycnal discharge depends on the balance between factors that increase ρ_b, e.g. entrainment of sediment or dense ambient water, and factors that decrease ρ_b, e.g. deposition of suspended sediment. Entrainment of sediment can be achieved through erosion from the seabed or by collapse or rainout from an overriding hypopycnal plume (Parsons et al., 2001). If sediment and ambient water are entrained more quickly than sediment is deposited, a flow will remain dense and continue into deep water as a sustained turbidity current. However, if sediment is deposited from the flow with relatively little ambient entrainment, ρ_b will decrease until it reaches an equivalent buoyancy with the ambient water,

at which point a plume will rise above the seabed in a process known as lofting (Sparks et al., 1993; Zavala and Arcuri, 2016).

The distinction between lofted and sustained flows is not trivial. Deposits from each flow type are suggested to display unique grain-size characteristics, geometries, and run-out distances, and lofting is a mechanism that can explain a variety of enigmatic deposits that do not directly fit classic turbidite or debrite facies models (Pritchard and Gladstone, 2009; Gladstone and Pritchard, 2010; Zavala and Arcuri, 2016). Sediment carried by the flow at the point of lofting will either be rapidly deposited or will remain in suspension within the rising plume (Pritchard and Gladstone, 2009). In laboratory flume experiments, lofted plumes rise and spread out along the water surface (Gladstone and Pritchard, 2010; Stevenson and Peakall, 2010). However, in stratified ocean basins, plumes may rise and spread along an intermediate depth of neutral buoyancy rather than the free surface, or may be carried away to more distal regions by cross-currents. Variability in ambient water stratification and ocean current dynamics leads to a number of possible architectures in lofted flow deposits, as fine sediment carried by the plume may settle over a widespread region around the point of buoyancy reversal or may be transported away from the area by ocean currents (Pritchard and Gladstone, 2009). Despite this variability, a diagnostic feature of the deposits created during experiments is a "snub-nosed" frontal geometry formed by rapid deposition during buoyancy reversal (Gladstone and Pritchard, 2010). Although theoretical models and laboratory experiments provide constraints on expected characteristics of lofted turbidity currents, field examples of lofted hyperpycnites validating these models have yet to be described.

2.1.2. GEOLOGIC SETTING

The SBC (34°N, 120°W) is the offshore extension of the Western Transverse Ranges province in southern California. The shelf in our study area is ~ 6 km wide and extends to ~ 100 m depth (Dartnell et al., 2015b). The six SBC fans imaged on the shelf lie in 25 m to 70 m water depth, and are disconnected but directly offshore from, and aligned with, creeks draining the Santa Ynez Mountains (Fig. 1). The majority of the sediment in these fans lies below 50 m water depth. The two largest fans are the Refugio Fan and Tajiguas Fan with estimated volumes of 1.7 x 10^6 m^3 and 1.5 x 10^6 m^3, respectively (Warrick et al., 2013). These fans are composed of elongate lobes with abrupt terminations. Relief of these features are 1–3 m, and lobe length to width ratios range from 4 to 13. The source watersheds (Refugio and Tajiguas creeks) have drainage areas of 21 and 16 km^2, respectively, have a total vertical relief of ~900 m, and are uplifting at ~2 mm yr^{-1} (Gurrola et al., 2014). Sediment delivery to the SBC is dominated by infrequent winter floods with exceptional discharge (Warrick and Mertes, 2009).

2.2 DATA AND METHODS

2.2.1 SEA FLOOR BATHYMETRY

High-resolution bathymetry and acoustic backscatter used in this study were collected by the U.S. Geological Survey as part of the California Seafloor Mapping Program (Dartnell et al., 2015a, b). Data extend from 10 m to 110 m water depth and were collected using 234.5 kHz phase-differencing sidescan sonar aboard the USGS R/V *Parke Snavely* (Dartnell et al., 2010).

2.2.2 HIGH-RESOLUTION SEISMIC SURVEYS

Shallow seismic surveys were conducted over the Tajiguas Creek and Refugio Creek fans in September 2012 and June 2013 aboard the R/V Connell operated by the University of California, Santa Barbara (Appendix I). The data were collected using an Edgetech 3100 Subbottom Profiler and a SB-216S Chirp system with a frequency sweep of 2.0 to 15.0 kHz and a recording length of 20 ms. A vertical resolution of ~20 cm is possible assuming an acoustic velocity of 1500 m/s.

2.2.3. SEDIMENT CORES AND GRAB SAMPLES

Six cores from the Tajiguas Fan, one core from the Refugio Fan, and one core from the shelf between the fans were collected aboard the *M/V Danny C* in October, 2013 (Fig. 1). Cores were supplemented with nine surface grab samples collected from the Tajiguas Fan and the shelf to the east of the fan aboard Theory Marine's *JAB* (Fig. 1). A pneumatic hammer coring system was used to collect all cores. Cores were driven to the point of refusal, assumed to be Neogene bedrock, which was sampled in two cores.

2.2.4. GRAIN SIZE ANALYSIS

All cores were sampled at 5 cm intervals for grain-size analysis. Samples were pretreated with 30% hydrogen peroxide (H_2O_2) and 10% hydrogen chloride (HCl). Grain-size was measured with a CILAS 1190 particle size analyzer capable of measuring grains within the 0.04 μm – 2,500 μm range, following the methods of Sperazza et al. (2004).

An algorithm for end-member modeling analysis (EMMA) was employed to quantify the differences in grain-size characteristics of the observed facies (Dietze et al., 2012). Sediment within the SBC was deposited by a variety of mechanisms and sources, and may have undergone post-depositional reworking. The EMMA algorithm 'unmixes' grain-size distributions in an effort to extract these processes and sources from samples (Dietze et al.,

2012). Four end-members were sufficient to describe 95 – 98 % of the grain-size variability in the SBC samples.

2.2.5. RADIOCARBON DATING

Four bivalves and ten plant fragments were sampled from cores for ^{14}C dating (Table 1; Appendix II). Terrestrial plant samples were measured by Atomic Mass Spectrometry (AMS) by DirectAMS in Seattle, Washington. Bivalve samples were measured at the University of Tokyo (Yokoyama et al., 2007). Bivalve ^{14}C ages were calibrated using the Marine04 calibration curve (Hughen et al., 2004), and plant fragment ^{14}C ages were calibrated using the IntCal04 calibration curve (Reimer et al., 2004) using the Calib Rev 7.0.2 program (Stuiver and Reimer, 1993).

2.3 RESULTS

2.3.1. SEDIMENTARY FACIES

Cores from the SBC fans contain structureless, well-sorted fine sand interbedded with muddy silt (Fig. 2; Appendix III). Mean percent clay for all cores within fan lobes range from 6.2% to 11.1%. However, off-fan samples range from 6.4% to 16.3% clay, with all samples except for surface sample A1 ranging between 13% and 16.3% clay. Tajiguas Fan sediment displays a basinward-fining trend (Fig. 2). All cores from the fan lobes contain scattered shells and shell fragments, ranging from ~1 mm to 7 cm in size, and plant fragments. Due to the well-sorted nature of the deposits, individual beds are difficult to distinguish and results from EMMA provided a quantifiable metric for distinguishing sedimentary facies and beds. Three sedimentary facies and four end-member grain-size distributions were identified in cores and grab samples (Fig. 2). Goodness of fit between the original dataset and EMMA results provides

mean r^2 values ranging from 0.57 to 0.98 in all cores collected from fan lobes (Fig. 3), with the exception of core RF13-02, which has a lower goodness of fit of $r^2 = 0.49$ due to the small sample size from this core (n=4). EMMA results for SBC sediment provides the most robust results for grain-size classes of <10ϕ and >2ϕ (Fig. 3).

Facies S_1 consists of subrounded, well sorted fine silt to fine sand with ~ 10% - 20% clay. This facies is primarily composed of EMMA end-members EM1 and EM2, which have polymodal grain-size distributions with modes ranging from 13 μm to 170 μm. Facies S_1 is bioturbated and contains very few plant fragments larger than two mm in diameter, and less than 5% shells, some of which are articulated bivalves. Facies S_1 beds are ~5 cm to ~25 cm thick in all cores and comprises all off-fan grab samples.

Facies S_2 is composed of subrounded, very well sorted, fine silt to medium sand with less than 10% clay. This facies is primarily composed of EMMA end-member EM3, which is positively skewed and contains a mode near 150 μm (Fig. 2). Facies S_2 contains abundant plant fragments including twigs and wood fragments up to 3 cm long and ~5% - 30% by volume shells and shell fragments, which are predominantly the gastropod *Turritella*. Facies S_2 beds are ~5 cm to ~40 cm thick, and are present in all fan cores, but absent in off-fan grab samples.

Facies S_3 is composed of very well-sorted, subrounded, fine silt to fine sand with less than 10% clay. Facies S_3 is predominantly composed of EMMA end-member EM4, which has a positively skewed distribution with a mode near 80 μm. Facies S_3 contains less than 5% shell fragments and less than 5% plant fragments. This facies is found only at the base of two cores: TG13-02 and TG13-03.

2.3.2. RADIOCARBON RESULTS

Fourteen ^{14}C ages were obtained from six cores in the SBC (Table 1). Ages range from 500 to 12,677 calibrated years BP (cal yr BP). Two ages obtained from ~8 mg plant fragments in core TG13-02, at 33 cm and 43 cm, are out of sequence. All radiocarbon samples collected from individual S_2 beds in the Tajiguas Fan provide unique ages, while those within the same S_2 bed returned overlapping ages (Fig 2; Table 1).

2.4 DISCUSSION

2.4.1. FACIES INTERPRETATIONS

Facies S_1 is the least sorted facies within the SBC fan samples, with polymodal distributions containing fine-grained modes in addition to modes shared by other facies (Fig 2). All off-fan shelf samples are composed of facies S_1. Although minor, bioturbation throughout S_1 beds suggests deposition during quiescent periods. Therefore, facies S_1 is interpreted to represent a combination of hemipelagic shelf sedimentation and sedimentation from lofted plumes. Facies S_1 contains a higher percentage of silt and sand than might be expected in hemipelagic sediment, which is perhaps due to the presence of sediment from buoyant plumes and from hypopycnal river effluent.

Facies S_2 contains abundant terrestrial plant fragments that indicate rapid burial from river-derived outflow (Zavala and Arcuri, 2016). Scattered shell fragments require a bottom-hugging turbulent flow capable of entraining and distributing shelf material. Radiocarbon samples from the base and top of one of these beds (TG13-02 61cm and 69cm) are the same age, ~5400 cal yr BP (Table 1; Appendix II), suggesting that S_2 beds were deposited as discrete events in a short period of time, rather than by continuous gradual sediment accumulation.

Individual S_2 beds provide distinct ^{14}C ages, suggesting that each lobe is composed of multiple events (Fig. 2; Table 1). These beds are relatively coarse-grained, unimodal deposits, which we interpret as fan-building hyperpycnites. Multiple hyperpycnites of facies S_2 ranging from ~5 cm to ~40 cm thick are separated by facies S_1 (Fig. 2). The EM3 grain-size mode decreases from 160 μm in the shallowest core to 130 μm in the deepest core, indicating a basinward-fining trend within the hyperpycnites. Lobes sampled in the Tajiguas Fan were each constructed by 3 – 6 hyperpycnal flows; six flows are identified in core TG13-01, five in TG13-02 and TG13-06, and three in TG13-03, TG13-04, and TG13-05 (Fig. 2).

A transgressive ravinement surface (TRS) was sampled at or near the base of five cores. The TRS contains abundant shell fragments from a wide range of environments, and ^{14}C ages from material directly below this surface correlate well to a local relative sea-level curve (Reynolds and Simms, 2015). Where sampled, S_3 beds are only present directly below the TRS and likely represent early Holocene shoreface deposits (Fig. 2).

2.4.2. LOFTED HYPERPYCNAL FLOWS IN THE SBC

Based on the abundance of wood and plant fragments, we conclude that the SBC fans on the shelf were deposited by river-derived flows (Myrow et al., 2008; Zavala and Arcuri, 2016). Although scattered shelf-derived shell fragments suggest an initially turbulent hyperpycnal flow, abrupt lobe terminations, lack of tractional structures, and convolute bedding from rapid dewatering indicate *en masse* deposition. This contrasts with the traction-laminated hyperpycnites described from some deep-water slope and shelf deposits (Myrow et al., 2002; Plink-Bjorklund and Steel, 2004; Olariu et al., 2010), where lamination is thought to have developed during pulsed aggradation of the bed while flows continued to bypass. If suspended-sediment within a hyperpycnal flow is deposited quickly and ambient water

entrainment is slow, ρ_b will decrease until the flow becomes a lofting plume. This process results in *en masse* deposition of the base of the flow, which contains the coarsest grain-size fraction (Fig. 4). Further support for the role of buoyancy reversal in the deposition of these features lies in the well-sorted nature of the deposits; sediment from the modern shoreface and watersheds are much more poorly sorted than sediment deposited in SBC fans. Hyperpycnal flows transport sediment in suspension, which explains the lack of coarse-grained material (e.g. coarse sand or cobbles) in the SBC fans, but SBC deposits also have a lower clay percentage than would be expected based on watershed characteristics and off-fan samples. Pritchard and Gladstone (2009) suggest that the finest grain-size fraction in suspension at the point of lofting will be carried away with the rising plume; the analogous process of buoyancy reversal in pyroclastic flows results in coarse-tailed deposits (Walker and McBroome, 1983). A lofted hyperpycnal flow may therefore deposit a well-sorted and slightly normally graded sand bed (Pritchard and Gladstone, 2009), as observed in the fines-depleted hyperpycnal beds of the SBC fans (Fig. 2). Hyperpycnal beds are capped by facies S_1. This sediment was likely deposited through settling of fines from lofted plumes and background shelf processes between flow events, analogous to the fine-tailed pyroclastic deposits of Walker and McBroome (1983) (Fig. 4).

Wave climate may play a role in the deposition of hyperpycnites in the Santa Barbara Channel. Fair-weather wave base in the Santa Barbara Channel is less than 20 m water depth, and estimates of storm wave base range from 35 m to 70 m water depth (Sommerfield et al., 2009). However, this study site lies in a region of the Santa Barbara Channel sheltered from large swells by the Channel Islands, and storm wave base is likely to be closer to 35 m water depth (Sommerfield et al., 2009; Johnson et al., 2013). Waves have been known to enhance

turbulence in turbidity currents (Wright et al., 2001; Myrow et al., 2002), and although wave conditions during deposition of the SBC fans are unknown, turbulence within the hyperpycnal flows was likely modified by waves, which may have led to enhanced sediment transport across the shelf. In addition to typical Bouma-type features, wave-modified turbidity currents are expected to deposit hummocky cross stratification and combined-flow ripple cross-stratification (Myrow et al., 2002). Fan deposits in the Santa Barbara Channel do not display such diagnostic sedimentary structures, perhaps because they were deposited below storm wave base or because buoyancy reversal hinders the development of such features.

2.4.3. DEPOSITION OF HIGHSTAND SHELF FANS

The present study is important because it demonstrates that hyperpycnal plunging of river-mouth sediment-laden water allows for the development of underflows and the delivery of sand well beyond the high-energy coastline, where sandy sediment is commonly confined during sea-level highstands. Far beyond the river-mouth plunge-point, buoyancy reversal in hyperpycnal plumes provides a mechanism through which sediment is abruptly deposited on the continental shelf rather than continuing onto the deep-water slope or continental rise. This suggests that active margins may not only deliver sediments to deep-water basins during sea-level highstands (Covault et al., 2007), but also to the continental shelf. The existence of these fans in the Santa Barbara Channel challenges conventional thinking that significant sand deposition does not occur on the continental shelf during sea-level highstands, and provides a modern field example for the importance of hyperpycnal flow in across-shelf sediment transport. The preservation of Holocene SBC fans is likely due to the steep continental shelf gradients, which allow for sediment to be deposited within a short distance of the coastline yet still below fair-weather wave base.

Standard hyperpycnite models suggest a coarsening-to-fining upward deposit profile associated with waxing and waning flood stages (Mulder et al., 2003; Zavala et al., 2006). However, these models do not take into account the effects of buoyancy reversal, which may be more prolific in turbidite systems than is currently acknowledged. The lack of sedimentary structures in any cores from the SBC fans suggests that lofting, and therefore rapid deposition of sediment, occurred along the entire length of the flow rather than simply lofting at the head of the flow while the body and tail remained bed-attached. Turbidity currents are stratified, with sediment concentration and grain-size decreasing upwards (e.g. Kneller and Buckee, 2000; Hansen et al., 2015; Peakall and Sumner, 2015). This stratification could cause the upper portions of the flow, which are more dilute, to loft earlier than the base of the flow and to progressively remove fine material during the course of the flow. Furthermore, the lift-off point of the flow head is likely to migrate downstream due to the effects that lofting has on the density of ambient fluid surrounding the current (Stevenson and Peakall, 2010). The combination of lift-off point migration, lofting along the upper margins of the entire flow, and the short length of the fan system (<2 km) is likely responsible for rapid deposition and the lack of sedimentary structures within the deposits.

Hyperpycnal flows in marine basins are particularly susceptible to buoyancy reversal due to the density contrasts between fresh interstitial water and salty ambient water. However, any environment conducive to generating turbidity currents with light interstitial fluid, including currents flowing through a density stratified ocean or lake basin, is capable of producing lofting turbidity currents. Buoyancy reversal in turbidity currents that initiate on the shelf or upper slope and travel into colder deep water provides an additional, and commonly overlooked, mechanism for the deposition of massive deep-water sands (Shanmugam, 1996;

Stow and Johansson, 2000). Because buoyancy reversal may be responsible for the formation of well-sorted, structureless sands in a range of shallow or deep-water environments, the presence of fluvially-influenced indicators, such as terrestrial plant fragments, can aid in the distinction between river-derived hyperpycnites and turbidites that originated within a marine or lacustrine basin (Myrow et al., 2008; Zavala and Arcuri, 2016).

Highstand shelf fans in the SBC differ from previously described shelf sand bodies formed by wave processes or tidal currents (Bergman and Snedden, 1999) in their distinct fluvially-influenced signature. Conventional models suggest that lowstand shelf-edge deltas, which feed sediment directly onto the continental slope, are needed to produce well-developed hyperpycnal flow and thick hyperpycnite beds (Olariu et al., 2010). However, highstand shelf fans in the SBC show that hyperpycnal flows are capable of depositing thick shelf sand bodies. The recognition of highstand shelf fans may aid in the interpretation of sand bodies that would otherwise be incorrectly interpreted as deep-water or lowstand deposits. Additionally, the sorting and cleaning of sand through the process of buoyancy reversal could explain the abundance of structureless beds interpreted as turbidites, but lacking typical Bouma-type features (Stow and Johansson, 2000; Stevenson and Peakall, 2010). In conclusion, the results of this study reveal that hyperpycnal flows are capable of depositing more significant shelf sandbodies than previously recognized, and buoyancy reversal and subsequent lofting of hyperpycnal plumes allowed for the deposition of previously undescribed shelf sand bodies that are sorted through the stripping of fine-grained material in suspension at the point of lift-off.

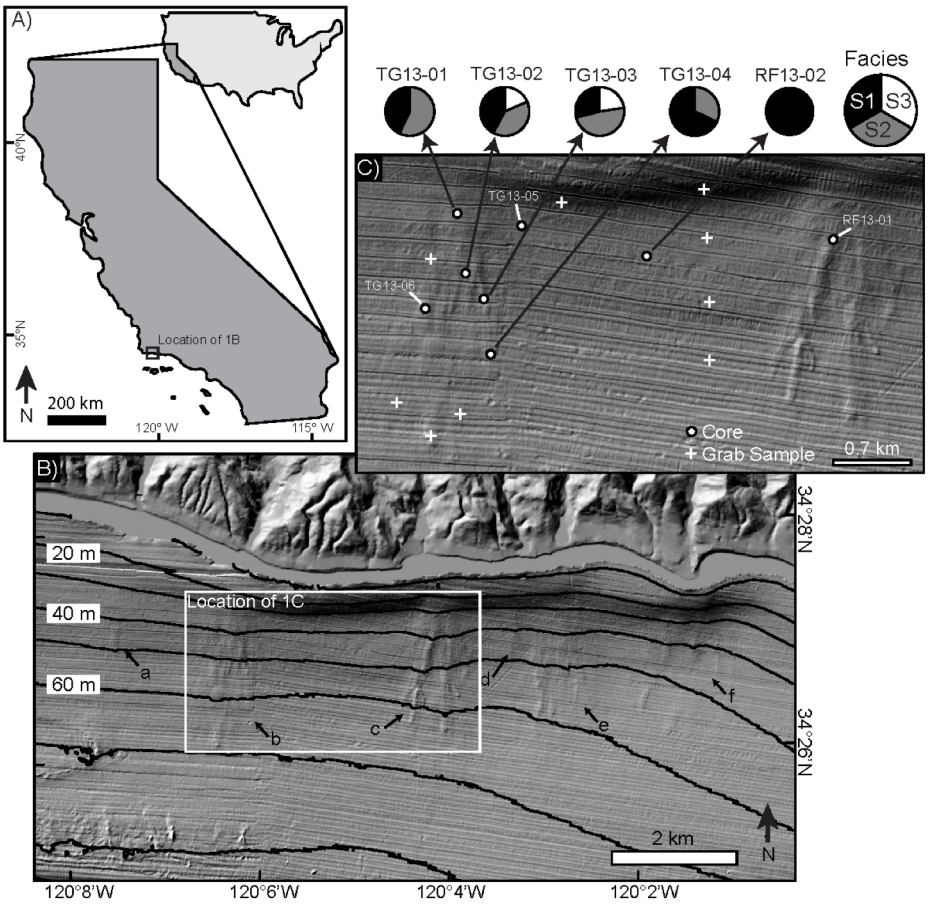

Figure 1. Bathymetry of six submarine fans on the shelf of the northern Santa Barbara Channel, California. (A) Location of study area in Southern California. The location Figure 1B is indicated by the black box. (B) Fans lie between 25 m and 70 m water depth offshore from Arroyo Quemada (a), Tajiguas Creek (b), Refugio Creek (c), Venadito Creek (d), Las Flores Creek (e), and El Capitan Creek (f). (C) Core and grab sample locations from the Tajiguas Fan (left) and the Refugio Fan (right). Pie charts show facies composition of four Tajiguas Fan cores and one off-fan core.

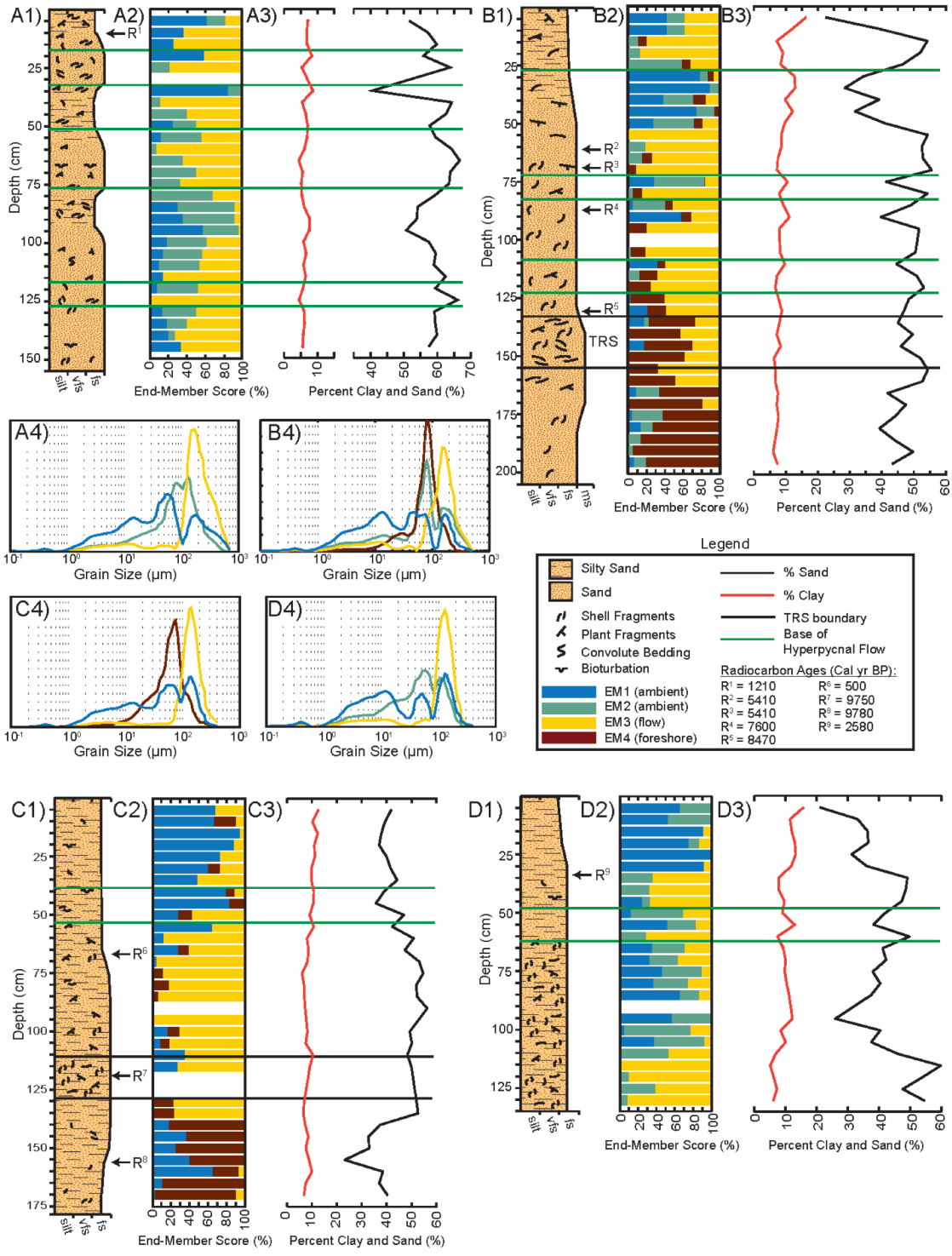
A1)
A2)
A3)
B1)
B2)
B3)
C1)
C2)
C3)
D1)
D2)
D3)
A4)
B4)
C4)
D4)
Depth (cm)
End-Member Score (%)
Percent Clay and Sand (%)
Grain Size (μm)
TRS
Legend
Silty Sand
Sand
Shell Fragments
Plant Fragments
Convolute Bedding
Bioturbation
EM1 (ambient)
EM2 (ambient)
EM3 (flow)
EM4 (foreshore)
% Sand
% Clay
TRS boundary
Base of Hyperpycnal Flow
Radiocarbon Ages (Cal yr BP):
R1 = 1210
R2 = 5410
R3 = 5410
R4 = 7600
R5 = 8470
R6 = 500
R7 = 9750
R8 = 9780
R9 = 2580

Figure 2. (previous page) Core description, EMMA results, and percent clay and sand for cores TG13-01, TG13-02, TG13-03, and TG13-04. See Figure 1 for core locations. (A1) Core description for TG13-01. (A2) EMMA results for TG13-01. (A3) Percent clay and sand in TG13-01. The boundary marking the base of hyperpycnites is marked by a decrease in clay and an increase in sand. (A4) End-member distributions corresponding to A2. (B1-B4) Core description, EMMA results, percent clay and sand, and end-member distributions for core TG13-02. (C1-C4) Core description, EMMA results, percent clay and sand, and end-member distributions for core TG13-03. (D1-D4) Core description, EMMA results, percent clay and sand, and end-member distributions for core TG13-04. Green lines mark the base of hyperpycnites. Hyperpycnite tops are not indicated because the boundary between plume fall-out and hemipelagic sediment is difficult to distinguish. However, the top of the sediment deposited by the bed-attached flow occurs where the EM3 (yellow) bar becomes less dominant compared to EM1 (blue) and EM2 (green). Six flows are identified in TG13-01, five flows in TG13-02, and three flows in both TG13-03 and TG13-04. The transgressive ravinement surface (TRS) is bounded by black lines. A basinward-fining trend is indicated by a shift in the EM3 (yellow) grain size peak from core TG13-01 (A4) to TG13-04 (D4).

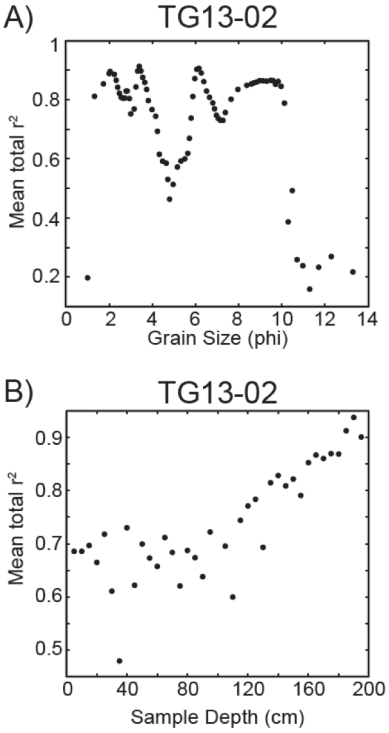

Figure 3. Goodness of fit plots from EMMA end-member analysis from core TG13-02. All cores from Santa Barbara Channel fans provide similar results. The mean coefficient of determination (r^2) is a quantitative error estimate that compares model results to the original dataset. (A) The relationship between grain size and mean r^2 values. EMMA results from the SBC fans are most accurate for grain sizes between 2Φ and 10Φ. (B) The relationship between sample depth and mean r^2 values.

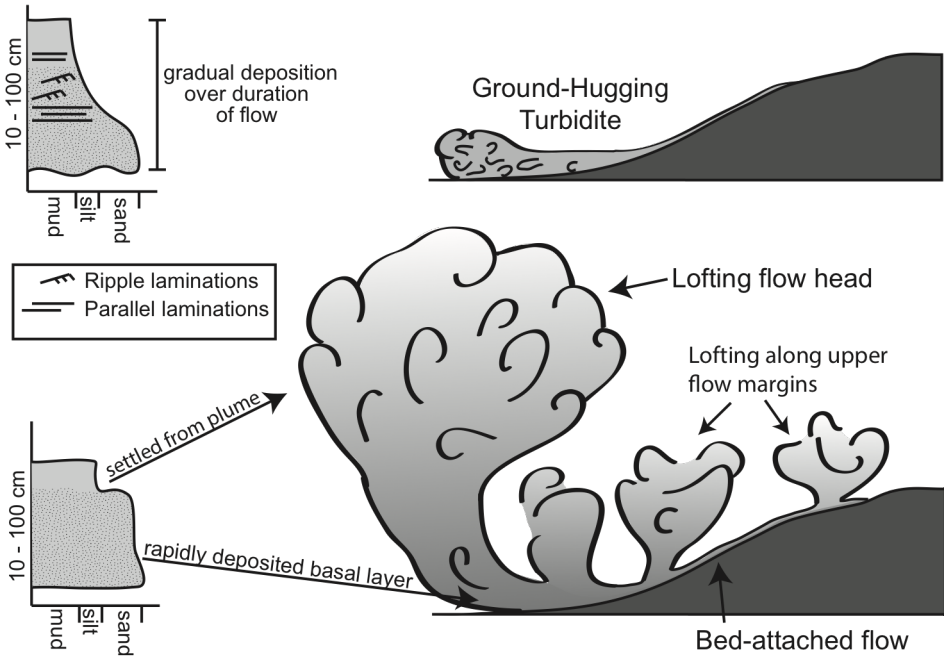

Figure 4. Schematic diagram illustrating the difference between a ground-hugging turbidity current and a lofting turbidity current. The ground-hugging flow will deposit commonly recognized turbidites with Bouma or Lowe sequences. Lofting flows deposit beds with a massive, fines-depleted basal layer and a fine-grained cap deposited by sediment settling from the lofted plume. Lofting may occur at the flow head or along the length of the flow due to lofting of dilute upper flow margins.

TABLE 1. RADIOCARBON AGES FROM THE TAJIGUAS FAN AND REFUGIO FAN

Lab ID	Core Name	Depth (cm)	Material	$\delta^{13}C$ (per mil)	^{14}C age ± 1σ (years BP)	Calibrated Age (Cal years BP)*
YAUT-007625	TG13-01	10	Bivalve	3.50	1215 ± 18	412 - 714
D-AMS 008757	TG13-02	33	Plant	- 29.10	6615 ± 35	7440 - 7568
D-AMS 008758	TG13-02	43	Plant	- 14.30	7766 ± 36	8448 - 8603
D-AMS 008007	TG13-02	61	Plant	- 28.40	4708 ± 29	5323 - 5579
D-AMS 008759	TG13-02	69	Plant	- 17.00	4648 ± 33	5310 - 5467
D-AMS 008008	TG13-02	87	Plant	- 29.20	6739 ± 30	7568 - 7662
D-AMS 008009	TG13-02	133	Plant	- 23.70	7680 ± 36	8408 - 8542
D-AMS 008011	TG13-03	69	Plant	- 26.70	427 ± 23	345 - 520
D-AMS 008010	TG13-03	122	Plant	- 33.50	8619 ± 38	9529 - 9669
YAUT-007629	TG13-03	156	Bivalve	- 0.23	9780 ± 29	10,182 - 10,617
D-AMS 008013	TG13-04	29	Plant	- 10.30	2477 ± 30	2381 - 2721
D-AMS 008012	TG13-06	225	Plant	- 11.90	10720 ± 43	12,590 - 12, 728
YAUT-007630	RF13-01	81	Bivalve	4.66	5191 ± 22	4969 - 5507
YAUT-007631	RF13-01	160	Bivalve	1.64	5537 ± 22	5459 - 5876

*Bivalve ^{14}C ages were corrected using the Marine04 calibration curve and ΔR 252 ± 93 ^{14}C years (Hughen et al., 2004). Terrestrial ^{14}C ages were corrected using the IntCal04 calibration curve (Reimer et al., 2004). All dates were calibrated using Calib 7.0.7 (Stuiver and Reimer, 1993).

2.5 ACKNOWLEDGEMENTS

This work was supported in part by funds from the Geological Society of America and the AAPG Grants-in-Aid John E. Kilkenny Memorial Grant. Acknowledgement is made to the Donors of the American Chemical Society Petroleum Research Fund for support of this research. Bivalve ^{14}C measurements were supported by grant JSPS-KAKENHI 26247085. We also thank the captain and crew of the M/V Danny C and JAB for help in collecting offshore data and Olivia Nicholson for assistance in lab work.

2.6 REFERENCES CITED

Bergman, K.M., and Snedden, J.W., eds., 1999, Isolated shallow marine sand bodies: Sequence stratigraphic analysis and sedimentologic interpretation: SEPM Special Publication No. 64, 362 p.

Covault, J.A., Normark, W.R., Romans, B.W., and Graham, S.A., 2007, Highstand fans in the California borderland: The overlooked deep-water depositional systems: Geology, v. 35, p. 783-786.

Dartnell, P., Finlayson, D. P., Conrad, J. E., Cochrane, G., and Johnson, S., 2010, Bathymetry and acoustic backscatter: Northern Santa Barbara Channel, Southern California: U.S. Geological survey open-file report 2009-1289.

Dartnell, P., Phillips, E. L., and Finlayson, D. P., 2015a, Backscatter -- offshore of Refugio Beach, California: California State Waters Map Series Data Catalog, U.S. Geological Survey.

Dartnell, P., Phillips, E. L., and Finlayson, D. P., 2015b, Bathymetry -- offshore of Refugio Beach, California: California State Waters Map Series Data Catalog, U.S. Geological Survey.

Dietze, E., Hartmann, K., Diekmann, B., IJmker, J., Lehmkuhl, F., Opitz, S., Stauch, G., Wünnemann, B., and Borchers, A., 2012, An end-member algorithm for deciphering modern detrital processes from lake sediments of Lake Donggi Cona, NE Tibetan Plateau, China: Sedimentary Geology, v. 243, p. 169-180.

Felix, M., Peakall, J. and McCaffrey, W.D., 2006, Relative importance of processes that govern the generation of particulate hyperpycnal flows: Journal of Sedimentary Research, v. 76, p. 382-387.

Gladstone, C., and Pritchard, D., 2010, Patterns of deposition from experimental turbidity currents with reversing buoyancy: Sedimentology, v. 57, no. 1, p. 53-84.

Gurrola, L.D., Keller, E.A., Chen, J.H., Owen, L.A., and Spencer, J.Q., 2014, Tectonic geomorphology of marine terraces : Santa Barbara fold belt, California: Geological Society of America Bulletin, v. 126, no. 1, p. 219-233.

Hansen, L.A.S., Callow, R.H.T., Kane, I.A., Gamberi, F., Rovere, M., Cronin, B.T., and Kneller, B.C., 2015, Genesis and character of thin-bedded turbidites associated with submarine channels: Marine and Petroleum Geology, v. 67, p. 852-879.

Hughen, K. A. et al., 2004, Marine04 marine radiocarbon age calibration, 0-26 ka BP: Radiocarbon, v. 46, p. 1059-1086.

Johnson et al., 2013, California State Waters Map Series – Offshore of Carpinteria, California: Scientific Investigations Map 3261, U.S. Geological Survey, 42 p., http://pubs.usgs.gov/sim/3261/.

Kneller, B., and Buckee, C., 2000, The structure and fluid mechanics of turbidity currents: a review of some recent studies and their geological implications: Sedimentology, v. 47, p. 62-94.

Lamb, M. P., Myrow, P. M., Lukens, C., Houck, K., and Strauss, J., 2008, Deposits from wave-influenced turbidity currents: Pennsylvanian Minturn Formation, Colorado, U.S.A: Journal of Sedimentary Research, v. 78, no. 7, p. 480-498.

Milliman, J. D., Lin, S. W., Kao, S. J., Liu, J. P., Liu, C. S., Chiu, J. K., and Lin, Y. C., 2007, Short-term changes in seafloor character due to flood-derived hyperpycnal discharge: Typhoon Mindulle, Taiwan, July 2004: Geology, v. 35, no. 9, p. 779.

Mulder, T., and Syvitski, J. P., 1995, Turbidity currents generated at river mouths during exceptional discharges to the world oceans: The Journal of Geology, p. 285-299.

Mulder, T., Syvitski, J.P.M., Migeon, S., Faugeres, J.C., Savoye, B., 2003, Marine hyperpycnal flows: initiation, behavior and related deposits. A review: Marine and Petroleum Geology, v. 20, p. 861-882.

Myrow, P.M., Fischer, W., and Goodge, J.W., 2002, Wave modified turbidites: combined-flow shoreline and shelf deposits, Cambrian, Central Transantarctic Mountains: Journal of Sedimentary Research, v. 72, p. 641-656.

Myrow, P.M., Lukens, C., Lamb, M.P., Houck, K., and Strauss, J., 2008, Dynamics of a transgressive prodeltaic system: Implications for geography and climate with a Pennsylvanian intracratonic basin: Journal of Sedimentary Research, v. 78, p. 512-528.

Normark, W. R., and Piper, D. J. W., 1991, Initiation processes and flow evolution of turbidity currents: Implications for the depositional record: Shoreline to Abyss: SEPM Special Publication, v. 46, p. 207-230.

Olariu, C., Steel, R. J., and Petter, A. L., 2010, Delta-front hyperpycnal bed geometry and implications for reservoir modeling: Cretaceous Panther Tongue Delta, Book Cliffs, Utah: AAPG Bulletin, v. 94, no. 6, p. 819-845.

Parsons, J.D., Bush, J.W.M., and Syvitski, J.P.M, 2001, Hyperpycnal plume formation from riverine outflow with small sediment concentrations: Sedimentology, v. 48, p. 465-478.

Peakall, J., and Sumner, E.J., 2015, Submarine channel flow processes and deposits: A process-product perspective: Geomorphology, v. 244, p. 95-120.

Plink-Bjorklund, P. and Steel, R.J., 2004, Initiation of turbidity currents: outcrop evidence for Eocene hyperpycnal-flow turbidites: Sedimentary Geology, v. 165, p. 29-52

Posamentier, H. W., and Allen, G. P., 1999, Siliciclastic sequence stratigraphy: Concepts and applications: Tulsa, Oklahoma, Society for Sedimentary Geology, SEPM concepts in sedimentology and paleontology no. 7, 205 p.

Pritchard, D., and Gladstone, C., 2009, Reversing buoyancy in turbidity currents: Developing a hypothesis for flow transformation and for deposit facies and architecture: Marine and Petroleum Geology, v. 26, no. 10, p. 1997-2010.

Reimer, P. J., et al., 2004, Intcal04 terrestrial radiocarbon age calibration, 0-26 cal kyr BP: Radiocarbon, v. 48, no. 3, p. 1029-1058.

Reynolds, L., and Simms, A. R., 2015, Late Quaternary relative sea level in Southern California and Monterey Bay: Quaternary Science Reviews, v. 126, p. 57-66.

Shanmugam, G., 1996, High-density turbidity currents: are they sandy debris flows?: Journal of Sedimentary Research, v. 66, p. 2-10.

Sommerfield, C.K., Lee, H.J., and Normark, W.R., 2009, Postglacial sedimentary record of the Southern California continental shelf and slope, Point Conception to Dana Point, *in* Lee, H.J., and Normark, W.R., eds., Earth Science in the Urban Ocean: The Southern California Continental Borderland: Geological Society of America, Special Paper 454, p. 89-115.

Sparks, R. S. J., Bonnecaze, R. T., Huppert, H. E., Lister, J. R., Hallworth, M. A., Mader, H., and Phillips, J., 1993, Sediment-laden gravity currents with reversing buoyancy: Earth and Planetary Science Letters, v. 114, no. 2, p. 243-257.

Sperazza, M., Moore, J. N., and Hendrix, M. S., 2004, High-resolution particle size analysis of naturally occurring very fine-grained sediment through laser diffractometry: Research methods papers: Journal of Sedimentary Research, v. 74, no. 5, p. 736-743.

Stevenson, C.J., and Peakall, J., 2010, Effects of topography on lofting gravity flows: Implications for the deposition of deep-water massive sands: Marine and Petroleum Geology, v. 27, p. 1366-1378.

Stow, D.A., and Johansson, M., 2000, Deep-water massive sands: nature, origin and hydrocarbon implications: Marine and Petroleum Geology, v. 17, p. 145-174.

Stuiver, M., and Reimer, J., 1993, Extended 14c database and revised calib 3.014 c age calibration program: Radiocarbon, v. 35, no. 1, p. 215-230.

Walker, G. P., and McBroome, L. A., 1983, Mount St. Helens 1980 and Mount Pelée 1902—flow or surge?: Geology, v. 11, no. 10, p. 571-574.

Warrick, J. A., and Mertes, L. A. K., 2009, Sediment yield from the tectonically active semiarid Western Transverse Ranges of California: Geological Society of America Bulletin, v. 121, no. 7-8, p. 1054-1070.

Warrick, J. A., Simms, A. R., Ritchie, A., Steel, E., Dartnell, P., Conrad, J. E., and Finlayson, D. P., 2013, Hyperpycnal plume-derived fans in the Santa Barbara Channel, California: Geophysical Research Letters, v. 40, no. 10, p. 2081-2086.

Wright, L., Yang, Z.-S., Bornhold, B., Keller, G., Prior, D., and Wiseman Jr, W., 1986, Hyperpycnal plumes and plume fronts over the Huanghe (Yellow River) delta front: Geo-Marine Letters, v. 6, no. 2, p. 97-105.

Wright, L.D., Friedrichs, C.T., Kim, S.C., Scully, M.E., 2001, Effects of ambient currents and waves on gravity-driven sediment transport on continental shelves: Marine Geology, v. 175, p. 25-45.

Yokoyama, Y., Miyairi, Y., Matsuzaki, H., and Tsunomori, F., 2007, Relations between acid dissolution time in the vacuum test tube and time required for graphitization for AMS target preparation: Nuclear Instruments and Methods in Physics Research B, v. 259, p. 330-334.

Zavala, C., Ponce, J. J., Arcuri, M., Drittanti, D., Freije, H., and Asensio, M., 2006, Ancient lacustrine hyperpycnites: A depositional model from a case study in the Rayoso Formation (Cretaceous) of west-central Argentina: Journal of Sedimentary Research, v. 76, no. 1, p. 41-59.

Zavala, C., and Arcuri, M., 2016, Intrabasinal and extrabasinal turbidites: Origin and distinctive characteristics: Sedimentary Geology, v. 337, p. 36-54.

CHAPTER 3

THE ROLE OF BUOYANCY REVERSAL IN TURBIDITE DEPOSITION AND SUBMARINE FAN GEOMETRY

3.1 INTRODUCTION

Ancient submarine fans serve as prolific hydrocarbon reservoirs and provide records of climatic and tectonic activity. Hence, the economic recovery of hydrocarbons and accurate interpretation of the geologic record rely on the understanding of factors that control fan morphology and architecture. Basin configuration, sediment supply, and antecedent topography are commonly cited factors in controlling the geometry of submarine fan lobes (e.g., Normark and Piper, 1991; Reading and Richards, 1994; Fernandez et al., 2014). However, gravity current characteristics such as sediment concentration and the relationship between current density and ambient water density may also significantly affect the morphology of a submarine fan.

A version of this chapter is published as a paper in Geology under the citation:
Steel, E., Buttles, J., Simms, A., Mohrig, D., and Meiburg, E., 2017, The role of buoyancy reversal in turbidite deposition and submarine fan geometry: Geology, v. 45, no. 1, p. 35-38.

Turbidity currents can be classified as ground-hugging currents or lofting currents (Fig. 5) (Meiburg and Kneller, 2010). Lofting, or buoyancy reversal, occurs when an initially ground-hugging turbulent underflow becomes less dense than the surrounding fluid and rises from the basin floor. Despite an abundance of fluid dynamics studies describing lofting, few geologists have investigated its impact on turbidite systems (e.g., Hurzeler et al., 1995; Huppert, 1998; Pritchard and Gladstone, 2009; Zavala and Arcuri, 2016; Steel et al., 2016). Lofting significantly alters the spreading geometry of submarine currents and the extent of their deposits, and should no longer be overlooked in the context of submarine deposition. The purpose of this paper is to use a three dimensional experimental model to examine how lofting, basin-floor gradient, and sediment concentration affect turbidity currents and submarine fan geometry.

3.2 BACKGROUND

The relationship between ambient water density, interstitial water density, and bulk current density plays a critical role in the evolution of a turbidity current. In the case of a current with relatively light interstitial fluid, bulk current density exceeds ambient water density due to suspended sediment, and a dense underflow travels across the basin floor. The current remains ground-hugging as long as bulk density exceeds the surrounding water density (Sparks et al., 1993). As the current progresses, bulk current density may decrease by settling of sediment, or may increase by entrainment of sediment or ambient water. If sediment settles from suspension more rapidly than replacement of interstitial fluid with ambient water, bulk flow density will lighten until it reaches a point of reversing buoyancy. At this point, a buoyant plume will rise from the basin floor (Sparks et al., 1993; Sequeiros et al., 2009). These

conditions occur in nature when fresh, sediment-laden rivers meet ocean basins or when turbidity currents initiated in warm, shallow-water environments travel into deeper and colder water (Sparks et al., 1993). Previous studies have focused on understanding two-dimensional aspects of buoyancy reversal, such as spreading rate of flow fronts (Hurzeler et al., 1995), and lift-off points (Sparks et al., 1993; Hogg et al., 1999; Sequeiros et al., 2009; Stevenson and Peakall, 2010), but few studies have explored the effects of buoyancy reversal on lateral spreading of flows and its impact on three-dimensional deposit geometry (Zavala et al., 2011).

Ground-hugging currents spread as a logarithmic function of time, and the rate of lateral spreading decreases as slope angle increases (Alavian, 1986; Choi and Garcia, 2001). Buoyancy reversal is likely to alter the spreading rates of currents, and may prevent them from reaching their predicted maximum width (Zavala et al., 2011). Furthermore, the decrease in velocity at a slope-break can lead to rapid sedimentation, which may enhance or initiate lofting. Therefore, a discussion of lofting dynamics is incomplete without an understanding of the links between lofting and basin geometry.

3.3 EXPERIMENTAL SETUP

In this study we conducted 12 experimental turbidity currents, 9 of which lofted (Table 2). Experiments were performed on a 2.4 m long by 1.8 m wide tilted ramp inside the Experimental Deep Water Basin at the University of Texas. The basin is 4 m wide, 8 m long, and 2 m deep (Fig. 6). Video cameras recorded currents from inside the tank (underwater), from outside the tank through an observation window, and from a raised platform. Overhead photos were taken every 10 seconds during runs. Density contrasts between interstitial current water and ambient tank water were achieved by heating the interstitial water to 31 °C and

keeping ambient water at 23 °C. Plastic sediment with a d_{50} grain size of 206 μm and density of 1.15 g/cm^3 was mixed with the warm interstitial water and piped onto the submerged ramp. Currents were run across three ramp geometries: 5° slope to flat, constant 5° slope, and constant 8° slope. On each ramp geometry, currents with warm interstitial water were conducted with 1.5%, 2%, and 3% sediment concentration. Currents with the same ambient and interstitial water densities were conducted with 1.6% sediment concentration in order to allow comparisons between ground-hugging and lofting currents of similar sediment concentrations as well as those of the same bulk densities (Table 2). Bulk inlet discharge was 278.1 cm^3/s and currents were run for 12 min. After the completion of each run, the deposit was scanned using a high-resolution underwater laser scanner (Fig. 7). The water was drained and the tank cleaned before running subsequent currents.

Lateral flow lofting in each run was identified using a combination of overhead photos and side videos. The maximum flow width as a function of time was measured from a sequence of overhead photos (Figs. 8 and 9). Lofting was defined as the point where four successive width measurements were repeated. There was no point where the curve became constant for ground-hugging currents because they grew wider than the ramp.

3.4 RESULTS

All currents with light interstitial fluid were initially ground-hugging (bed-attached) on all ramp geometries (Fig. 10a). Lofting initiated along the current fronts and lateral margins while the interior remained bed-attached (Fig. 10b). Lofting along the margins induced an inward flow of ambient fluid, which first reduced the current spreading rate and eventually stopped lateral spreading altogether (Fig. 10c). This is in contrast to ground-hugging currents

which continued to spread and flow over ramp edges (Fig. 5b). During lofting, the rising plume maintained both forward and upward momentum, carrying with it suspended sediment. Gradually, the plume spread along the free water surface in all directions.

A comparison of the maximum half-width through time for lofting and ground-hugging currents clearly shows the width-limiting nature of lofting (Fig. 11a; 8; 9). Following the methods of Choi and Garcia (2001), half-width lengths and times were normalized by characteristic plume length, l_p, and time, t_p, scales, which approximate the length and time scales at which a density current transitions from jet (momentum) dominated to buoyancy (plume) dominated flow. The ground-hugging currents spread laterally through time as predicted by Choi and Garcia (2001) (Run H; Fig. 11a). In contrast, lofting currents spread laterally with time until reaching a constant half-width that was then maintained for the remainder of the flow (Fig. 11a). The maximum half-width length and time to lofting increased with higher initial suspended sediment concentration (Fig. 11a).

The shape of deposits from lofting currents is distinct from those formed by currents that remained ground-hugging; lofting currents formed narrower deposits than ground-hugging currents of similar or greater sediment concentration in all cases (Fig. 11b; 12).Once the current lofted, a thin layer of sediment settled from the plume over a wide area, resulting in an initially narrow deposit that broadens in its most distal reaches. The ground-hugging current on the 8° ramp (Run L) had a lower spreading rate than the ground-hugging current on the 5° ramp (Run H) and therefore a narrower current and deposit. This confirms predictions that steeper gradients result in lower rates of lateral spreading in ground-hugging flows (Alavian, 1986).

Lofting currents with higher sediment concentrations began to loft later, and were therefore wider and deposited wider lobes (Fig. 11). Additionally, flows on the 8° ramp had a

higher frontal velocity, underwent buoyancy reversal farther basinward, and deposited wider lobes than those traveling across the 5° and 5°-to-flat ramps.

3.5 DISCUSSION

3.5.1. DYNAMICS OF BUOYANCY REVERSAL

Despite the importance of predicting the geometry of sandbodies, particularly for the economic extraction of hydrocarbons, little is known about the three-dimensionality of lofted-current deposits. Observing buoyancy reversal in a 3-dimensional setting allows the effects of light interstitial fluid on lateral spreading of currents to be seen, as well as the resulting changes in length-to-width ratios of their deposits.

The flow margins of currents with light interstitial fluid are more dilute than the flow center, and therefore have a lower contrast between the flow and ambient water densities. Because of this density gradient, as sediment settles from suspension and bulk current density decreases, current margins reach a point of neutral buoyancy before the current interior. Once current margins become buoyant, lateral spreading of the current ceases and vortices form, pulling fluid from the edges of the current inwards and upwards (Fig. 10). In addition to the rise of the current margins, the current head expands significantly as forward velocity of the current decreases. The vertical expansion at the head of a ground-hugging turbidity current is due to shear instabilities causing Kelvin-Helmholtz billows and entrainment of ambient water (Britter and Simpson, 1978). However, the expansion at the head of the currents with light interstitial fluid is likely to result from loss of sediment, causing decreased current density and rising of a buoyant plume. If significant entrainment of ambient water occurred, interstitial water would be replaced and currents would continue as ground-hugging rather than lofting.

When the current lifts off from the basin floor, any sediment left in suspension rises with it and is distributed over a broad area. Depending on local conditions, the rising plume may be carried away by cross-currents or may deposit a thin layer of fine sediment on top of the narrow lobe emplaced by the bed-attached portion of the current.

3.5.2. EFFECTS OF SEDIMENT CONCENTRATION AND RAMP GRADIENT ON DEPOSIT GEOMETRY

A strong correlation is observed between current width and deposit width, and factors that affect lateral spreading of currents will similarly affect deposit geometry (Fig. 11b). Currents with higher sediment concentrations produced wider deposits and began to loft farther basinward than flows with lower sediment concentrations. The higher sediment concentration results in higher bulk current density, and therefore a greater contrast between the initial current and ambient water density. For the current to reach a point of neutral or positive buoyancy, a current with high suspended sediment concentration must deposit more sediment and travel farther across the basin floor before lofting. Thus the current will have more time to spread laterally before lofting, resulting in an overall wider flow and deposit. In natural systems, sediment grain size will also play a role in the lofting distance and currents with high concentrations of mud-sized sediment may loft much later or not at all due to hindered sediment settling (Zavala and Arcuri, 2016).

Lofting flows traveling across steeper ramp gradients result in farther basinward lofting points and wider deposits. This behavior occurs because currents moving across steeper gradients travel a greater distance basinward and spread farther laterally in a comparable amount of time preceding lofting (Fig. 9). However, because ground-hugging currents have lower rates of lateral spreading on steeper ramps (Alavian, 1986), and because lofting will not

limit their maximum width, ground-hugging currents on steep ramps should produce narrower deposits than ground-hugging currents on shallow ramps, as seen in Run L on the 8° ramp compared to Run H on the 5° ramp (Table 2; Fig. 11b).

In all lofting cases, the 5°-to-flat deposits were wider than the 5° ramp deposits. The effect of a break in slope on deposit width is likely a reflection of Taylor-Görtler vortices (Taylor, 1921; Panton, 1984). When a current travels over a concave surface, and is relatively thick compared to the radius of curvature of the surface, centrifugal force begins to act on the fluid and pushes the current down into the basin floor (Fig. 13). Centrifugal force acts more strongly on faster moving fluid particles, meaning that it will be greater on particles in the central portion of the current than on the slower-moving particles near the base or top of the current. This downward-directed centrifugal force forms Taylor-Görtler vortices, which effectively cause the current to spread laterally as an upper part of the current is pushed down and lower-flow particles are pushed out (Taylor, 1921; Panton, 1984). The original goal of designing a ramp with a slope-break was to explore its effects on the location of the lofting point. However, although not measured directly, the widening effects of Taylor- Görtler vortices likely play a more significant role in flow dynamics of these experimental currents. The effects of Taylor-Görtler vortices may be enhanced by a decrease in velocity at the slope break causing current competency to decrease and promoting sediment deposition. The Taylor-Görtler vortices do not appear to have such a strong effect on ground-hugging flows, perhaps because all flows overran the platform boundary and never achieved a true 'maximum width.'

Both Taylor-Görtler vortices (5°-to-flat ramp) and a basinward shift in the lofting point (8° ramp) appear to cause wider currents, making a comparison between the two ramp geometries complex. Other factors beyond the scope of this study, such as flow inertia and

grain-size distribution, may also affect lofting and current width. However, this study shows that the primary width-limiting process is buoyancy reversal, and that within lofting currents the location of the lift-off point, which adjusts due to changes in sediment concentration or ramp geometry, controls the ultimate width of the deposit.

3.5.3. COMPARISON TO ANCIENT AND MODERN DEPOSITS

Based on this study and previous work on lofting turbidity currents, lofted deposits are expected to have narrow lobes with abrupt frontal and lateral terminations (Gladstone and Pritchard, 2010). Previous studies show that the internal architecture of lofted deposits is expected to consist of a fines-depleted basal layer, deposited by the bed-attached flow, and a fines-enriched mantle, deposited by the lofted plume (Walker and McBroome, 1983). The fines-enriched mantle may not be present if the plume is carried far from its point of lift-off. The basal layer is rapidly deposited by the bed-attached portion of the current once buoyancy reversal begins, resulting in a bed that may more closely resemble a sandy debrite (Shanmugam, 1996; Amy et al., 2005) rather than the typical Bouma-type features associated with ground-hugging turbidity currents (Steel et al., 2016). Lofting currents frequently contain river-derived plant fragments that settle from the lofted plume more slowly than clastic material, resulting in 'lofted rhythmites' comprised of sand-silt couplets bounded by thin layers of plant debris (Zavala et al., 2012).

Evidence for turbidites with reversing buoyancy can be found in both modern and ancient turbidite successions around the world. The shelf of the Santa Barbara Channel in southern California contains at least six Holocene fans built by hyperpycnal currents (Warrick et al., 2013). The lobes within these fans are narrow, contain distinct margins, and are composed of well-sorted, structureless sand, indicating that the hyperpycnal currents were

modified by buoyancy reversal (Steel et al., 2016). In another case, the Mid-Jurassic Lajas Formation of the Neuquén Basin in western Argentina, which is comprised of continental shelf deposits, contains outer-shelf, river-derived turbidites with partial Bouma sequences, as well as occurrences of enigmatic beds that are comprised of well-sorted, medium-grained sandstones that contain parallel laminations (Paim et al., 2010; Ron Steel, personal commun., 2016). Individual beds of this type on the slope are on the order of 40 m wide, and are better sorted and significantly narrower than the majority of the turbidites in the lower slope and basin floor succession (Shin, 2015). Their well-sorted nature and narrow geometry suggest that these unusual beds may be another example of deposition from river-derived turbidity currents with reversing buoyancy.

3.6 CONCLUSIONS

Buoyancy reversal is an overlooked process in turbidites. The distinction between ground-hugging and lofting turbidity currents is not pedantic, as it affects the length-to-width ratios of individual sandbodies and the degree of sediment sorting within beds. Ocean stratification leads to conditions in which the fluid within a turbidity current may be less dense than the surrounding ambient water, meaning that buoyancy reversal could play a role in the evolution of the current if suspended sediment settles relatively quickly. Shelf-edge deltaic systems feeding fresh-water hyperpycnal currents directly onto the continental slope create ideal conditions for currents with reversing buoyancy. Other factors such as basin floor gradient and sediment concentration can alter submarine fan geometry, and disentangling various flow characteristics from the ultimate geometry of turbidites is a difficult task. However, this study provides data intended to advance this understanding of how factors such as sediment concentration, basin configuration, and fluid density control deposit morphology.

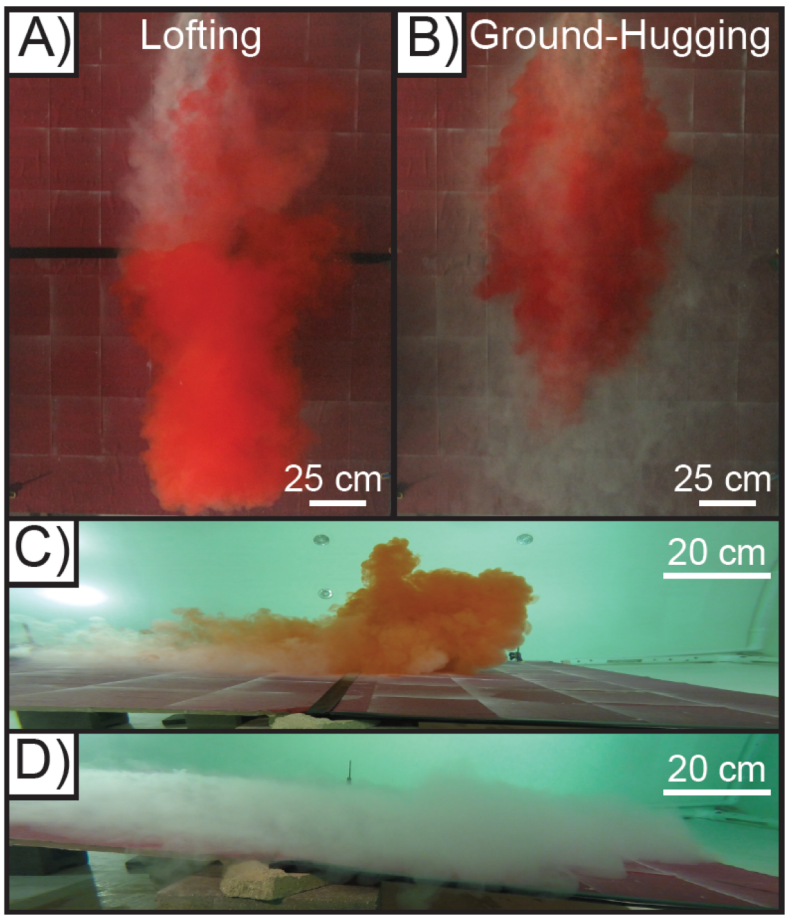

Figure 5. A comparison of a lofting turbidity current (Run G) and a ground-hugging turbidity current (Run H) with similar initial sediment concentrations, discharge and bottom slopes. (A) and (B) show overhead photos taken during experiments G and H, respectively. Red dye was injected into the currents to enhance visibility. The current in (A) contained light interstitial fluid and a buoyant plume rose along the head and the edges -limiting both the longitudinal and lateral spreading. The current in (B) remained ground-hugging and was wider than the lofting current. Side views of the lofting (E) and ground-hugging (F) currents taken from a camera within the tank show the contrasts between the width and heights of lofting vs ground-hugging currents.

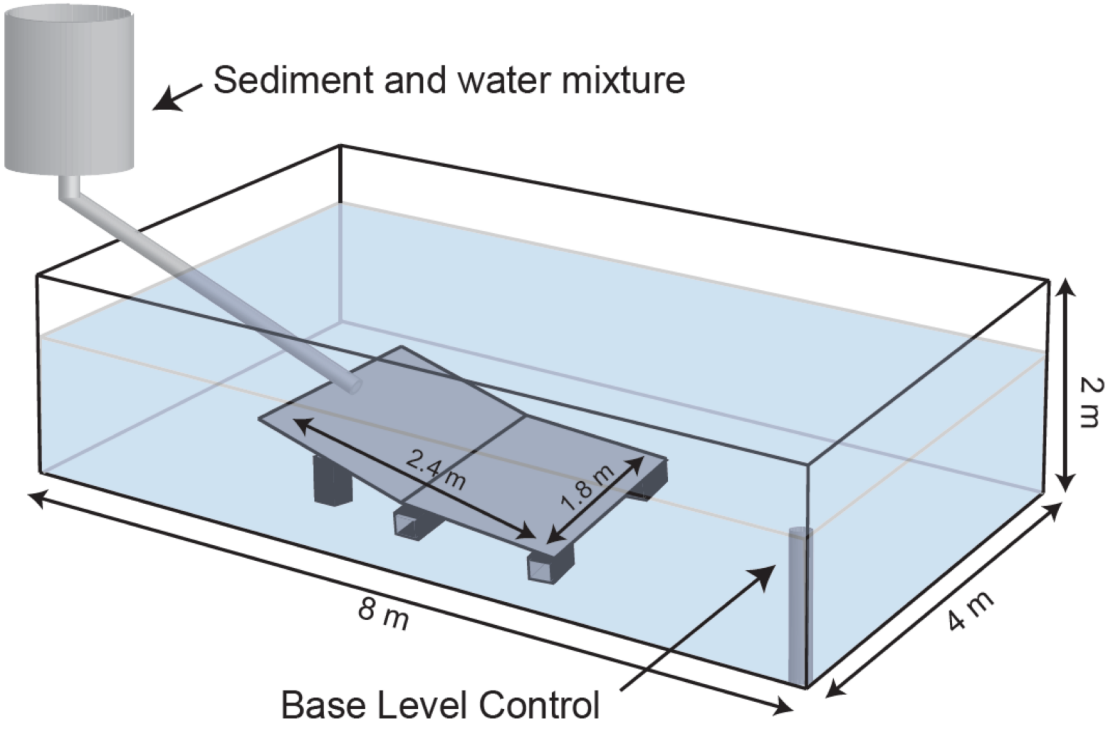

Figure 6. Diagram of the basin used for these experiments. Sediment and water were mixed in a 400-liter tank and piped into the large basin. Water in this tank was heated to 31° for runs with light interstitial fluid. Water in the basin was 23° for all experiments. A pulse of red dye was injected into the pipe in order to enhance visibility. The platform inside the tank was made of Plexiglas and covered in red sandpaper. Windows on two sides of the tank and a platform around two edges of the tank allowed for the experiments to be viewed from many angles. One video camera filmed the flows from inside the tank, one video camera filmed through a window on the long side of the tank, and one video camera filmed from the raised platform. An overhead camera took photos every 10 seconds during each run.

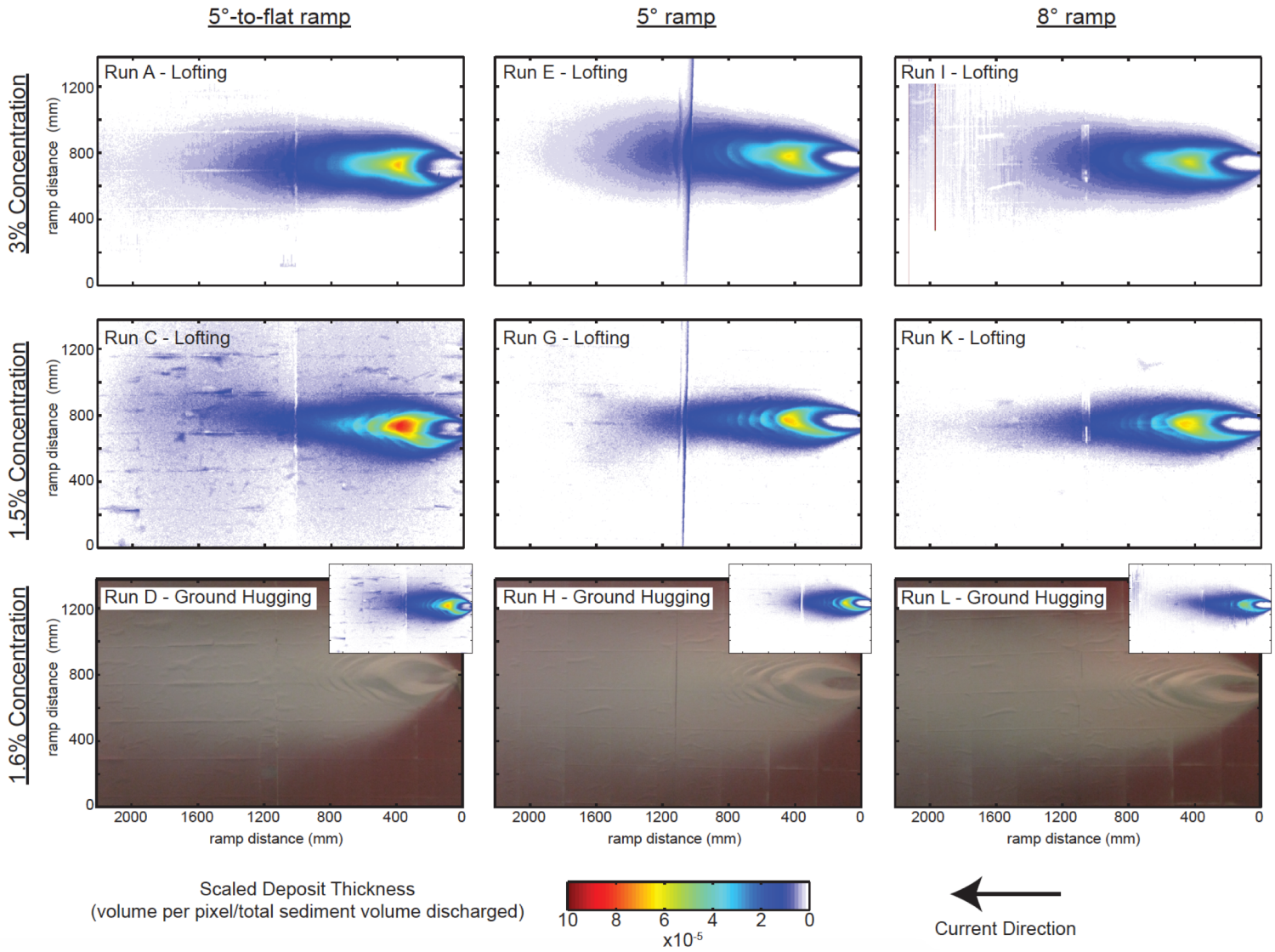
5°-to-flat ramp
5° ramp
8° ramp
3% Concentration
1.5% Concentration
1.6% Concentration
Run A - Lofting
Run E - Lofting
Run I - Lofting
Run C - Lofting
Run G - Lofting
Run K - Lofting
Run D - Ground Hugging
Run H - Ground Hugging
Run L - Ground Hugging
ramp distance (mm)
1200
800
400
0
2000
1600
1200
800
400
0
Scaled Deposit Thickness
(volume per pixel/total sediment volume discharged)
10
8
6
4
2
0
x10-5
Current Direction

Figure 7. (Previous page) Scaled deposit thickness maps and overhead photos from currents with 3%, 1.5% and 1.6% sediment concentration on all ramp geometries. The deposit surface was mapped after each run using a high-resolution underwater laser scanner and then subtracted from a laser scan of the bare ramp surface to produce deposit thickness. To make the deposits from different flow conditions comparable, deposit volume at each pixel was scaled by the total sediment volume discharged for each run (volume per pixel/total sediment volume discharged). Lofted-current deposit widths were measured from cross-sectional laser profiles as the distance between inflection points on each side of the deposit. Ground-hugging deposit margins thinned below the laser resolution (runs D, H, L insets) but were visually apparent (runs D, H, L photos). Therefore, ground-hugging deposit widths were determined using overhead photos and measured as the width at which the light colored sediment could no longer be identified on top of the dark colored ramp. Currents travelled from right to left across the platform. A vertical line running across the ramp at approximately 1000 mm is an artifact of the ramp set-up and marks the break between plexiglass boards. Poor scans of the deposit from run I resulted in a striped appearance in several locations. These are errors associated with water clarity and should be disregarded.

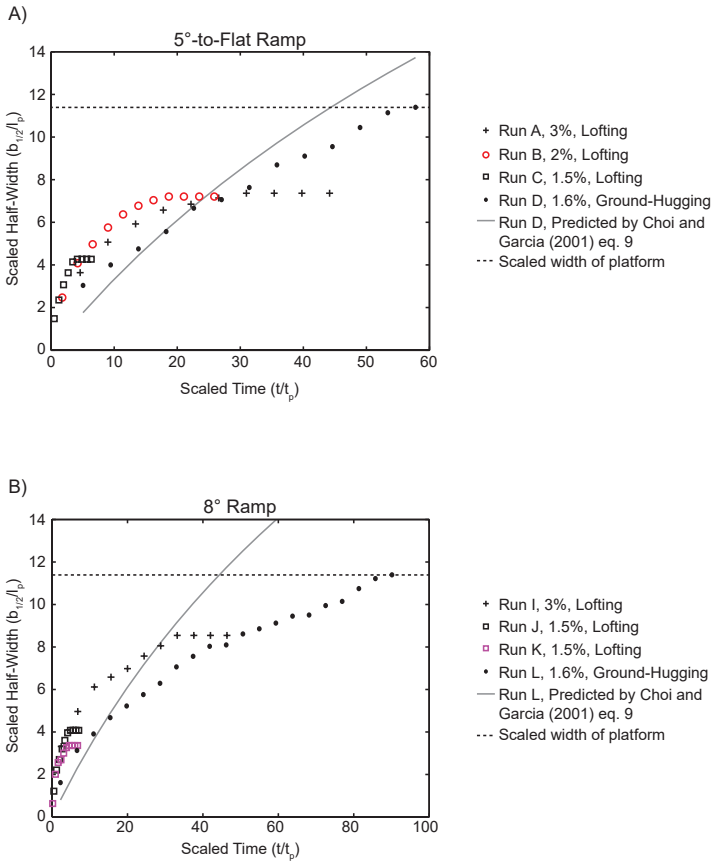

Figure 8. Comparison of scaled maximum current half-width with scaled time for runs on the 5°-to-flat ramp (A) and 8° ramp (B). Half-width and time are normalized by characteristic length and time scales, l_p and t_p, using Equations 3 and 4 of Choi and Garcia (2001). The solid line is the empirically predicted fit for the lateral spreading of the ground-hugging current (black dots) using Equation 9 of Choi and Garcia (2001). The dashed black line is the scaled width of the platform, which ground-hugging currents exceeded. The ground-hugging current in (B) does not match the predicted spreading rate as well as in (A) or in Fig. 11A. This is most likely because the predicted spreading calculation is insensitive to slope, which appears to play a role in spreading rates. Additionally, the current front of run L reached the edge of the platform before the current edges reached the sides of the platform at $t/t_p = 41.8$. At this point there is a change in the spreading rate, and it may have altered flow dynamics. Despite these complications, both (A) and (B) show that current half-width remains constant beyond the point of lofting, in contrast to ground-hugging flows which continue to spread until they overflow the platform boundary.

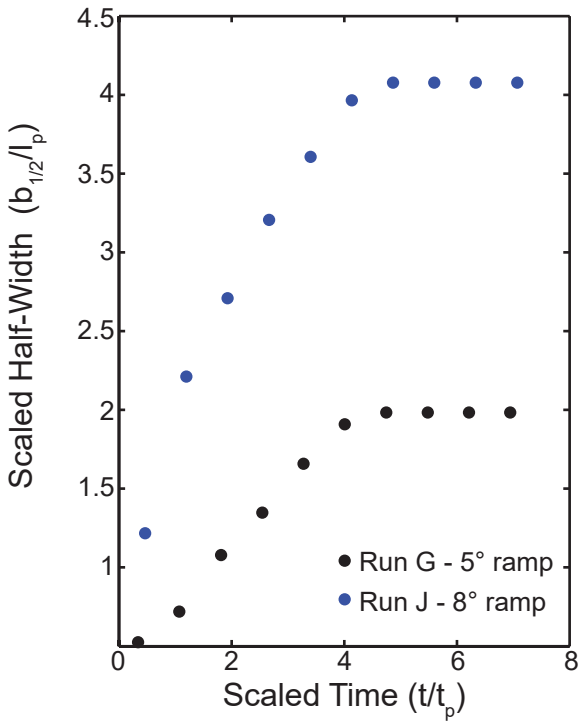

Figure 9. Spreading rate of runs G and J. Both of these flows had 1.5% sediment concentration, but were flowing across 5° and 8° ramps, respectively. Run J, which flowed across the steeper ramp, was travelling at a faster velocity and spread farther both laterally and basinward before lofting. Maximum half-width and time are normalized by l_p and t_p, using equations 3 and 4 of Choi and Garcia (2001).

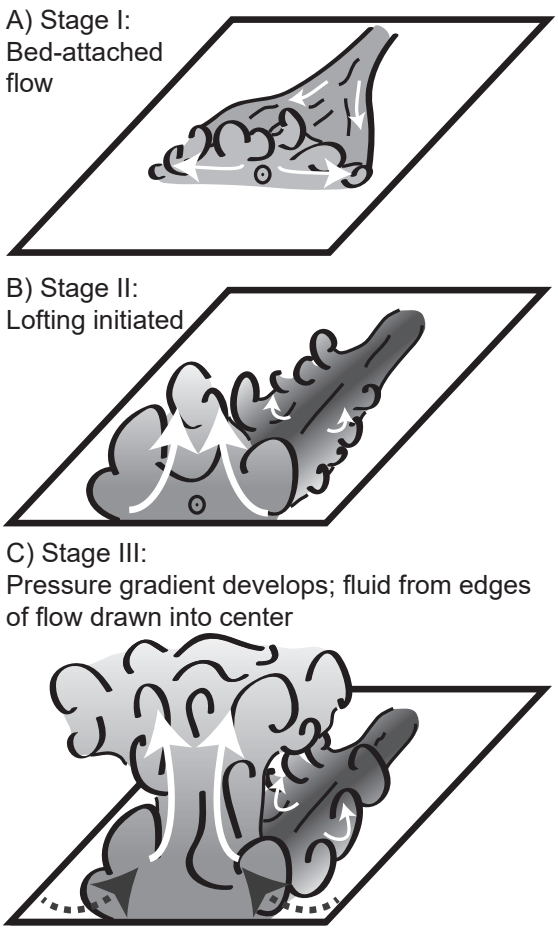

Figure 10. Schematic diagram of the lofting process. A) In stage 1, the current is ground-hugging and spreads both laterally and longitudinally. B) As sediment is deposited from the current, bulk density decreases and the current becomes buoyant and lofts at the front and lateral margins. C) A low pressure zone develops below the lofting portions of the current, creating pressure gradients that slow and then stop longitudinal and lateral spreading. Sediment that remains in suspension during lofting settles from the plume over a broad area.

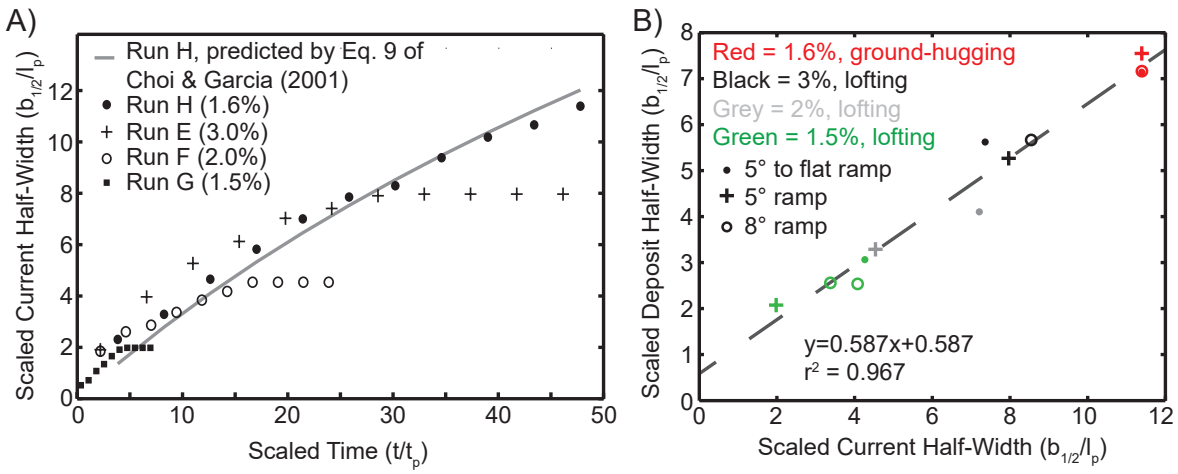

Figure 11. A) Comparison of scaled maximum current half-width with scaled time for runs on the 5° ramp. Half-width and time are normalized by characteristic length and time scales l_p and t_p, using Equations 3 and 4 of Choi and Garcia (2001). The solid line is the empirically predicted fit for the lateral spreading of a ground-hugging current (black dots) using the methods of Choi and Garcia (2001). Lofting currents spread until they begin to loft, at which point they maintain a constant width. Currents with higher sediment concentrations loft later, and therefore are wider. B) Comparison of current half-width and deposit half-width. There is a strong linear relationship between current half-width and deposit half-width. Despite having a low sediment concentration, ground-hugging flows (red) are the widest and produce the widest deposits. Current half-widths were measured using overhead photos taken every 10 seconds. Deposit half-widths were measured using laser scans for lofting flows and overhead photos for ground-hugging flows because deposits were below the resolution of the laser scanner.

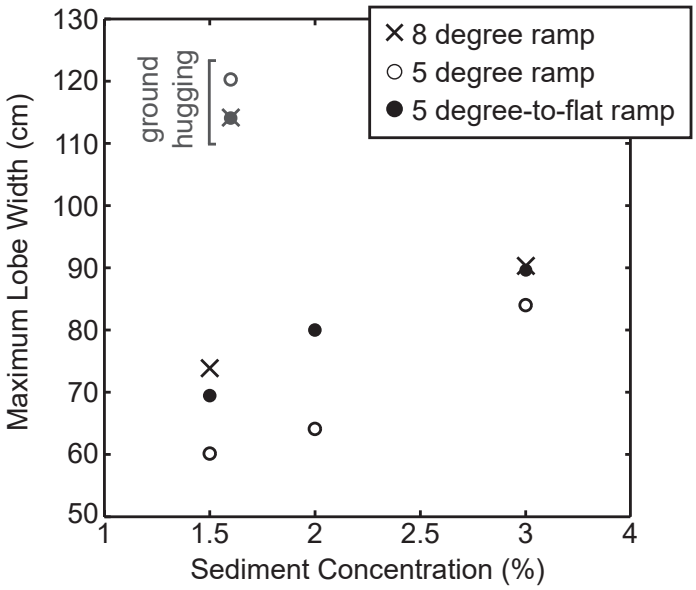

Figure 12. Plot of sediment concentration versus maximum lobe width. In all cases, ground-hugging turbidity currents (gray) deposited wider lobes than lofting currents (black). Currents that lofted farther basinward, i.e., currents with higher sediment concentrations or currents on the 8° ramp, deposited wider sediment lobes. The break in slope on the 5°-to-flat ramp increased the maximum deposit width in all lofting cases. Maximum lofted-current deposit width measurements were taken within a distance of 1 m from the inlet to exclude the deposit associated with the lofted plume. Lofted-current deposit widths were measured from cross-sectional laser profiles as the distance between inflection points on each side of the deposit. Ground-hugging deposit margins thinned below the laser resolution but were visually apparent (Fig. 7). Therefore, ground-hugging deposit widths were determined using overhead photos and measured as the width at which the light colored sediment could no longer be identified on top of the dark colored ramp.

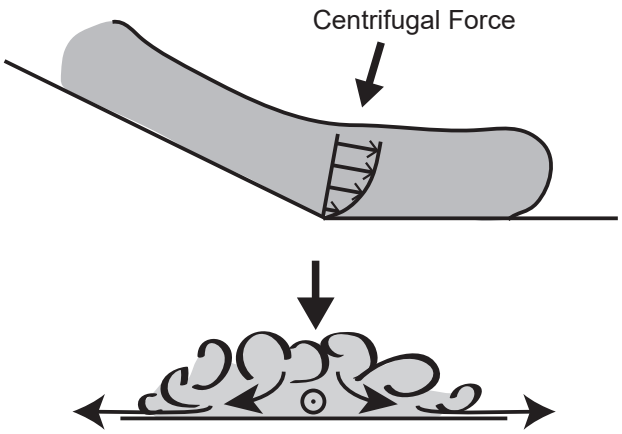

Figure 13. When a current travels over a concave surface, centrifugal force begins to push downwards on the current. Due to the velocity gradient within turbidity currents, centrifugal force acts more strongly on central portions of the current, resulting in widening of the current as lower material is displaced outward. The vortices that develop, known as Taylor-Görtler vortices, are likely responsible for widening of currents travelling over the 5°-to-flat ramp geometry. This widening of the currents resulted in the deposition of wider experimental deposits.

TABLE 2. EXPERIMENTAL CONDITIONS

Run	Interstitial water temperature (°C)	Ambient water temperature (°C)	Interstitial water denstiy (kg/m^3)	Ambient water density (kg/m^3)	Sediment concentration (%)	Bulk flow density (kg/m^3)	Ramp geometry
A	31	23	995.3	997.5	3.0	1000.0	5° to Flat
B	31	23	995.3	997.5	2.0	998.4	5° to Flat
C	31	23	995.3	997.5	1.5	997.7	5° to Flat
D	23	23	997.5	997.5	1.6	1000.0	5° to Flat
E	31	23	995.3	997.5	3.0	1000.0	5°
F	31	23	995.3	997.5	2.0	998.4	5°
G	31	23	995.3	997.5	1.5	997.7	5°
H	23	23	997.5	997.5	1.6	1000.0	5°
I	31	23	995.3	997.5	3.0	1000.0	8°
J	31	23	995.3	997.5	1.5	997.7	8°
K	31	23	995.3	997.5	1.5	997.7	8°
L	23	23	997.5	997.5	1.6	1000.0	8°

Note: All experiments were conducted with plastic sediment with a density of 1150 kg/m^3 and median grain size of 206 μm.

3.7 ACKNOWLDEGEMENTS

Acknowledgment is made to the Donors of the American Chemical Society Petroleum Research Fund for support of this research. This work was also supported in part by a Geological Society of America Graduate Student Research Grant and the UT-CSU RoiMAR Industry Consortium.

3.8 REFERENCES CITED

Alavian, V., 1986, Behavior of density currents on an incline: Journal of Hydraulic Engineering, v. 112, p. 27-42.

Amy, L.A., Talling, P.J., Peakall, J., Wynn, R.B., and Arzola Thynne, R.G., 2005, Bed geometry used to test recognition criteria of turbidites and (sandy) debrites: Sedimentary Geology, v. 179, p. 163–174, doi:10.1016/j.sedgeo.2005.04.007.

Britter, R.E., and Simpson, J.E., 1978, Experiments on the dynamics of a gravity current head: Journal of Fluid Mechanics, v. 88, p. 223–240, doi:10.1017/S0022112078002074.

Choi, S.U., and Garcia, M.H., 2001, Spreading of gravity plumes on an incline: Coastal Engineering Journal, v. 43, p. 221–237, doi:10.1142/S0578563401000359.

Fernandez, R.L., Cantelli, A., Pirmez, C., Sequeiros, O., and Parker, G., 2014, Growth patterns of subaqueous depositional channel lobe systems developed over a basement with a downdip break in slope: Laboratory experiments: Journal of Sedimentary Research, v. 84, p. 168–182, doi:10.2110/jsr.2014.10.

Gladstone, C., and Pritchard, D., 2010, Patterns of deposition from experimental turbidity currents with reversing buoyancy: Sedimentology, v. 57, p. 53–84, doi:10.1111/j.1365-3091.2009.01087.x.

Hogg, A.J., Huppert, H.E., and Hallworth, M.A., 1999, Reversing buoyancy of particle-driven gravity currents: Physics of Fluids, v. 11, p. 2891, doi:10.1063/1.870147.

Huppert, H.E., 1998, Quantitative modelling of granular suspension flows: Philosophical Transactions: Mathematical: Physical and Engineering Sciences, v. 356, p. 2471–2496, doi:10.1098/rsta.1998.0282.

Hurzeler, B.E., Ivey, G.N., and Imberger, J., 1995, Spreading model for a turbidity current with reversing buoyancy from a constant-volume release: Marine & Freshwater Research, v. 46, p. 393–408.

Meiburg, E., and Kneller, B., 2010, Turbidity currents and their deposits: Annual Review of Fluid Mechanics, v. 42, p. 135–156, doi:10.1146/annurev-fluid-121108-145618.

Normark, W.R., and Piper, D.J.W., 1991, Initiation processes and flow evolution of turbidity currents: Implications for the depositional record: Shoreline to Abyss: SEPM Special Publication, v. 46, p. 207–230.

Paim, P.S.G., Lavina, E.L.C., Faccini, U.F., Silveira, A.S., Leanza, H., and d'Avila, R.S.F., 2010, Fluvial-derived turbidites in the Los Molles formation (Jurassic of the Neuquén basin): Initiation, transport, and deposition, in Slatt, R.M., and Zavala, C., eds., Sediment transfer from shelf to deep water – revisiting the delivery system: AAPG Studies in Geology 61, p. 1–22.

Panton, R.L., 1984, Incompressible Flow: New York, John Wiley & Sons, 780 p.

Pritchard, D., and Gladstone, C., 2009, Reversing buoyancy in turbidity currents: Developing a hypothesis for flow transformation and for deposit facies and architecture: Marine and Petroleum Geology, v. 26, p. 1997–2010, doi:10.1016/j.marpetgeo.2009.02.010.

Reading, H.G., and Richards, M., 1994, Turbidite systems in deep-water basin margins classified by grain size and feeder system: AAPG Bulletin, v. 78, no. 5, p. 792-822

Sequeiros, O.E., Cantelli, A., Viparelli, E., White, J.D.L., Garcia, M.H., and Parker, G., 2009, Modeling turbidity currents with nonuniform sediment and reverse buoyancy: Water Resources Research, v. 45, W06408, doi:10.1029/2008WR007422.

Shanmugam, G., 1996, High-density turbidity currents: Are they sandy debris flows?: Journal of Sedimentary Research, v. 66, p. 2–10, doi:10.1306/D426828E-2B26-11D7-8648000102C1865D.

Shin, M., 2015, Architecture of coarse grained (conglomeratic) deep water lobes at the base of a sandstone dominated fan, Jurassic Los Molles Formation, Neuquen Basin, Argentina [M.S. Thesis]: University of Texas at Austin, 116 p.

Sparks, R.S.J., Bonnecaze, R.T., Huppert, H.E., Lister, J.R., Hallworth, M.A., Mader, H., and Phillips, J., 1993, Sediment-laden gravity currents with reversing buoyancy: Earth and Planetary Science Letters, v. 114, p. 243–257, doi:10.1016/0012-821X(93)90028-8.

Steel, R.J., Personal Communication, 2016.

Steel, E., Simms, A.R., Warrick, J., and Yokoyama, Y., 2016, Highstand shelf fans: The role of buoyancy reversal in the deposition of a new type of shelf sand body: Geological Society of America Bulletin, v. 128, no. 11-12, p. 1717-1724. doi:10.1130/B31438.1.

Stevenson, C.J., and Peakall, J., 2010, Effects of topography on lofting gravity flows: Implications for the deposition of deep-water massive sands: Marine and Petroleum Geology, v. 27, p. 1366-1378, doi:10.1016/j.marpetgeo.2010.03.010

Taylor, G.I., 1921, Experiments with rotating fluids: Proceedings of the Royal Society of London. Series A, Containing Papers of a Mathematical and Physical Character, v. 100, p. 114–121, doi:10.1098/rspa.1921.0075.

Walker, G.P., and McBroome, L.A., 1983, Mount St. Helens 1980 and Mount Pelée 1902—flow or surge?: Geology, v. 11, p. 571–574, doi:10.1130/0091-7613(1983)11<571:MSHAMP>2.0.CO;2.

Warrick, J.A., Simms, A.R., Ritchie, A., Steel, E., Dartnell, P., Conrad, J.E., and Finlayson, D.P., 2013, Hyperpycnal plume-derived fans in the Santa Barbara Channel, California: Geophysical Research Letters, v. 40, p. 2081–2086, doi:10.1002/grl.50488.

Zavala, C., Arcuri, M., Di Meglio, M., Diaz, H.G., and Contreras, C., 2011, A genetic facies tract for the analysis of sustained hyperpycnal flow deposits: in Slatt, R.M., and Zavala, C., eds., Sediment transfer from shelf to deep water – revisiting the delivery system: AAPG Studies in Geology 61, p. 31-51

Zavala, C., and Arcuri, M., 2016, Intrabasinal and extrabasinal turbidites: Origin and distinctive characteristics: Sedimentary Geology, v. 337, p. 36–54, doi:10.1016/j.sedgeo.2016.03.008.

CHAPTER 4

HYPERPYCNAL DELIVERY OF SAND TO THE CONTINENTAL SHELF: AN EXAMPLE FROM THE JURASSIC LAJAS FORMATION, NEUQUÉN BASIN, ARGENTINA

4.1 INTRODUCTION

Although deepwater deposits dominate the literature regarding sediment gravity flows, gravity-driven processes operating on continental shelves may also play an important role in the transport of sediment from source-to-sink (e.g. Middleton and Hampton, 1976; Lowe, 1982; Normark and Piper, 1991; Mulder and Alexander, 2001; Mutti et al., 2003). Sand deposition on the continental shelf remains understudied, primarily because mechanisms to explain significant cross-shelf transport of sand, particularly during sea-level highstand, are lacking. Processes commonly considered to affect deposition of sediment on continental shelves include tides, waves, and shore-parallel geostrophic currents (Cacchione and Drake, 1990; Myrow and Southard, 1996; Midtgaard, 1996). These processes alone may be capable of suspending enough sediment to induce cross-shelf gravity-driven flow, and the addition of pulses of river-derived sediment to the continental shelf can generate hyperpycnal currents capable of transporting and depositing large volumes of sand beyond the high energy shoreline (Wright et al., 1988; Mutti et al., 1996; Mutti et al., 2003; Warrick et al., 2013; Steel et al., 2016). Recognition of river-derived gravity currents on the continental shelf is critical because it allows for more accurate interpretations of the depositional record, including improved

paleoenvironmental models, and a broader understanding of mechanisms capable of producing shelf sand bodies, which has implications for sediment dispersal into basins and for hydrocarbon reservoir modeling.

Previous work on shelf sand bodies has primarily focused on reworked transgressive features or relict lowstand deposits (e.g. Houbolt, 1968; Bergman and Snedden, 1999, and references therein; Leva López et al., 2016). However, relatively few studies document shelf sand bodies deposited by hyperpycnal currents in the rock record or on modern shelves (Mutti et al., 2003; Lamb et al., 2008; Warrick et al., 2013; Steel et al., 2016). Hyperpycnal currents are gaining recognition as important mechanisms for cross-shelf transport of sediment, and early work on hyperpycnal currents has led to an improved understanding of conditions conducive to the generation of hyperpycnal currents and their deposit characteristics. Mulder and Syvitski (1995) showed the importance of relatively small rivers in the generation of hyperpycnal currents. Studies of modern and ancient hyperycnites found that deposits commonly contain an abundance of terrestrial organic debris due to the plunging of river outflow as it enters salt water (Plink-Bjorklund and Steel, 2004; Zavala et al., 2006; Myrow et al., 2008; Zavala et al., 2012). Furthermore, freshwater within hyperpycnal currents may result in lofting, also known as buoyancy reversal, in which the current becomes lighter than the surrounding ambient water and lifts off from the basin floor (Fig. 14; Sparks et al., 1993; Hurzeler et al., 1995; Hogg et al., 1999). Lofting has been shown to affect grain sorting (e.g. Pritchard and Gladstone, 2009; Zavala et al., 2011; Steel et al., 2016) and bed geometry of hyperpycnites (Plink-Bjorklund and Steel, 2004; Gladstone and Pritchard, 2010; Steel et al., 2017). A facies model proposed by Zavala et al. (2011) breaks hyperpycnal deposits into facies formed through bed-load, suspended load, and lofting transport processes, and is applicable to

many depositional settings (Fig. 14). Though hyperpycnites are gaining recognition, wider acceptance and promotion of hyperpycnite facies models necessitates a broader range of studies describing their facies variability and stratigraphic architecture, specifically in continental shelf settings which have largely been overlooked.

The objectives of this work are 1) to describe the geometry, internal architecture, and facies variability of shelfal sandstones deposited on the continental shelf of the Neuquén Basin in southwestern Argentina, and 2) to place them in the context of previously described shelf sand bodies in order to understand the processes responsible for their deposition. The hypotheses are that 1) lobate sand bodies in the La Jardinera region of the Neuquén Basin were deposited by hyperpycnal currents fed by relatively small fluvial systems and that 2) these sandstones are well-sorted due to processes inherent to hyperpycnal currents, such as lofting and low flow competence (Sparks et al., 1993; Zavala et al., 2011.; Steel et al., 2016). These aims have implications for understanding basin evolution and source-to-sink sediment transport, particularly in foreland basins that are characterized by steep basin catchments, narrow margins, and high sediment-water ratios, which are conducive to the generation of hyperpycnal currents. Furthermore, if these sand bodies in the Neuquén Basin were deposited by hyperpycnal currents, describing their facies variability and depositional architecture will help to confirm or modify existing hyperpycnal facies models (Fig. 14).

4.2. STUDY AREA

4.2.1. GEOLOGIC SETTING

The Neuquén Basin lies in central Chile and western Argentina between 32° and 40° S latitude (Fig. 15A). The basin is bounded to the west by the Andean magmatic arc, to the

northeast by the Sierra Pintada Massif, and to the south by the North Patagonian Massif (Fig. 15A). The Neuquén basin spans an area of over 120,000 km^2 and contains a sedimentary succession which is up to 4000 m thick and records deposition through various phases of basin evolution: a pre-Andean extensional phase, a thermal sag phase, and a foreland phase (Yrigoyen 1991; Franzese and Spalletti, 2001; Howell et al., 2005). Late Triassic - Early Jurassic pre-Andean extension associated with the collapse of the Gondwana orogen created a series of narrow, elongate half-grabens (Uliana et al., 1989; Franzese and Spalletti, 2001; Franzese et al., 2003). In the Early Jurassic, development of a magmatic arc along the western edge of Gondwana led to a transition from mechanical to thermal subsidence and caused integration of the many depocenters into the larger Neuquén back-arc basin (Franzese et al., 2003). During the early Cretaceous, continued thermal subsidence resulted in widespread marine deposition in all Patagonian back-arc basins and the Neuquén Basin reached its maximum sag phase (Franzese et al., 2003; Howell et al., 2005). Andean compressional tectonics associated with a shallowly dipping subduction zone in the Late-Cretaceous initiated a retro-arc foreland basin phase, which resulted in a lost connection to the Proto-Pacific Ocean (Introcaso et al., 1992).

4.2.2. LOCAL STRATIGRAPHY

A thick and relatively continuous stratigraphic succession records the evolution of the Neuquén Basin during the Late Triassic – Early Cenozoic (Legarreta and Gulisano, 1989; Legarreta and Uliana, 1991; Vergani et al., 1995; Howell et al., 2005). The succession contains an excellent record of marine invertebrates, leading to a refined biostratigraphic framework with over 30 Jurassic ammonite biozones (Leanza, 1981; Riccardi, 1983; Howell et al., 2005). During a period of thermal subsidence in the Mid-Jurassic to Early Cretaceous, thick

sedimentary successions of the Cuyo, Lotena, and Mendoza groups were deposited in the Neuquén Basin, where they record various transgressive-regressive cycles due to complex relationships between tectonics and eustatic sea level changes (Fig. 15B; Howell et al., 2005). One of the third-order transgressive-regressive cycles is recorded within the Middle Jurassic Cuyo Group, which consists of alluvial conglomerates and sandstones of the Sierra Chacaico Formation, a thick marine shale and turbidite succession of the Los Molles Formation, coeval shelf and shelf-edge deposits of the Lajas Formation, and alluvial plain sediments of the Challaco Formation (Fig. 15B; Paim et al., 2008). The focus of this study is the Bajocian (169.2 – 176.5 Ma; Gradstein et al., 1994) Lajas Formation, directly above the transition from the Los Molles Formation. This study area provides insight into processes operating on the outer continental shelf and to the deposition of well-sorted shelf sand bodies (Paim et al., 2008).

4.3 METHODOLOGY

This study focuses on a locality within the La Jardinera region of the Neuquén Basin outcropping near 39°24'30" S and 70°42' W (Figs. 15, 16, 17). Detailed stratigraphy immediately above the transition from the Los Molles Formation to the Lajas Formation was analyzed by measuring seven, closely spaced sedimentary sections (Figs. 17 and 18; Appendix IV). These measured sections provide a high resolution analysis of grain size trends, sedimentary structures, and bed characteristics of a ~40 m thick succession that spans a width of ~300 meters. Measured sections are supplemented with outcrop photographs, drone photographs, and paleocurrent measurements.

4.4 RESULTS

The lower part of the Lajas Formation in this region displays a 40-m-thick, coarsening-upward succession in which shale and thin sandstones are overlain by well-sorted, lobate sandstone bodies with thick, parallel laminations. The well-sorted, lobate sandstone bodies are encased by shale and organic-rich siltstone and sandstone, and display oblique migration and compensational stacking. The sandstone bodies are capped by thickly bedded conglomerates and cross-stratified coarse sandstones. The bedding geometry is described in more detail below.

4.4.1. SEDIMENTARY FACIES

The following sedimentary facies are present in the lower deposits of the Lajas formation of the Neuquén Basin near La Jardinera:

Thickly-laminated well-sorted sandstone – Facies S_L

Facies S_L consists of very well-sorted sandstone with grain sizes ranging from medium-lower to coarse-upper sand (Figs. 19A and 19B). The most distinctive features of facies S_L are the continuous planar-laminations that range in thickness from a few mm up to ~5 cm thick. In some beds, laminations thicken enough to become thinly bedded units. Beds are sharp-based and some beds contain tool marks indicating paleoflow direction. Some beds contain intense bioturbation that disrupts laminations and gives them a structureless appearance (Fig. 20B). The tops of some facies S_L beds are cross-stratified (Fig. 18). This facies has a quartz:feldspar:lithic ratio (QFL) of 50:40:10.

Hummocky cross-stratified sandstone – Facies S_{HCS}

Facies S_{HCS} is found near the base of the section as well as at the top of some packages of facies S_L (Fig. 18). This facies consists of well-sorted fine- to medium-grained sandstone

containing hummocky cross-stratification (HCS) with meter-scale wavelengths (Fig. 19C; Harms et al., 1975; Hamblin and Walker, 1979; Dott and Bourgeois, 1982). Over distances of tens of meters, some beds with HCS transition laterally to beds of the same thickness that contain mm-scale wavy laminations.

Heterolithic sandstone, siltstone, shale - Facies S_H

Facies S_H is commonly found below, lateral to, and above most beds of facies S_L (Fig. 18). This facies is heterolithic, with alternating mm-scale laminations of fine-grained sandstone, siltstone, and shale (Fig. 19D). The most predominant lithology in this facies is fine-grained sandstone with mm-scale parallel laminations. Charcoal, plant fragments, and organic debris are abundant and are typically aligned along laminations and bedding planes (Figs. 19D and 20E). The QFL ratio for this facies is 40:50:10.

Coarse-grained cross-stratified sandstone –Facies S_C

Facies S_C is characterized by very coarse-grained sandstone that commonly contains floating granules and pebbles (Fig. 19E). Beds of facies S_C are commonly trough cross-stratified, contain scour-and-fill structures, and sometimes contain bi-directional cross-stratification. Mud rip-up clasts are common at the base of these beds. Granules and coarse sand grains sometimes form laminations. These beds are found at the top of the section and in association with conglomerates of Facies C_C (Fig. 18).

Channelized conglomerate – Facies C_C

Facies C_C is characterized by pebble conglomerates with scoured bases and abundant internal scours (Fig. 19F). Large (dm) pieces of petrified wood are common. Conglomerates form sedimentary bodies that are tens of meters wide and ~1 m thick with concave-up basal contacts and are interpreted as channels. Multiple sets of truncated surfaces within channel

bodies suggests they were built by several episodes of scour and fill. Beds are poorly sorted and display coarse-tail fining-upwards patterns, typically from cobble-sized to coarse sand.

Tabular Pebble Conglomerate – Facies C_T

Facies C_T predominantly comprises clast-supported pebble conglomerates, although beds range from very coarse-grained sandstone to cobble conglomerates (Fig. 19G). Pebbles and coarse grains commonly form faint laminations or coarse lenses within beds. Beds commonly contain mud clasts ranging from 1 mm up to 30 cm in diameter, and some beds contain internal scours filled with gravel. Average pebble conglomerate bed thickness is ~1 m, but beds can reach up to 2.5 m thick.

Massive, organic-rich sandstone – Facies S_M

Facies S_M is characterized by structureless, organic-rich, fine- to medium-grained sandstone (Fig. 19H). These sandstone beds contain scattered organic fragments and shell fragments up to 1 cm in diameter and are more poorly sorted than other sandstone facies, with grains ranging from coarse silt to medium-grained sand. Beds of this facies are most common at the base of the section, but can also be found between S_L beds and the overlying conglomeratic beds (Fig. 18). This facies has a QFL ratio of 50:30:20.

Fine-grained sandstone – Facies S_F

Facies S_F is characterized by very fine- to fine-grained sandstone that commonly contains mm-scale laminations (Fig. 19I). This facies weathers easily and typically has very poor exposures. This facies has more lithic grains than facies S_L and is moderately sorted, with a QFL of 35:30:35.

Shale – M

Facies *M* is found at the base of all measured sections (Fig. 18) and consists of laminated shale, with rare siltstone and sandstone interbeds (Fig. 19J). Siltstone and sandstone interbeds are commonly cm-thick, but can be up to 5 cm in thickness. Facies M becomes less abundant higher in the succession.

4.4.2. SANDSTONE LOBE GEOMETRY

The apparent cross-sectional geometry of the deposits is lobate (flat base and convex-up, with a thick center that thins laterally), rather than channelized (convex-down and flat top) (Fig. 21). Sandstone beds in this succession are organized into four discrete lobate packages, which are on the order of 10 m thick and ~150 m wide (Figs. 18 and 21). Beds coarsen and thicken upwards within lobes. A hierarchy exists in which 1- 10 cm thick beds amalgamate to form bedsets of facies S_L, and bedsets stack together, in some cases separated by heterolithic facies S_H, to create lobes (Fig. 22). Organic rich, heterolithic beds of facies S_H typically lie below, in between, and lateral to individual lobes (Figs. 18, 21 and 22).

Lobes contain many amalgamation surfaces and internal scour-and-fill structures (Figs. 18 and 21). Some bedsets display a thickening-to-thinning upward sequence, with cm- or mm-scale laminations at the base and at the top and beds up to ~10 cm in the center (Fig. 18). Sandstone beds commonly contain moderate amounts of charcoal and organic debris and some beds are bioturbated. Hummocky cross-stratification and scour and fill can be found at the top of lobes (Figs. 18 and 19C). Lobes thin and pinch out over a few hundred meters to the west and east (Fig. 21).

4.4.3. LARGE-SCALE STACKING PATTERNS

Lobes are offset laterally and migrate to the east through the succession (Fig. 21) with the surfaces between the lobes dipping at ~ 8 degrees relative to flat-lying strata. In addition to

beds coarsening and thickening upward within individual lobes, there is an overall coarsening and thickening upward trend between lobes (Fig. 18). The outcrop stratigraphy records a transition from shale deposition with few thin sandstone and siltstone beds (facies M) and hummocky cross-stratified beds (facies S_{HCS}), to lobate sand bodies migrating laterally and prograding to the northeast, back to deposition of finer-grained facies M and S_H, and finally capped by the deposition of very coarse sandstones and conglomerates (facies C_T, C_C and S_C) (Fig. 18).

4.5 INTERPRETATIONS

4.5.1. INTERPRETATION OF THICKLY-LAMINATED WELL-SORTED SANDSTONE FACIES (S_L)

We interpret beds of facies S_L to represent deposition by hyperpycnal currents. Packages of facies S_L are distinctive in their lobate geometry, well-sorted nature, and extensive thick laminations. Sharp or erosional based, dm thick, parallel laminated sandstone are typical for sustained gravity flows and have been commonly interpreted as river-derived hyperpycnites (Mulder et al., 2001; Mulder et al., 2003; Mutti et al., 2003; Plink-Bjorklund and Steel, 2004; Petter and Steel, 2006). Modern hyperpycnites with similar characteristics are identified in the Var submarine system (Mulder et al., 2001). Some laminations within beds display a thickening-to-thinning upward pattern over vertical scales of ~10 cm to ~ 20 cm, which may record a waxing-to-waning flood cycle with laminations formed by pulses within a single flood. As discussed later, laminae within hyperpycnites may also record superposition of oscillatory wave motion on hyperpycnal currents (Myrow and Southard, 1996; Macquaker et al., 2010). The pattern of coarsening- and thickening-upward beds within lobes is interpreted

as evidence of lobe progradation, because thicker and coarser beds suggest more proximal deposition. Paleocurrent measurements are limited, but tool marks at the base of facies S_L beds suggest a paleoflow to the northeast (with the exception of one southeastward measurement) (Figs. 18 and 21), which match the regional paleoflow directions of nearby slope channels, suggesting offshore-directed flow (Vann, 2013; Tudor, 2014; R. Steel et al., 2017). Cross-stratification at the tops of facies S_L beds primarily record east-southeastward paleoflow directions and one westward paleoflow direction (Figs. 18 and 21). The orientation of these cross-strata suggest a different process, likely reflecting post-depositional reworking of hyperpycnites by shelf currents. Care should be taken, however, when interpreting paleocurrent measurements in this study because there are few measurements and many measurements come from similar horizons within the stratigraphy.

4.5.2. INTERPRETATION OF HUMMOCKY CROSS-STRATIFIED FACIES (S_{HCS})

The presence of hummocky cross-stratified facies S_{HCS} above and below the sand lobes suggests shelfal water depth (tens of meters) that record storm activities (Harms et al., 1975; Hamblin and Walker, 1979; Dott and Bourgeois, 1982). In addition to providing a context for depositional environment, hummocky cross-stratification suggests periods of non-deposition and reworking. HCS is only found at the top of lobes, which suggests that non-deposition and reworking most likely occurred after the locus of deposition migrated to the east, resulting in the development and progradation of a new lobe. However, it is also possible that reworking and formation of HCS occurred within lobes, between flood events, but the HCS beds were removed by successive hyperpycnal currents. Moderate bioturbation also suggests quiescent periods between deposition of bedsets and following lobe abandonment.

4.5.3. INTERPRETATION OF THINLY LAMINATED, HETEROLITHIC SANDSTONE FACIES (S_H)

In La Jardinera, the thinly laminated, organic-rich facies S_H are interpreted as deposits from lofted plumes. Freshwater within hyperpycnal currents has the potential to loft from the flow and rise vertically, or to induce buoyancy reversal of the entire current (Sparks et al., 1993). The lofting plume can carry with it light constituents such as fine-grained sediment and organic matter, which eventually settle out over a broader region (Zavala et al., 2011; Pritchard and Gladstone, 2009). These beds are analogous to lofted rhythmites of Zavala et al., 2006.

4.5.4. DEPOSITION OF HYPERPYCNAL LOBES

Further evidence for a hyperpycnal origin of these shelf sands is the abundance of charcoal along bedding planes (Figs. 19E and 19F). Common occurrence of coal and charcoal fragments supports the proximity of the shorelines, and in ancient deposits has been linked to river floods (Petter and Steel, 2006; Zavala et al., 2012). The occurrence of wildfires in drainage basins is known to "prime" rivers for significant suspended sediment loads during subsequent floods (e.g. Florsheim et al., 1991; Silins et al., 2009; DiBiase and Lamb, 2013), making rivers more likely to produce hyperpycnal effluent. The presence of charcoal, which can reach 1 cm in diameter in Lajas sandstones, may reflect this process in which wildfire leads to excessive sediment discharge. Finally, internal scouring and amalgamation of beds, as well as tool marks at the base of bedsets, suggests that these sandstones were deposited by turbulent currents capable of scouring into the substrate. Although a lofting flow will have a slower-moving head, the bed-attached portion of the current is still expected to be capable or eroding the substrate. However, lofting flows are unlikely to be as erosive as surge-type turbidity

currents: a contrast that is reflected by the relatively small number of tool marks at the base of beds in this study area compared to many "classic" turbidite systems.

Deposits are characterized as hyperpycnal "lobes" based on the geometry of the deposits in addition to the facies interpretation. The sandstone bodies range in thickness from ~1 to 8 meters, and thin laterally to the east and west over ~150 m. The resulting overall geometry is a relatively flat base with a thick "axis" and thinner beds laterally (Figs. 18 and 21). Modern hyperpycnites on the shelf of the Santa Barbara Channel show similar geometries to those seen in the Lajas Formation (Warrick et al., 2013; Steel et al., 2016).

4.5.5. INTERPRETATION OF MUD FACIES (M), FINE GRAINED SANDSTONE FACIES (S_F), AND STRUCTURELESS SANDSTONE FACIES (S_M)

Strata below the hyperpycnal lobes are characterized by facies M, which is composed of shale and few thin sandstone beds, and by fine-grained sandstone of facies S_F. Thin sand beds within facies M are interpreted as distal turbidites deposited either on the axial margins or basinward reaches of hyperpycnite deposition. The origin of facies S_F is more difficult to interpret, primarily because these deposits are heavily weathered and poorly exposed. These S_F sandstones are thinly laminated and very fine grained, and they contain organic debris and few shell fragments. Plunging of river effluent and the subsequent generation of hyperpycnal currents requires very high suspended sediment concentrations, and rivers more commonly generate hypopycnal plumes in which freshwater and suspended sediment override the ambient salt water and eventually settle from suspension (Bates, 1953). A possible explanation is that beds of facies S_F were deposited by hypopycnal plumes from local rivers and were possibly reworked or re-distributed by background shelf processes (e.g. tides, waves). Beds of facies

S_M make up a small proportion of the section, but are observed both below and above hyperpycnal lobes. These beds are structureless and contain scattered shells and organic fragments. The origin of this facies is unclear, but potential interpretations include debris flow deposition or tidally reworked shelf sands.

4.5.6. INTERPRETATION OF TABULAR CONGLOMERATE FACIES (C_T)

Conglomerates and very coarse sandstone beds of facies C_T were deposited above the hyperpycnites and are interpreted to represent the near-shore fall out of coarse material or part of the fluvial system feeding the hyperpycnites. These flows are likely to have low competency compared to surge-type turbidity currents, due to their fresh interstitial water rather than saline interstitial water, which will limit their ability to carry very coarse sand and gravel far beyond the shoreline. These conglomerates contain scour and fill structures, faint parallel laminations, and some beds contain mud clasts at their base. They are interpreted as proximal equivalents of the hyperpycnal sandstone beds of facies S_L. However, they are more likely to be affected by shallow-water processes such as wave reworking, which would explain the faint laminations, scouring, and discontinuous coarse-grained lenses.

4.5.7. INTERPRETATION OF COARSE-GRAINED SANDSTONE FACIES (S_C) AND CHANNELIZED CONGLOMERATE FACIES (C_C)

The stratigraphic section is capped by trough-cross stratified sandstone and channelized conglomerates of facies S_C and C_C. These facies are interpreted as deposits from the relatively small rivers feeding the hyperpycnal currents. Beds contain abundant petrified wood, fining-upward patterns, and erosional bases. The absence of lateral accretion in these deposits supports the interpretation of a small, braided system, rather than a larger, meandering river (Miall, 1994).

4.5.8. PALEOGEOGRAPHY OF THE LAJAS SHELF IN THE STUDY AREA

Progradation is recorded by the succession of outer-shelf or possibly upper-slope shale and thin sandstone beds overlain by shelf hyperpycnites (facies S_L), which are capped by hypopycnal deposits (facies S_F) and coarser shallow-water gravel beds and channelized fluvial deposits (facies C_T, C_C, S_C). The shelf edge indicated in Figure 17 is estimated by previous workers based on a marked shift to mudstones, which contain distal turbidites that are more characteristic of typical surge-type turbidity currents (e.g. partial Bouma sequences and some evidence of chaotic bedding and soft-sediment deformation associated with rapid deposition of sediment; Vann, 2013; Tudor, 2014). Within ~10 km of this study area, portions of the Lajas – Los Molles system contained large, well-developed fluvial and submarine canyon systems which are interpreted to indicate significant bypass of the continental shelf and transport of coarse-grained conglomeratic material across the slope break into deep water (Paim et al., 2008; Vann, 2013; R. Steel et al., 2017). In these other locales, thick fluvial successions within the Challaco Formation are seen up-dip from these conglomeratic slope channels (Viega, 1998; Paim et al., 2008). The present study area is interpreted to represent a system in which smaller rivers fed hyperpycnal sand lobes on the continental shelf (Fig. 23A). These hyperpycnal shelf sand bodies are likely to be found adjacent to systems in which rivers connect with canyons, and channels in the continental slope feed deep-water fans (Fig. 23B). The fluvial systems feeding the Lajas shelf in the present study area are interpreted as relatively small systems based on the size of the channels seen at the top of the succession, which have widths of ~15 m and depths of ~1 m (Figs. 19F and 21). Furthermore, large rivers are less likely to induce hyperpycnal currents than small mountainous rivers due to the storage of sediment within their

extensive floodplains and deltas preventing the high sediment concentrations necessary to induce plunging of river effluent (Mulder and Syvitski, 1995).

A hypothesized paleogeography of the study area is shown in Figure 23. It's worth noting that, in the hyperpycnal shelf systems, the coarse-grained material is likely to be trapped within the fluvial environment or at the high-energy shoreline, and clay-sized particles may be stripped from the flow through lofting of fresh interstitial water, resulting in well-sorted shelf sands (Steel et al., 2016). This scenario is in contrast to larger systems that connect with slope conduits and which may be capable of bypassing the shelf and sending coarse-grained material onto the slope or continental rise. This sediment partitioning of hyperpycnal systems is explored in more detail in the discussion.

4.6 DISCUSSION

4.6.1. RECOGNITION OF HYPERPYCNITES

Distinguishing hyperpycnites from "classic" turbidites (extrabasinal vs. intrabasinal turbidites, *sensu* Zavala et al., 2016) is critical to accurate paleoenvironmental interpretations. However, the distinction can be challenging to make, because both are deposited by turbulent sediment gravity flows. Despite this challenge, hyperpycnal currents have several unique characteristics which can alter both their dynamics and their deposit characteristics with respect to "classic" turbidites. A diagnostic criterion for the recognition of hyperpycnites is the abundance of terrestrial organic matter (Plink-Bjorklund and Steel, 2004; Petter and Steel, 2006; Myrow et al., 2008; Zavala et al., 2012). Additionally, hyperpycnal currents are distinct from other turbidity currents in that they are river-derived and, therefore, contain fresh interstitial water. In many cases, lofting of this fresh interstitial water from the flow can

enhance sorting, because light constituents such as plant fragments, very fine sand, silt, and clay are stripped from the bed-attached portion of the current by the rising freshwater plume (Pritchard and Gladstone, 2009; Zavala and Arcuri, 2016), and can also result in narrower deposits than expected from "classic" turbidity currents that remain ground-hugging (E. Steel et al., 2017).

The Lajas hyperpycnites share many similarities with existing hyperpycnite models, including the abundance of terrestrial organic matter, the well-sorted nature of the deposits, and their overall morphology and architecture (e.g. Mulder et al., 2003; Zavala et al., 2006; Zavala et al., 2011; Steel et al., 2016). Hyperpycnal currents in the Var submarine system deposited well-sorted sands containing thick laminations, suggested to represent individual floods of the Var River (Mulder et al., 2001). These Mediterranean hyperpycnites are 3 – 12 cm thick and do not exceed fine-grained sand. Individual laminations are difficult to distinguish visually in the Var submarine system, and were only recognized through detailed grain size analysis (Mulder et al., 2001). Similarly, Holocene hyperpycnites on the continental shelf of the Santa Barbara Channel, Southern California (Warrick et al., 2013; Steel et al., 2016) contain well-sorted fine-grained sand with individual beds that are only distinguished through detailed grain-size analysis (Steel et al., 2016). Although the Lajas sand bodies are medium-grained rather than fine-grained, their well-sorted nature is analogous to observations from the Mediterranean and the Santa Barbara Channel hyperpycnites. This difference in grain size may simply be attributed to differences in the velocity of the currents or in the size-distribution of the material in the fluvial system.

Lajas hyperpycnites form lobate sand bodies that are ~150 m wide and have maximum thicknesses of ~2 – 8 m. This narrow geometry is analogous to shelf hyperpycnites of Southern

California (Steel et al., 2016) and to flume experiments on lofting turbidity currents (E. Steel et al., 2017). The lobes consist largely of well-sorted parallel laminated sandstones (facies S_L), surrounded by thinly laminated fine-grained sandstone and siltstone with abundant plant debris (facies S_H). These facies correspond to previously described hyperpycnite facies of Zavala et al. (2011), in which the bed-attached portion of the current produces parallel laminated sandstone (S2) and the lofting plume produces laminated sandstone and silt with plant debris (L), termed lofted rhythmites. The presence of light interstitial fluid within hyperpycnal currents is likely to reduce flow competency, resulting in rapid fall-out of coarse grain-size fractions near the shoreline (facies B of Zavala et al., 2011). The distinct lack of coarse-grained material in the Lajas hyperpycnal lobes, shelf hyperpycnites of the Santa Barbara Channel (Steel et al., 2016), and Var River hyperpycnites in the Mediterranean (Mulder et al., 2001) reflects this low flow competence. Pebbly sandstones and conglomerates of facies C_T deposited above the Lajas hyperpycnal lobes are interpreted to represent coarse material deposited in front of the river mouth, near the shoreline. These conglomerates may be deposited by normal river discharge, or could potentially reflect coarse fall-out due to the low competency of hyperpycnal currents.

One of the most distinctive characteristics of the sandstone beds in the study area is their extensive thick laminations and thin beds, which amalgamate to form bedsets. Lobes are composed of several bedsets separated by thinly-laminated, organic rich beds of facies S_H (Fig. 22). Several mechanisms may be operating to produce the thick laminations and thin beds observed within these sandstones. The combination of storm wave oscillations and hyperpycnal currents could produce pulses within the current and cause the deposition of laminae (Myrow and Southard, 1996). Laminae may also be the result of pulses in flood

strength or possibly the migration of the flow axis during floods (Best et al., 2005). Storm waves or flood pulses can also explain internal scour-and-fill structures observed within some of the hyperpycnites. Alternatively, thicker laminations may represent individual hyperpycnal events. It is most likely that the observed architecture is developed due to a combination of many hyperpycnal events, modified by flood pulses and oscillatory wave motion.

4.6.2. PREVIOUSLY DESCRIBED SHELF SAND BODIES

An assortment of explanations has been proposed for the origin of shelf sand bodies, many of which are large-scale transgressive features commonly oriented at an oblique angle to the strongest tidal current (e.g. Houbolt, 1968; Bergman and Snedden, 1999; Reynaud and Dalrymple, 2012). The various models include tidal sand ridges, which grow from irregularities in the seabed (Fig. 24A; e.g. Houbolt, 1968; Tillman and Martinsen, 1984; Rine et al., 1991), recycled lowstand shoreface deposits (Fig. 24B; Posamentier et al., 1992; Berné et al., 1998), reworked ebb-tidal deltas (Fig. 24C; Snedden et al., 1999), and overstepped barrier islands (Fig. 24D; Rodriguez et al., 1999). Despite some similarities, such as sharp-based, prograding, well-sorted sandstones, existing models of shelf sand bodies do not easily explain the origin of the Lajas shelf sandstones. The Lajas deposits studied do not exhibit the deep incisions or high-angle clinoforms observed in sandstone ridges composed of recycled lowstand shorefaces (24B) (Berné et al., 1998). Furthermore, based on limited paleocurrent data from this study, as well as regional paleocurrent directions (Tudor, 2014), the Lajas sandstone bodies are smaller and appear to be less laterally extensive (hundreds of meters to km) than would be expected if they originated from a lowstand shoreface. Even considering the possibility that the sandstones in this study are features from a minor transgression within an overall regression, the existing sand ridge models cannot explain the extensive thick parallel

laminations characteristic of the Lajas sandstones (Figs. 18 and 19). Tidal currents play a strong role in shaping and reworking sediment in tidal sand ridges, and the extensive compound cross-bedding typically associated with these processes (Dalrymple, 2010; Leva-Lopez et al., 2016) is not observed in the study area. Furthermore, sand ridge models proposed by Snedden et al. (1999) and the Rodriguez et al. (1999) would imply that a filled tidal inlet or incised valley should be represented in the stratigraphy, but these features are not observed in the section or within tens of kilometers along strike from the study area. Overall, the lack of tidal mud drapes, the low abundance of cross-stratification, and the abundant parallel laminations deposited within a regressive sequence suggests that these sandstones are distinct from previously described shelf sandstone ridges (Fig. 24) (Leva-Lopez et al., 2016).

Storm-induced deposition of sediment on the continental shelf is shaped by a combination of waves, tides, geostrophic currents, and gravity-driven flow (Myrow and Southard, 1996). A model of tempestite deposition presented by Myrow and Southard (1996) suggests that, although storm-driven suspension of sediment on continental shelves may be capable of inducing turbidity currents (i.e. through an "excess weight force"), cross-shelf transport and deposition of sediment solely through storm waves and geostrophic currents is likely to be negligible. However, with the introduction of large sediment pulses from river floods or sediment failure triggered by earthquakes, it may be possible to deposit significant thicknesses of sand via sediment gravity flows (Myrow and Southard, 1996; Mutti et al., 2003; Steel et al., 2016). Storm waves can promote the continuation of hyperpycnal currents across the shelf by enhancing turbulence, and laminations may reflect pulsation of the currents from the addition of wave oscillations (Myrow and Southard, 1996; Wright and Friedrichs, 2006; Macquaker et al., 2010). Hummocky cross-stratification is commonly associated with

tempestites (Harms et al., 1975; Hamblin and Walker, 1979) and is found below, on top of, and within Lajas hyperpycnite lobes (Fig. 18), suggesting that hyperpycnal currents of the Lajas system were generated either in conjunction with storm conditions or that the hyperpycnites were later reworked by storm waves.

4.7 CONCLUSIONS

Deposits of the Lajas formation near La Jardinera, Argentina record the deposition of ~2- to 8-m-thick sandstone bodies on the continental shelf. These sandstones were deposited by hyperpycnal currents fed by small rivers and are predominantly characterized by well-sorted, medium-grained sandstones with cm- to dm-thick laminations. Deposits in this study area are part of a relatively short system (implied by the deposition of hyperpycnites on the shelf rather than on the slope or in deeper water) in which significant grain-size fractionation occurred, with gravel deposition near the shoreline, sand deposition by hyperpycnal currents on the shelf, and finer-grained sediment and organic debris stripped from the flow by lofting. Lofted material settled nearby on the shelf in this setting; however, in many ocean basins with cross-currents, the lofted plume and its constituents may be dispersed over a broad region on the shelf and therefore may not always be present in outcrop.

Hyperpycnal currents are beginning to gain recognition as important mechanisms for the deposition of large volumes of sand on the continental shelf (e.g. Mutti et al., 2003; Wright and Friedrichs, 2006; Pattison, 2005; Lamb et al., 2008; Steel et al., 2016). Facies models for hyperpycnites have been proposed (Mulder et al., 2001; Zavala et al., 2011), but the development of robust facies models necessitates a broad range of examples in a variety of settings. Understanding the ways in which hyperpycnites can be deposited in deep-water

settings is significant. However, recognizing their ability to build shelf sand bodies is equally important and will reduce the potential for these features to be misinterpreted as deep-water deposits. Finally, the well-sorted nature of these deposits makes them potentially high-quality hydrocarbon reservoirs. Accurate predictions of their reservoir quality, however, will require a deep understanding of their morphology, grain-size distributions, and internal architecture.

A)

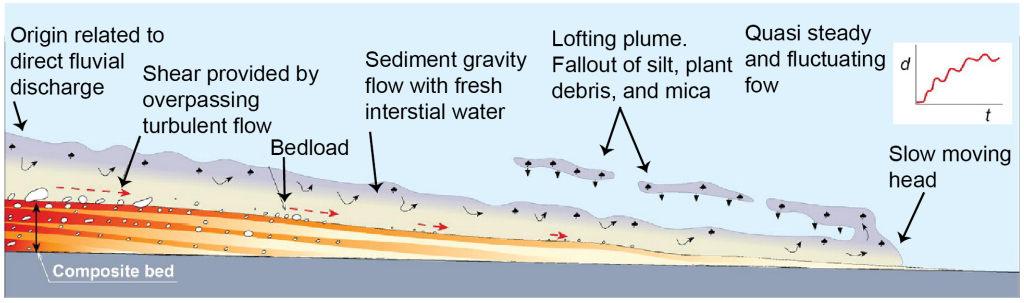

B)

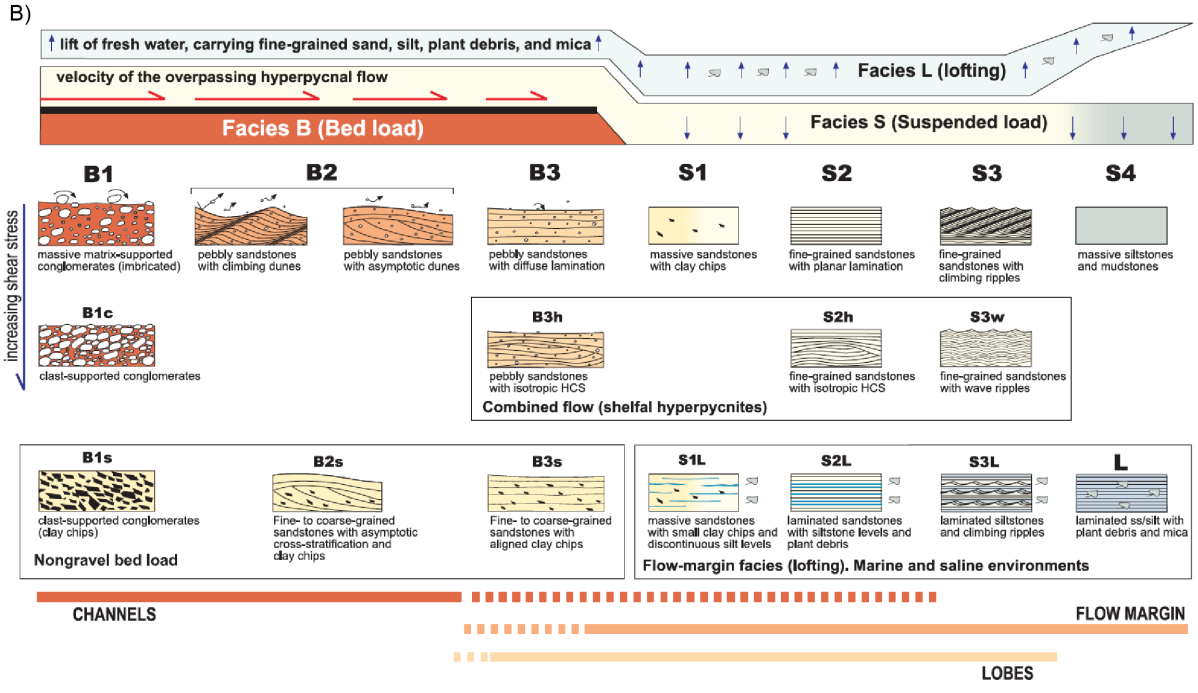

Figure 14. Schematic diagram of a lofting hyperpycnal current and associated sedimentary facies (*Modified from Zavala et al., 2011)*. A) Components of a lofting hyperpycnal current. Fresh interstitial water can allow for lofting of freshwater and fine-grained flow constituents such as silt, mica, and plant material. B) The genetic facies model proposed by Zavala et al. (2011) breaks deposits into those associated with bedload transport (facies B), suspended load (facies S) and lofting (facies L). A variety of sedimentary structures may be formed by these currents, including sandstones with HCS (combined flow facies), planar laminated sandstones, pebbly sandstones with diffuse lamination, and imbricated conglomerates. See Zavala et al. (2011) and Zavala and Arcuri (2016) for more detailed discussion of hyperpycnite facies models.

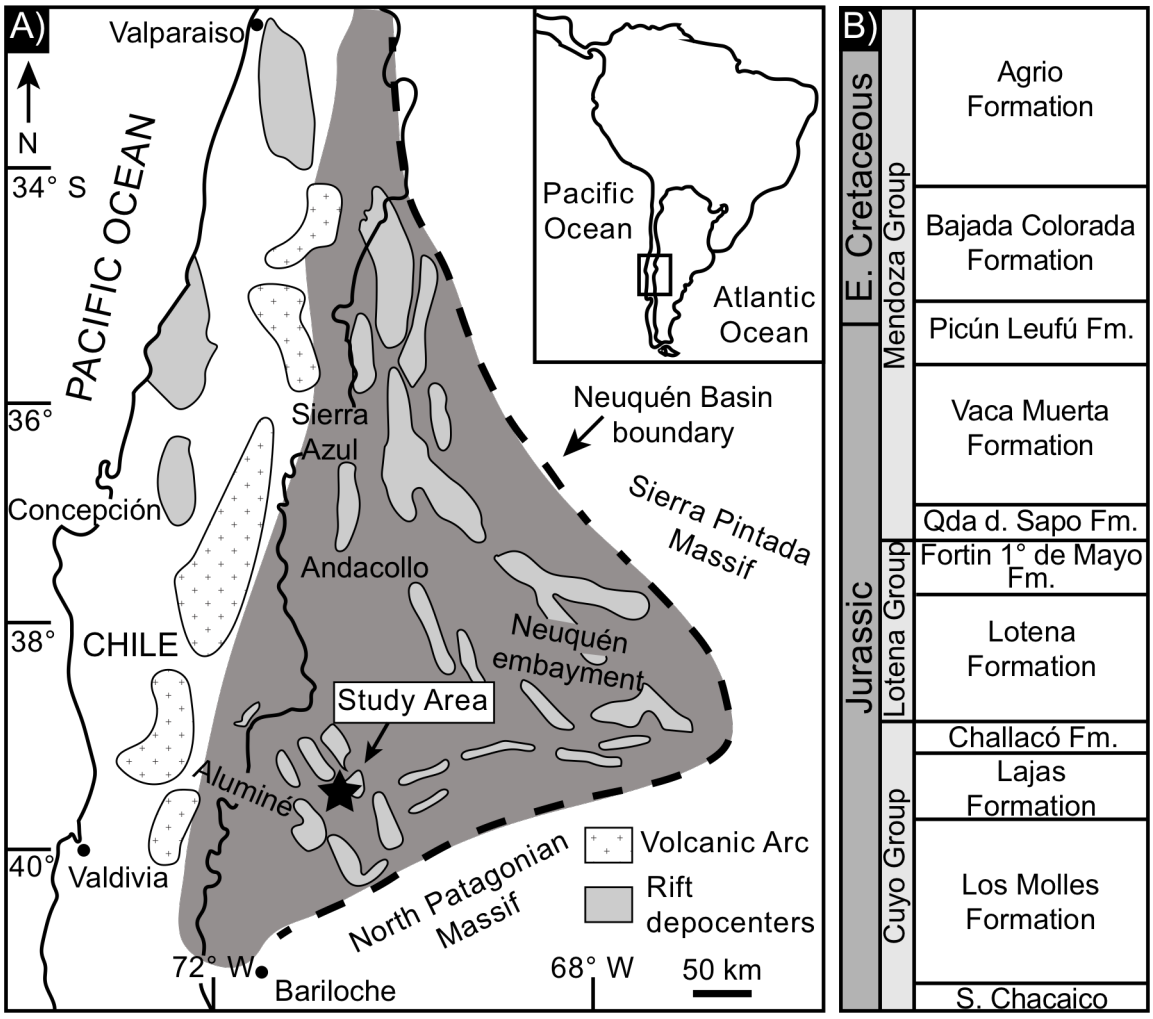

Figure 15. Study Area and Stratigraphy. A) Map of the Neuquén Basin, modified from Franzese et al., 2006. The Neuquén Basin, highlighted in dark grey, lies in Chile and western Argentina, between 32° and 40°S. The study area near La Jardinera is indicated by the black star. Rift depocenters associated with pre-Andean extension are indicated by grey polygons. The basin is bounded by the Sierra Pintada Massif and the North Patagonian Massif to the northeast and south, respectively. B) Jurassic and Early Cretaceous stratigraphy of the Neuquén Basin, modified from Paim et al., 2008. The focus of this study is the Lajas Formation, within the Jurassic Cuyo Group.

A)

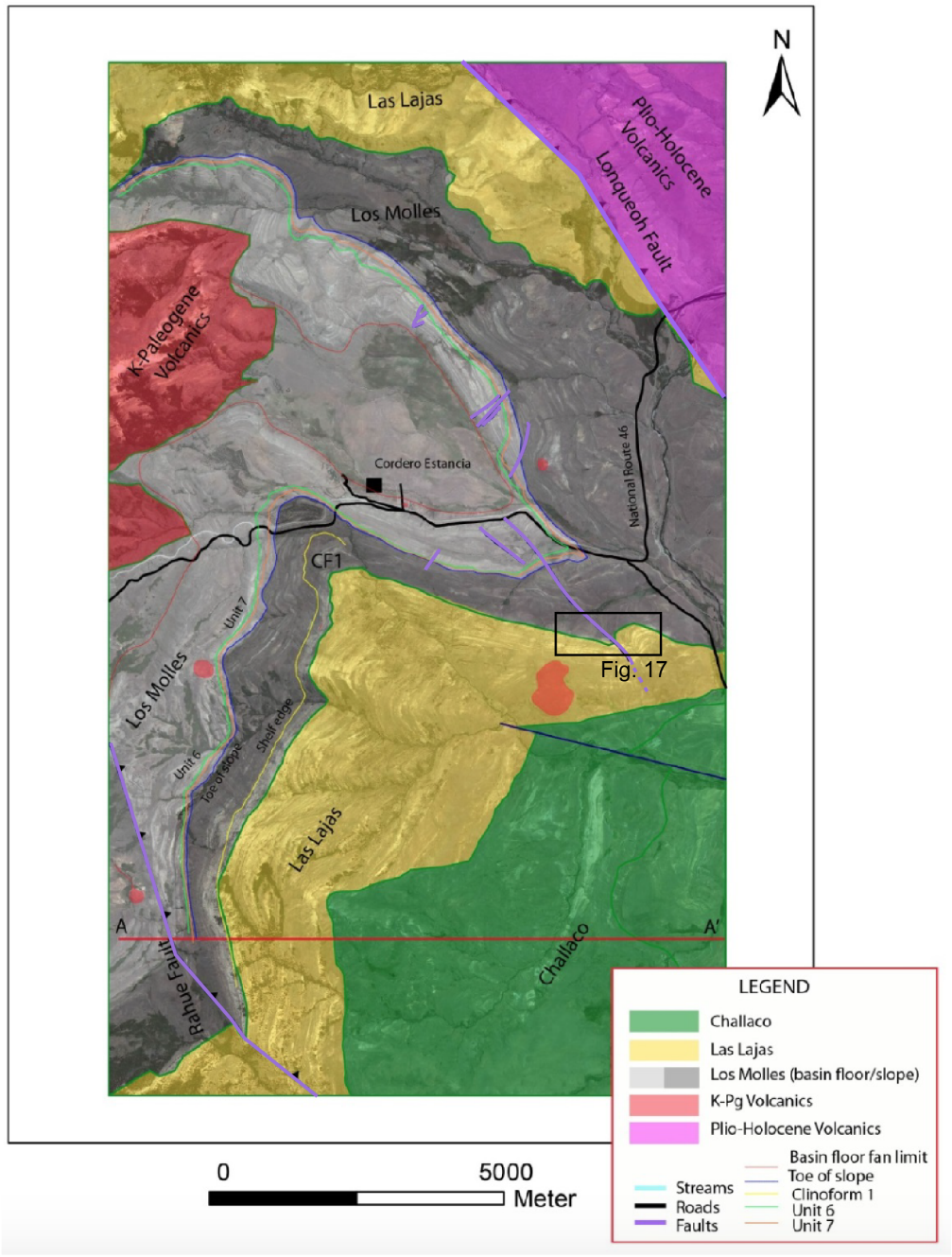
N
Las Lajas
Plio-Holocene Volcanics
Los Molles
Lonqueoh Fault
K-Paleogene Volcanics
Cordero Estancia
National Route 46
CF1
Unit 7
Los Molles
Fig. 17
Unit 6
Toe of slope
Shelf edge
Las Lajas
A
A'
Challaco
Rahue Fault
0
5000
Meter
LEGEND
Challaco
Las Lajas
Los Molles (basin floor/slope)
K-Pg Volcanics
Plio-Holocene Volcanics
Basin floor fan limit
Toe of slope
Clinoform 1
Unit 6
Unit 7
Streams
Roads
Faults

B)

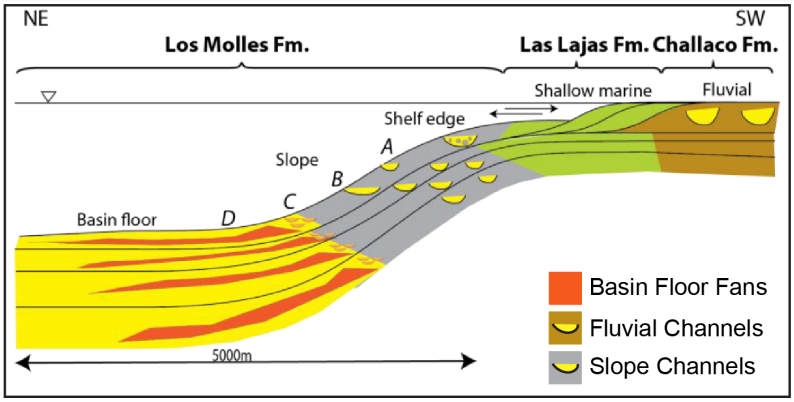
NE
SW
Los Molles Fm.
Las Lajas Fm.
Challaco Fm.
Shallow marine
Fluvial
Shelf edge
Slope
A
B
C
D
Basin floor
5000m
Basin Floor Fans
Fluvial Channels
Slope Channels

Figure 16. (Previous page) A) *Modified from Tudor, 2014*. Geologic map of the La Jardinera region, Neuquén Basin. The study area and location of Fig. 17 is indicated by the black box. B)Modified *from Vann, 2013*. Schematic diagram showing clinoforms of Los Molles Fm., Lajas Fm., and Challaco Fm as well as the overall SW-NE dip orientation of the depositional system.

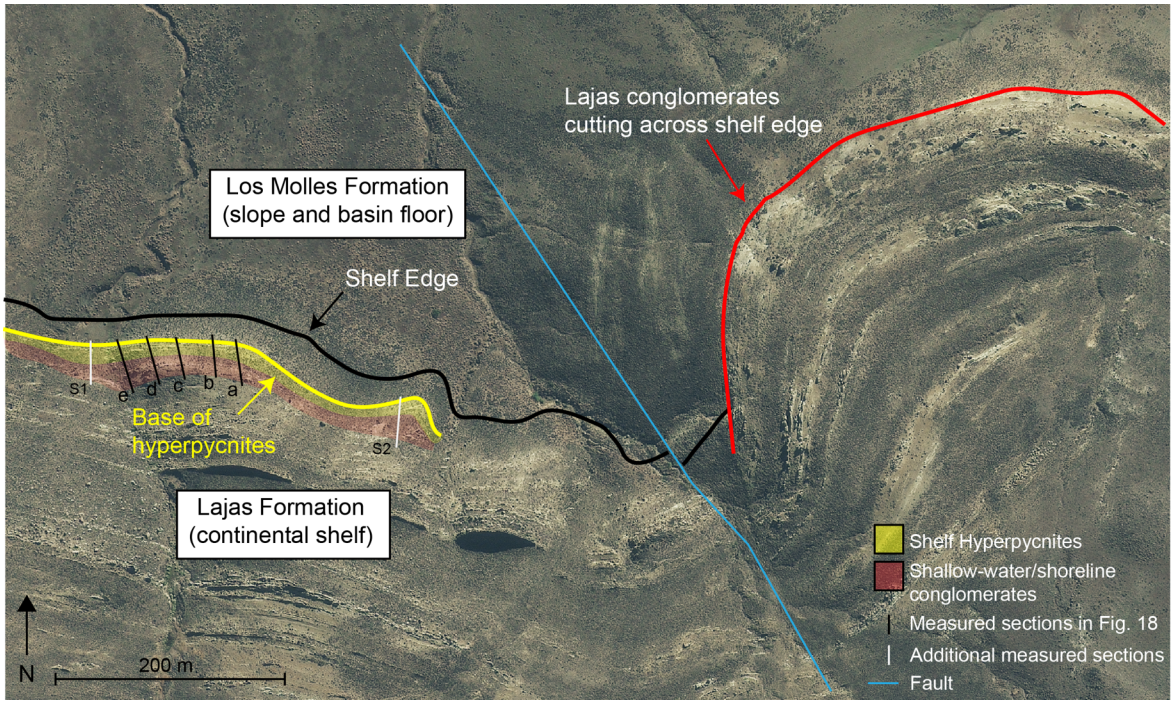

Figure 17. Aerial photo of study area. Hyperpycnites are highlighted in yellow and shallow-water/shoreline conglomerates are highlighted in red. The shelf edge, marked by the black line, was estimated by a marked shift to mudstones that contain distal turbidites in the west, and a change in conglomerates from subaerial fluvial textures to chaotic debris flows to the east. The hyperpycnites of the Lajas Formation lie above the shelf edge, whereas conglomeratic deposits to the east cut across and truncate the shelf edge as they transport coarse material onto the continental slope. The locations of measured sections are marked by solid lines in the region of the hyperpycnal sandstones. Sections S1 and S2 are included in Appendix IV.

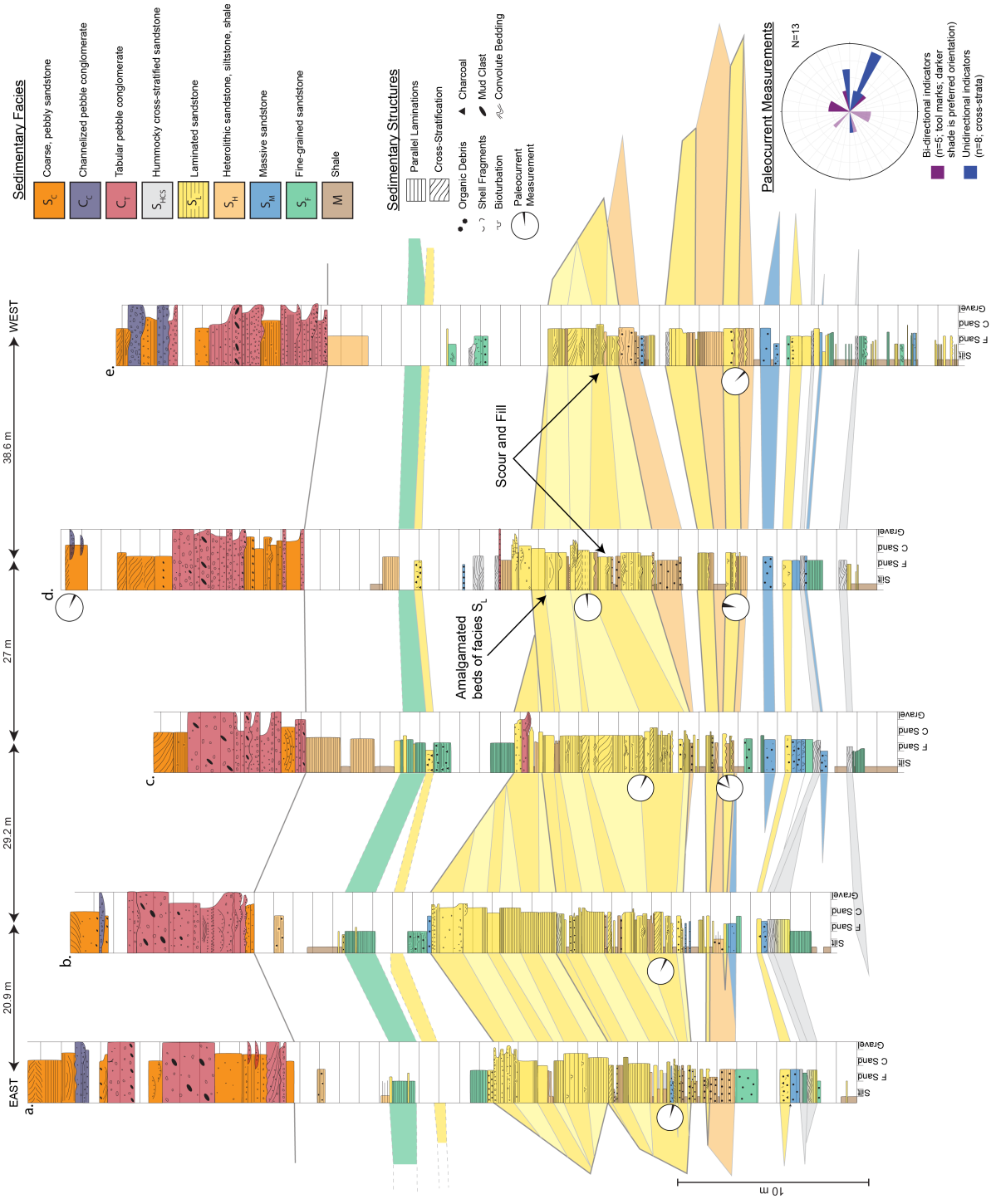
Sedimentary Facies
Coarse, pebbly sandstone
Channelized pebble conglomerate
Tabular pebble conglomerate
Hummocky cross-stratified sandstone
Laminated sandstone
Heterolithic sandstone, siltstone, shale
Massive sandstone
Fine-grained sandstone
Shale
Sedimentary Structures
Parallel Laminations
Cross-Stratification
Organic Debris
Charcoal
Shell Fragments
Mud Clast
Bioturbation
Convolute Bedding
Paleocurrent Measurement
Paleocurrent Measurements
N=13
Bi-directional indicators (n=5; tool marks; darker shade is preferred orientation)
Unidirectional indicators (n=8; cross-strata)
EAST
WEST
20.9 m
29.2 m
27 m
38.6 m
a.
b.
c.
d.
e.
Scour and Fill
Amalgamated beds of facies S_L
10 m
Slit
F Sand
C Sand
Gravel

Figure 18. (previous page) Correlation between measured sections. Section labels (a-e) refer to locations in Fig. 17. Units are colored by sedimentary facies, see text for facies descriptions. Hyperpycnal lobes (yellow) prograded to the east-southeast as indicated by paleocurrent measurements and bounding surfaces. Lobe boundaries are highlighted by thicker, dark grey lines. Measured sections reflect a regressive package in which fine-grained deposits and thin sandstone beds are overlain by hyperpycnal lobes and capped by coarse sandstones and conglomerates. Beds of facies S_{HCS}, shown in grey, contain hummocky cross stratification and suggest a continental shelf setting. Locations of the measured sections are indicated by black lines in Fig. 17.

Figure 19. (next page) Sedimentary facies in the study area. A) Stacked bedsets of facies S_L. B) Closer view of Facies S_L clearly showing the parallel laminations within these deposits. Pencil for scale is 14 cm long. C) Hummocky cross-stratification of facies S_{HCS}. D) Interbedded fine-grained sandstone, siltstone, and shale of facies S_H. Dark flecks visible along bedding planes are charcoal and organic debris. Field notebook is 12 cm wide. E) Coarse-grained sandstone representative of facies S_C. F) Channel fill consisting of conglomerates and coarse-grained sandstone of facies C_C. This channel has several fining-upward packages with scoured bases and pinches out laterally. Rock hammer for scale. G) Clast-supported pebble conglomerate characteristic of facies C_T, with some sandy lenses shown. H) Facies S_M is poorly-sorted sandstone with scattered organic debris and shell fragments. I) Facies S_F is fine-grained sandstone that is poorly exposed and easily weathered. This is an example of one of the best exposures of facies S_F. J) Laminated shale, characteristic of facies M.

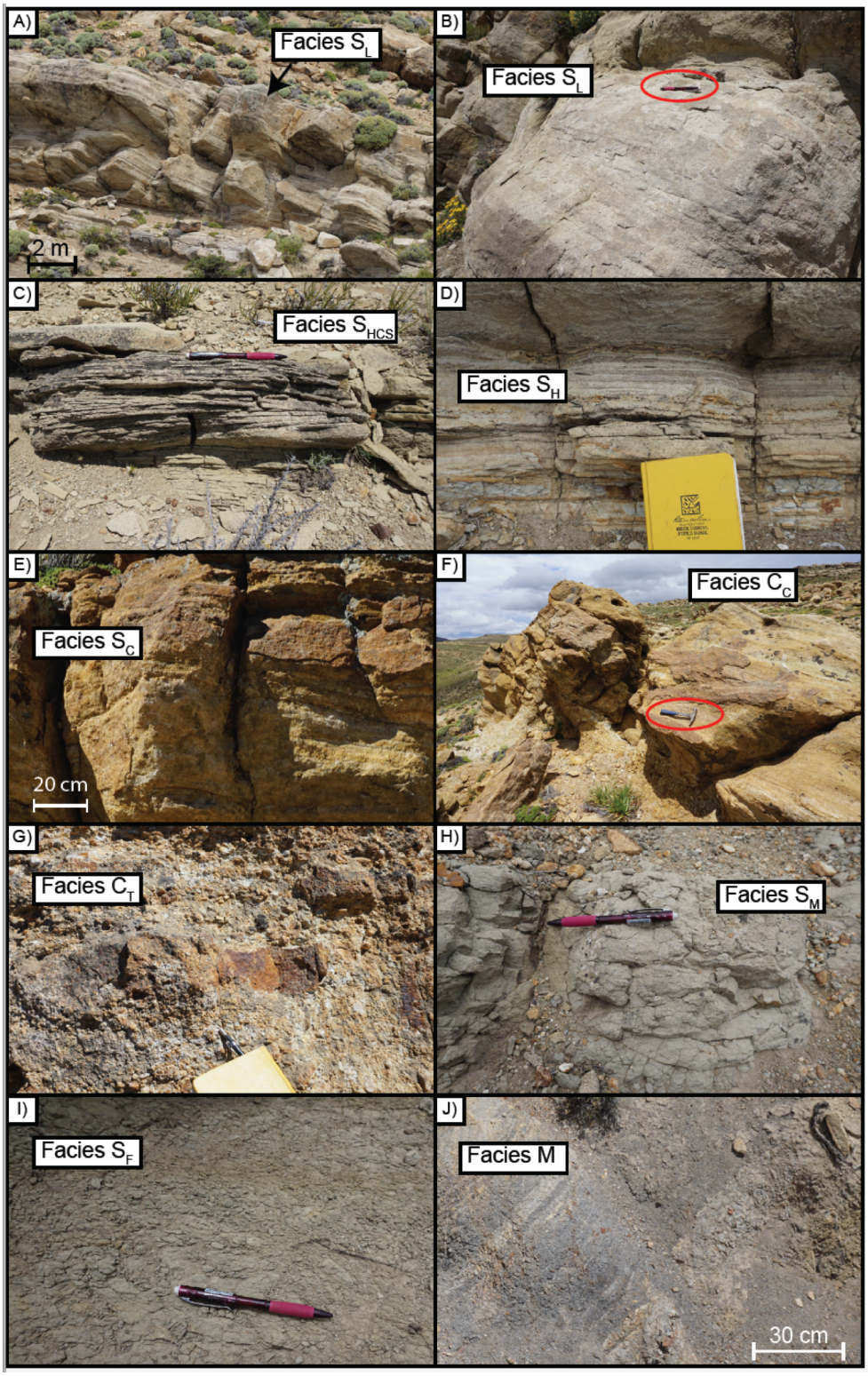
A)
Facies S_L
2 m
B)
Facies S_L
C)
Facies S_{HCS}
D)
Facies S_H
E)
Facies S_C
20 cm
F)
Facies C_C
G)
Facies C_T
H)
Facies S_M
I)
Facies S_F
J)
Facies M
30 cm

Figure 20. Photos of sedimentary structures and outcrop features. A) and B) examples of bioturbation within facies S_L. B) Bi-directional cross stratification at the top of a hyperpycnal lobe. Cross-stratification directions indicated by white arrows. D) Scoured surface filled with coarse-grained sandstone at the top of a bedset of facies S_L. Scour-and-fill structures such as these may be formed by reworking of sediment by storms or tides, or may reflect pulses in flood strength. E) Aligned organic material and charcoal at the base of a bed of facies S_L. F) Large charcoal fragment aligned with a bedding plane of facies S_L.

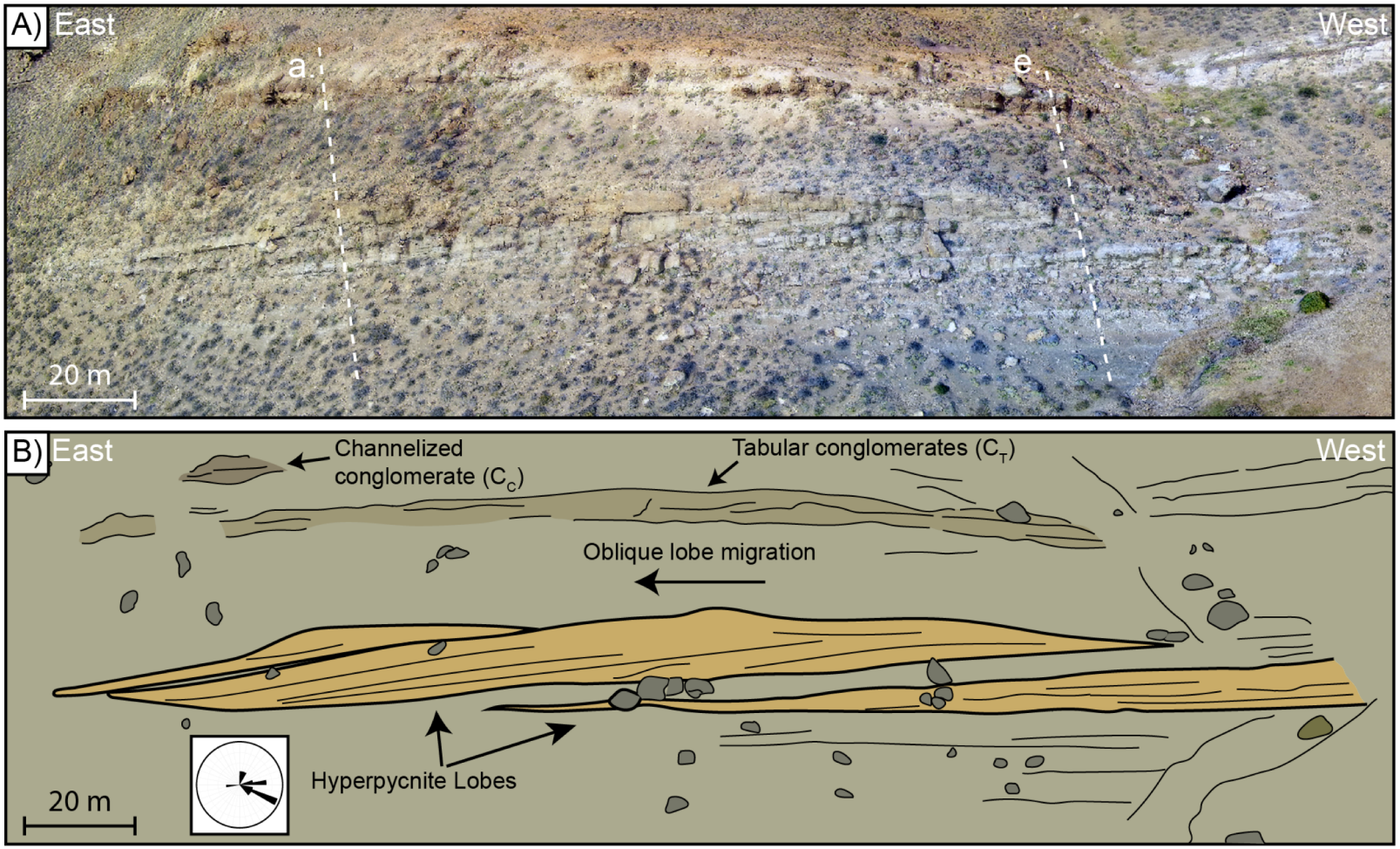
A) East
West
a
e
20 m
B) East
West
Channelized conglomerate (C_C)
Tabular conglomerates (C_T)
Oblique lobe migration
Hyperpycnite Lobes
20 m

Figure 21. (previous page) Outcrop geometry and stacking patterns. A) Composite drone photo of the study area. Eastward progradation of hyperpycnal sand lobes is visible in the middle of the section. Coarse-grained sandstones and conglomerates of facies S_C, C_T, and C_C form resistant beds at the top of the section. Locations of two measured sections (a and e) are included for reference. B) Simplified interpretation of outcrop geometry. Hyperpycnal sand lobes are outlined and highlighted in yellow. Packages of facies S_C and C_T are shaded in dark green, and a channel of facies C_C in the top-left corner is shaded in grey-brown. Rose diagram of paleocurrent measurements (n=13) indicates primarily east-southeast directed paleoflow directions.

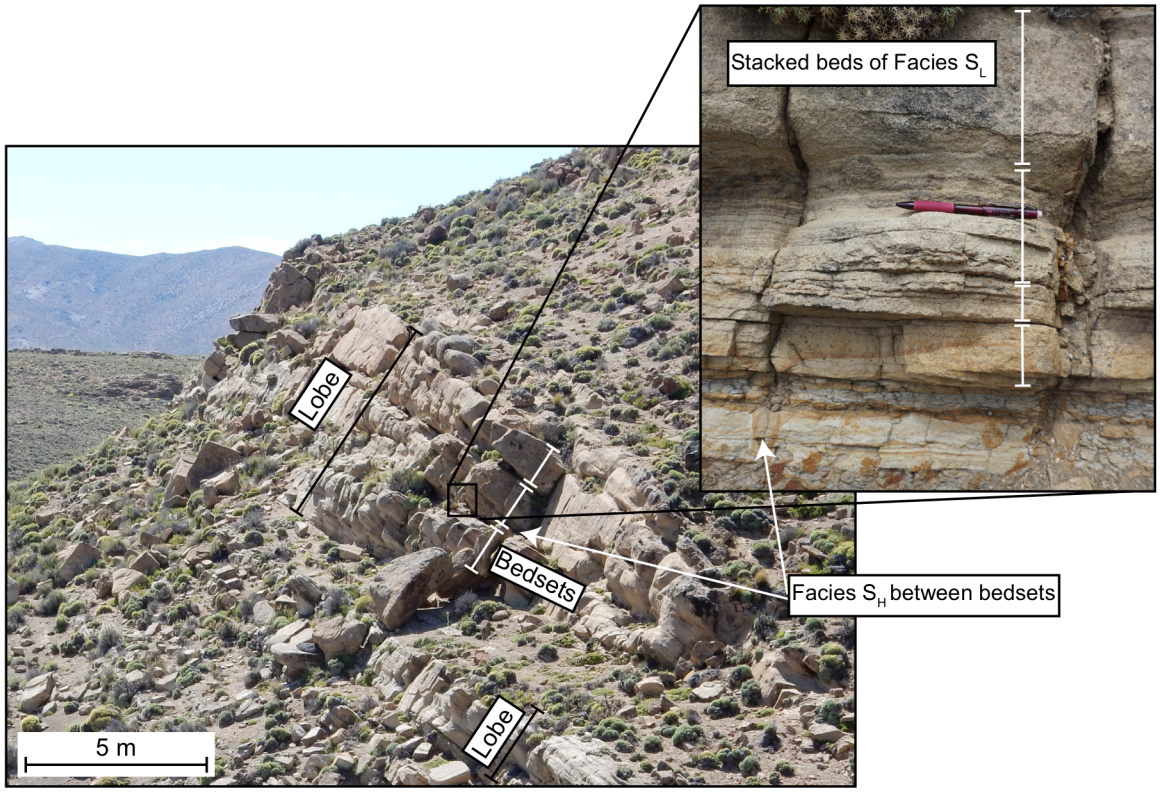

Figure 22. Hierarchy of Lajas hyperpycnites. View is of outcrop from Fig. 21, looking towards the east. Two hyperpycnal lobes can be seen stacked on top of one another, the upper lobe is thicker and is composed of several stacked bedsets. Inset photo shows a bedset composed of multiple beds, ranging in thickness from cm- to dm-scale. The wedge-shaped geometry and convex-up top surface of the sandstone lobes can be observed from this angle. Finer-grained, heterolithic beds of facies S_H lie between lobes and between bedsets.

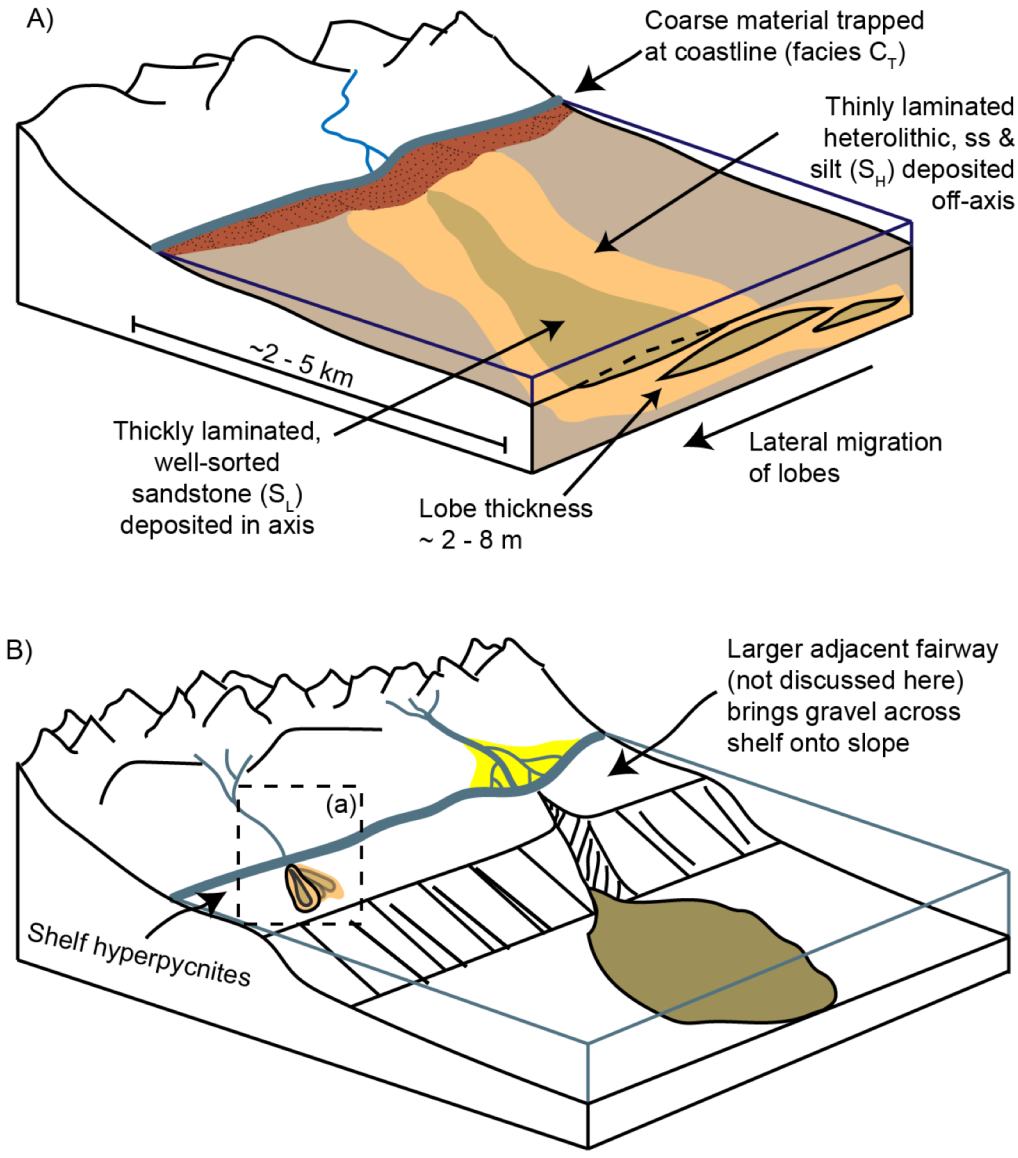

Figure 23. Schematic paleogeography of hyperpycnal shelf systems. A) Deposition of hyperpycnal lobes on the continental shelf offshore from small rivers. Coarse-grained material remains near the coastline due to low flow competence (shown in red). Dimensions may vary, but estimates based on modern systems (Steel et al., 2016) and on this study are provided. B) View of shelf hyperpycnites in a larger context. Small rivers induce hyperpycnal currents and deposit sand lobes on the shelf. Lateral to shelf systems, larger rivers bypass the continental shelf and feed coarse-grained material directly onto the slope or basin floor.

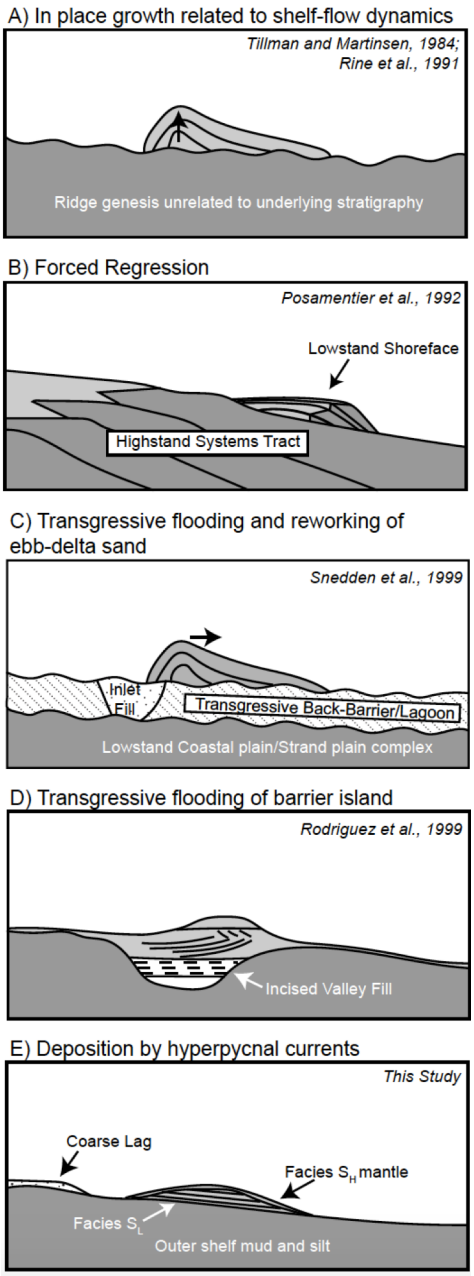

Figure 24. Models for formation of isolated shelf sand bodies, modified from Snedden et al. (1999). A) In-place ridge growth from shelf currents, B) Lowstand shoreface deposits from rapid forced regression, C) Reworking of ebb tidal delta sand during transgression, D) reworking of overstepped barrier island sediment during transgression, E) Deposition by hyperpycnal currents (this study).

4.8 ACKNOWLDEGEMENTS

Thank you to Elisa Medri, who served as both an excellent field assistant and a helpful translator. Thank you to Tanya Atwater and her Global Field Travel Grant for travel funding. Acknowledgement is made to the donors of the American Chemical Society Petroleum Research Fund for support of this research. We also thank PlusPetrol, YPF, and Shell for enthusiastic field discussion and financial support of the La Jardinera Project, of which this work is a part.

4.9 REFERENCES CITED

Bates, C.C., 1953, Rational Theory of Delta Formation: American Association of Petroleum Engineers Bulletin, v. 9, p. 2119-2162.

Bergman, K.M., and Snedden, J.W., eds., 1999, Isolated shallow marine sand bodies: Sequence stratigraphic analysis and sedimentologic interpretation: SEPM Special Publication No. 64, 362 p.

Berné, S., Lericolais, G., Marsset, T., Bourillet, J.F., and De Batist, M., 1998, Erosional offshore sand ridges and lowstand shorefaces: examples from tide-and wave-dominated environments of France: Journal of Sedimentary Research, v. 68, no. 4, p. 540-555.

Best, J.L., Kostaschuk, R.A., Peakall, J., Villard, P.V., and Franklin, M., 2005, Whole flow field dynamics and velocity pulsing within natural sediment-laden underflows: Geology, v. 33, no. 10, p. 765-768.

Cacchione, D. A., and Drake, D. E., 1990, Shelf sediment transport: an overview with applications to the northern California continental shelf, *in* LeMehaute, B., and

Handes, M.D., eds., The Sea, v. 9, Ocean Engineering Science: New York, Wiley Interscience, p. 729-773.

DiBiase, R.A. and Lamb, M.P., 2013, Vegetation and wildfire controls on sediment yield in bedrock landscapes: Geophysical Research Letters, v. 40, no. 6, p.1093-1097.

Dott, R.H. and Bourgeois, J., 1982, Hummocky stratification: significance of its variable bedding sequences: Geological Society of America Bulletin, v. 93, no. 8, p. 663-680.

Florsheim, J.L., Keller, E.A. and Best, D.W., 1991, Fluvial sediment transport in response to moderate storm flows following chaparral wildfire, Ventura County, southern California: Geological Society of America Bulletin, v. 103, no. 4, p. 504-511.

Franzese, J.R., and Spalletti, L.A., 2001, Late Triassic-early Jurassic continental extension in southwestern Gondwana: tectonic segmentation and pre-break-up rifting: Journal of South American Earth Sciences, v. 14, p. 257-270.

Franzese, J.R., Spalletti, L.A., Perez, I.G., and Macdonald, D., 2003, Tectonic and paleoenvironmental evolution of the Mesozoic sedimentary basins along the Andean foothills of Argentina (32°– 54°S): Journal of South American Earth Sciences, v. 16, p. 81-90.

Franzese, J.R., Viega, G.D., Schwarz, E., and Gomez-Perez, I., 2006, Tectonostratigraphic evolution of a Mesozoic graben border system: the Chachil depocentre, southern Neuquén Basin, Argentina: Journal of the Geological Society of London, v. 163, p. 207-221.

Gladstone, C., and Pritchard, D., 2010, Patterns of deposition from experimental turbidity currents with reversing buoyancy: Sedimentology, v. 57, no. 1, p. 53-84.

Gradstein, F.M., Agterberg, F.P., Ogg, J.G., Hardenbol, J., van Veen, P., Thierry, J., and Huang, Z., 1994, A Mesozoic time scale: Journal of Geophysical Research, v. 99, no. B12, p. 24,051 – 24, 074.

Hamblin, A.P. and Walker, R.G., 1979, Storm-dominated shallow marine deposits: the Fernie-Kootenay (Jurassic) transition, southern Rocky Mountains: Canadian Journal of Earth Sciences, v. 16, p. 1673-1690.

Harms, J.C., Southard, J.B., Spearing, D.R., and Walker, R.G., 1975, Depositional environments as interpreted from primary sedimentary structures and stratification sequences: Society of Economic Paleontologists and Mineralogists Short Course Notes no. 2, 161 p.

Hogg, A.J., Huppert, H.E., and Hallworth, M.A., 1999, Reversing buoyancy of particle-driven gravity currents: Physics of Fluids, v. 11, p. 2891, doi:10.1063/1.870147.

Houbolt, J., 1968, Recent sediments in the southern Bight of the North Sea: Geologie En Mijnbouw, v. 47, p. 245-273

Howell, J.A., Schwarz, E., Spalletti, L.A., and Veiga, G.D., The Neuquén Basin: an overview, in: Veiga, G.D., Spalletti, L.A., Howell, J.A., and Schwarz E., Eds., 2005, The Neuquén Basin, Argentina: A Case Study in Sequence Stratigraphy and Basin Dynamics: Geological Society of London, Special Publications, v. 252, p. 1-14.

Hurzeler, B.E., Ivey, G.N., and Imberger, J., 1995, Spreading model for a turbidity current with reversing buoyancy from a constant-volume release: Marine & Freshwater Research, v. 46, p. 393–408.

Introcaso, A., Pacino, M.C., and Fraga, H., 1991, Gravity, isostasy, and Andean crustal shortening between latitudes 30 and 35°S: Tectonophysics, v. 205, p. 31-48.

Lamb, M. P., Myrow, P. M., Lukens, C., Houck, K., and Strauss, J., 2008, Deposits from wave-influenced turbidity currents: Pennsylvanian Minturn Formation, Colorado, U.S.A: Journal of Sedimentary Research, v. 78, no. 7, p. 480-498.

Leanza, H. A., 1981, Faunas de ammonites del Jurásico superior y del Cretácico inferior de América del Sur, con especial consideración de la Argentina: Cuencas sedimentarias del Jurásico y Cretácico de América del Sur, v. 2, p. 559-597.

Legarreta, L., and Gulisano, C.A., 1989, Analisis estratigrafico secuencial de la Cuenca Neuquina (Triasico superior – Terciario inferior, Argentina), *in:* Chebli, G., and Spalletti, L., eds., Cuencas Sedimentarias Argentinas., Serie Correlacion Geologica, Universidad Nacional de Tucuman, v. 6, p. 221-243.

Legarreta, L., and Uliana, M.A., 1991, Jurassic-Cretaceous marine oscillations and geometry of back arc basin fill, Central Argentine Andes, *in:* Macdonald, D.I.M., ed., Sedimentation, Tectonics, and Eustasy – Sea-level Changes at Active Margins., International Association of Sedimentologists, Special Publications, v. 12, p. 429-450.

Leva López, J., Rossi, V. M., Olariu, C. and Steel, R. J. (2016), Architecture and recognition criteria of ancient shelf ridges; an example from Campanian Almond Formation in Hanna Basin, USA. Sedimentology, 63: 1651–1676. doi:10.1111/sed.12279

Lowe, D. R., 1982, Sediment gravity flows: II Depositional models with special reference to the deposits of high-density turbidity currents: Journal of Sedimentary Research, v. 52, no. 1, p. 279-297.

Macquaker, J.H.S., Bentley, S.J., and Bohacs, K.M., 2010, Wave-enhanced sediment-gravity flows and mud dispersal across continental shelves: Reappraising sediment transport

processes operating in ancient mudstone successions: Geology, v. 38, no. 10, p. 947-950.

Miall, A.D., 1977, A review of the braided-river depositional environment: Earth-Science Reviews, v. 13, no. 1, p. 1-62.

Middleton, G.V., and Hampton, M.A., 1976, Subaqueous sediment transport and deposition by sediment gravity flows: mechanics of flow and deposition, *in:* Middleton, G.V., Bouma, A.H., eds., Turbidites and Deep Water Sedimentation: Society of Economic Paleontologists and Mineralogists, Pacific Section Short Course Notes, p. 1 -38.

Midtgaard, H., 1996, Inner-shelf to lower shoreface hummocky sandstone bodies with evidence for geostrophic-influenced compbined flow, Lower Cretaceous, West Greenland: Journal of Sedimentary Research, v. 66, p. 343-353.

Mulder, T., and Syvitski, J.P., 1995, Turbidity currents generated at river mouths during exceptional discharges to the world oceans: The Journal of Geology, v. 103, p. 285-299.

Mulder, T., Migeon, S., Savoye, B., and Jouanneau, J.M., 2001, Twentieth century floods recorded in the deep Mediterranean sediments: Geology, v. 29, no. 11, p. 1011-1014.

Mulder, T., and Alexander, J., 2001, The physical character of subaqueous sedimentary density flows and their deposits: Sedimentology, v. 48, p. 269-299.

Mulder, T., Syvitski, J.P.M., Migeon, S., Faugeres, J.C., and Savoye, B., 2003, Marine hyperpycnal flows: initiation, behavior and related deposits. A review: Marine and Petroleum Geology, v. 20, p. 861-882.

Mutti, E., Davoli, G., Tinterri, R., and Zavala, C., 1996, The importance of ancient fluvio-deltaic systems dominated by catastrophic flooding in tectonically active basins: Memorie de Scienze Geologiche, v. 48, p. 233-291.

Mutti, E., Tinterri, R., Benevelli, G., di Biase, D., and Cavanna, G., 2003, Deltaic, mixed and turbidite sedimentation of ancient foreland basins: Marine and Petroleum Geology, v. 20, p. 733-755.

Myrow, P.M., and Southard, J.B., 1996, Tempestite Deposition: Journal of Sedimentary Research, v. 66, no. 5, p. 875-887.

Myrow, P.M., Lukens, C., Lamb, M.P., Houck, K., and Strauss, J., 2008, Dynamics of a transgressive prodeltaic system: implications for geography and climate within a Pennsylvanian intracratonic basin, Colorado, U.S.A.: Journal of Sedimentary Research, v. 78, p. 512-528.

Normark, W. R., and Piper, D. J. W., 1991, Initiation processes and flow evolution of turbidity currents: Implications for the depositional record: Shoreline to Abyss: SEPM Special Publication, v. 46, p. 207-230.

Paim, P.S., Silveira, A.S., Lavina, E.L., Faccini, U.F., Leanza, H.A., de Oliveira, J.T. and D'Avila, R.S., 2008, High resolution stratigraphy and gravity flow deposits in the Los Molles Formation (Cuyo Group, Jurassic) at La Jardinera region, Neuquén Basin, *in:* Revista de la Asociación Geológica Argentina. Simposio Jurásico de América del Sur, v. 63, no. 4, p. 728-753

Pattison, S.A.J., 2005, Storm-influenced prodelta turbidite complex in the lower Kenilworth Member at Hatch Mesa, Book Cliffs, Utah, U.S.A.: Implications for shallow marine facies models: Journal of Sedimentary Research, v. 75, no. 3, p. 420-439.

Petter, A.L., and Steel, R.J., 2006, Hyperpycnal flow variability and slope organization on an Eocene shelf margin, Central Basin, Spitsbergen, American Association of Petroleum Geologists Bulletin, v. 90, no. 10, p. 1451-1472.

Plink-Bjorklund, P. and Steel, R.J., 2004, Initiation of turbidity currents: outcrop evidence for Eocene hyperpycnal-flow turbidites: Sedimentary Geology, v. 165, p. 29-52.

Posamentier, H.W., Allen, G.P., James, D.P. and Tesson, M,1992, Forced regressions in a sequence stratigraphic framework: concepts, examples, and exploration significance: AAPG Bulletin , v. 76, p. 1687-1709.

Pritchard, D., and Gladstone, C., 2009, Reversing buoyancy in turbidity currents: Developing a hypothesis for flow transformation and for deposit facies and architecture: Marine and Petroleum Geology, v. 26, p. 1997–2010.

Reynaud, J.Y., and Dalrymple, R.W., 2012, Shallow-Marine Tidal Deposits, *in:* Davis, R.A. Jr. and Reynaud, J.Y., Principles of Tidal Sedimentology: Springer Netherlands, p. 335-369.

Riccardi, A.C., 1983, The Jurassic of Argentina and Chile, *in*: M. Moullade and A.E.M. Nairn, Eds., The Phanerozoic geology of the world II, the Mesozoic, B: Amsterdam, Elsevier, p. 201-263.

Rine, J.M., Tillman, R.W., Culver, S.J., and Swift, D.J.P., 1991, Generation of Late Holocene ridges on the middle continental shelf of New Jersey, USA – Evidence for formation in a mid-shelf setting based upon comparison with a nearshore ridge, In: Swift, D.J.P., Oertel, G.F., Tillman, R.W., and Thorne, J.A., eds., Shelf sand and sandstone, Geometry, Facies, and Sequence Stratigraphy: Oxford, International Association Sedimentologists Special Publication 14, p. 395-426.

Rodriguez, A.B., Anderson, J.B., Siringan, F.P., and Taviani, M., 1999, Sedimentary facies and genesis of Holocene sand banks on the east Texas inner continental shelf, In: Bergman, K.M., and Snedden, J.W., eds., Isolated shallow marine sand bodies: sequence stratigraphic analysis and sedimentologic interpretation: Society for Sedimentary Geology, Special Publication 64, p. 165-178.

Silins, U., Stone, M., Emelko, M.B., and Bladon, K, 2009, Sediment production following severe wildfire and post-fire salvage logging in the Rocky Mountain headwaters of the Oldman River Basin, Alberta: Catena, v. 79, no. 3, p. 189-197.

Snedden, J.W., Kreisa, R.D., Tillman, R.W., Culver, S.J., and Schweller, W.J., 1999, An expanded model or modern shelf sand ridge genesis and evolution on the New Jersey Atlantic shelf, In: Bergman, K.M., and Snedden, J.W., eds., Isolated shallow marine sand bodies: sequence stratigraphic analysis and sedimentologic interpretation: Society for Sedimentary Geology, Special Publication 64, p. 147-163.

Sparks, R. S. J., Bonnecaze, R. T., Huppert, H. E., Lister, J. R., Hallworth, M. A., Mader, H., and Phillips, J., 1993, Sediment-laden gravity currents with reversing buoyancy: Earth and Planetary Science Letters, v. 114, no. 2, p. 243-257.

Steel, E., Simms, A.R., Warrick, J., and Yokoyama, Y., 2016, Highstand shelf fans: The role of buoyancy reversal in the deposition of a new type of shelf sand body: Geological Society of America Bulletin, v. 128, no. 11-12, p. 1717-1724.

Steel, E., Buttles, J., Simms, A., Mohrig, D., and Meiburg, E., 2017, The role of buoyancy reversal in turbidite deposition and submarine fan geometry: Geology, v. 45, no. 1, p. 35-38.

Steel, R.J., Olariu, C., Rossi, V.M., Almeida, F., and Steel, E., 2017, Mid-Jurassic Shelf-Margin Growth in Neuquén Basin: Coarse-grained, river-tide interaction at the shelf edge, AAPG Annual Convention and Exhibition.

Tillman, R.W., and Martinsen, R.S., 1984, The Shannon shelf ridge sandstone complex, Salt Creek Anticline area, Powder River Basin, Wyoming, In: Tillman, R.W. and Siemers, C.T., eds., Siliciclasitc Shelf Sediments: Society for Sedimentary Geology, Special Publication 34, p. 1-34.

Tudor, E.P., 2014, Facies variability in deep water channel-to-lobe transition zone: Jurassic Los Molles Formation Neuquén Basin Argentina, M.S. Thesis, University of Texas at Austin, 90 p.

Uliana, M.A., Biddle, K.T., and Cerdan, J., 1989, Mesozoic extension and the formation of Argentine sedimentary basins, In: A.J. Tankard and H.R. Balkwill, Eds., Extensional Tectonics and Stratigraphy of the North Atlantic Margins: American Association of Petroleum Geology, Memoirs, V. 46, p. 509-614.

Vann, N.K., 2013, Slope to basin-floor evolution of channels to lobes, Jurassic Los Molles Formation, Neuquén Basin, Argentina: M.S. Thesis, University of Texas at Austin, 95 p.

Vergani, G. D., A. J. Tankard, H. J. Belotti, and H. J. Welsink, 1995, Tectonic evolution and paleogeography of the Neuquén basin, Argentina, *in:* A. J. Tankard, R. Suárez S., and H.J. Welsink, Petroleum basins of South America: AAPG Memoir 62, p. 383–402

Viega, G.D., 1998, Estratigrafíasecuencial en series continentales: aplicación a los depósitos de la Formación Challacó, Jurásico de la cuenca neuquina austral (Republica Argentina): Sociedad Geológica de España Revista, v. 11, p. 95-109.

Warrick, J.A., Simms, A.R., Ritchie, A., Steel, E., Dartnell, P., Conrad, J.E., and Finlayson, D.P., 2013, Hyperpycnal plume-derived fans in the Santa Barbara Channel, California: Geophysical Research Letters, v. 40, p. 2081–2086.

Wright, L. D., W. J. Wiseman, B. D. Bornhold, B. D. Prior, J. N. Suhayda, G. H. Keller, Z.-S. Yang, and Y. B. Fan, 1988, Marine dispersal and deposition of Yellow River silts by gravity-driven underflows: Nature, v. 332, p. 629– 632, doi:10.1038/332629a0.

Wright, L.D., and Friedrichs, C.T., 2006, Gravity-driven sediment transport on continental shelves: a status report: Continental Shelf Research, v. 26, p. 2092-2107.

Yrigoyen, M.R., 1991, Hydrocarbon resources from Argentina, In: World Petroleum Congress, Buenos Aires: Petrotecnia, v. 13, Special Issue, p. 38-54.

Zavala, C., Ponce, J. J., Arcuri, M., Drittanti, D., Freije, H., and Asensio, M., 2006, Ancient lacustrine hyperpycnites: A depositional model from a case study in the Rayoso Formation (Cretaceous) of west-central Argentina: Journal of Sedimentary Research, v. 76, no. 1, p. 41-59.

Zavala, C., Arcuri, M., Di Meglio, M., Diaz, H.G., and Contreras, C., 2011, A genetic facies tract for the analysis of sustained hyperpycnal flow deposits: in Slatt, R.M., and Zavala, C., eds., Sediment transfer from shelf to deep water – revisiting the delivery system: AAPG Studies in Geology 61, p. 31-51

Zavala, C., Arcuri, M., and Blanco Valiente, L., 2012, The importance of plant remains as a diagnostic criteria for the recognition of ancient hyperpycnites: Revue de Paleobiologie, v.11, p. 457-469.

Zavala, C., and Arcuri, M., 2016, Intrabasinal and extrabasinal turbidites: Origin and distinctive characteristics: Sedimentary Geology, v. 337, p. 36-54.

CHAPTER 5

FINAL REMARKS

The studies presented here demonstrate that hyperpycnal currents are capable of depositing sand bodies on the continental shelf. These sand bodies are likely to have high length-to-width ratios and consist largely of well-sorted fine or medium-grained sand. Holocene deposits on the shelf of the Santa Barbara Channel in southern California support previous work that highlights the role of small, mountainous rivers in the delivery of sediment to the continental shelf (Chapter 2; Milliman and Syvitski, 1992; Mulder and Syvitski, 1995). In addition to documenting the deposition and survival of river-derived sediment on the continental shelf, deposits in the Santa Barbara Channel provide a unique opportunity to sample Holocene shelf hyperpycnites and to compare them to existing facies models. The Santa Barbara Channel hyperpycnites are distinct from classic turbidites in their well-sorted nature, but also in their narrow, elongate morphology. Lofting, or buoyancy reversal, provides an explanation for both the grain sorting and the lobe geometry within these hyperpycnites. Turbidity currents that undergo lofting will be stripped of their finest grain sizes, leaving behind a well-sorted sand body (Walker and McBroome, 1983; Pritchard and Gladstone, 2009; Zavala and Arcuri, 2016). Furthermore, flume experiments suggest that lofting will hinder lateral spreading of turbidity currents and result in the deposition of narrower deposits than expected of currents that remain ground-hugging (Chapter 3).

The flume experiments discussed in Chapter 3 demonstrate that a turbidity current with light interstitial fluid will spread laterally until enough sediment has been deposited to induce lofting at the edges and at the head of the current. Beyond the lofting point, lateral spreading of the current will cease and the current will maintain a constant width. The strong correlation between turbidity current width and deposit width results in lofted turbidites with higher length-to-width ratios than those deposited by currents that remain ground-hugging. Furthermore, factors that push the lofting point basinward, such a higher initial sediment concentrations or steeper basin gradients result in wider currents and therefore wider deposits.

Jurassic hyperpycnites deposited on the shelf of the Neuquén basin of southwestern Argentina share many similarities with shelf hyperpycnites of the Santa Barbara Channel (Chapter 4). Both systems display well-sorted, lobate sand bodies that lie offshore from small fluvial systems. Terrestrial organic material is commonly used as a diagnostic criterion for hyperpycnites and is present in both the modern and ancient systems discussed here (Plink-Bjorklund and Steel, 2004; Zavala et al., 2006; Myrow et al., 2008; Zavala et al., 2012). The outcrops in the Neuquén basin provide a detailed view of the stratigraphic architecture and the stacking patterns of hyperpycnal lobes that is difficult to achieve with sediment cores. However, bathymetric surveys over the modern Santa Barbara Channel shelf provide an excellent view of the three-dimensional morphology of hyperpycnites, which is challenging to fully understand from outcrop geology. Furthermore, flume experiments provide the opportunity to understand the dynamics of hyperpycnal currents and the effects of various factors such as fluid density, sediment concentration, and basin geometry. Combining results from Holocene shelf sediments, outcrop stratigraphy, and analog experiments provides a

broader understanding of hyperpycnal current dynamics and the ways in which these processes are manifested in the resulting deposits.

Shelf hyperpycnites remain largely overlooked within source-to-sink systems. Continental shelves are flooded during sea-level highstand, causing many rivers to become disconnected from their associated deepwater fans (Posamentier and Allen, 1999). However, small, mountainous rivers can trigger hyperpycnal currents that are capable of delivering sand beyond the high-energy shoreline and depositing lobate sand bodies during sea-level highstand. These sand bodies provide a connection between continental and marine environments and may serve as archives of extreme river floods. Yet, accurate interpretation of these archives necessitates more examples of shelf hyperpycnites in both modern and ancient basins. Broader recognition of these features and refinement of hyperpycnite facies models is critical to preventing misinterpretation of shelf hyperpycnites as fluvial deposits or as deepwater turbidites.

REFERENCES

Milliman, J.D., and Syvitski, J.P.M, 1992, Geomorphic/tectonic control of sediment discharge to the ocean: Importance of small mountainous rivers: The Journal of Geology, v. 100, p. 525-544.

Mulder, T., and Syvitski, J.P., 1995, Turbidity currents generated at river mouths during exceptional discharges to the world oceans: The Journal of Geology, v. 103, p. 285-299.

Myrow, P.M., Lukens, C., Lamb, M.P., Houck, K., and Strauss, J., 2008, Dynamics of a transgressive prodeltaic system: Implications for geography and climate with a

Pennsylvanian intracratonic basin: Journal of Sedimentary Research, v. 78, p. 512-528.

Walker, G. P., and McBroome, L. A., 1983, Mount St. Helens 1980 and Mount Pelée 1902—flow or surge?: Geology, v. 11, no. 10, p. 571-574.

Plink-Bjorklund, P. and Steel, R.J., 2004, Initiation of turbidity currents: outcrop evidence for Eocene hyperpycnal-flow turbidites: Sedimentary Geology, v. 165, p. 29-52

Posamentier, H. W., and Allen, G. P., 1999, Siliciclastic sequence stratigraphy: Concepts and applications: Tulsa, Oklahoma, Society for Sedimentary Geology, SEPM concepts in sedimentology and paleontology no. 7, 205 p.

Pritchard, D., and Gladstone, C., 2009, Reversing buoyancy in turbidity currents: Developing a hypothesis for flow transformation and for deposit facies and architecture: Marine and Petroleum Geology, v. 26, p. 1997–2010.

Zavala, C., Ponce, J. J., Arcuri, M., Drittanti, D., Freije, H., and Asensio, M., 2006, Ancient lacustrine hyperpycnites: A depositional model from a case study in the Rayoso Formation (Cretaceous) of west-central Argentina: Journal of Sedimentary Research, v. 76, no. 1, p. 41-59.

Zavala, C., Arcuri, M., and Blanco Valiente, L., 2012, The importance of plant remains as a diagnostic criteria for the recognition of ancient hyperpycnites: Revue de Paleobiologie, v.11, p. 457-469.

Zavala, C., and Arcuri, M., 2016, Intrabasinal and extrabasinal turbidites: Origin and distinctive characteristics: Sedimentary Geology, v. 337, p. 36-54.

APPENDIX I – SEISMIC DATA COLLECTED FROM REFUGIO CREEK FAN, SANTA BARBARA CHANNEL, CA

Seismic lines collected from the Refugio fan in September 2012. (a) Line A-A′ crosses several lobes of the fan. The base of the fan is indicated by the semi-continuous reflection marked in red. Some faint reflections are also apparent above this surface and potentially represent overlying flow packages. (b) Line B-B′ shows clearly the continuous hard reflection truncating abundant southward-dipping reflections. This surface is interpreted as separating deformed Plio-Pleistocene strata from Upper Pleistocene-Holocene deposits. (c) Map of the Refugio fan indicating locations of a and b.

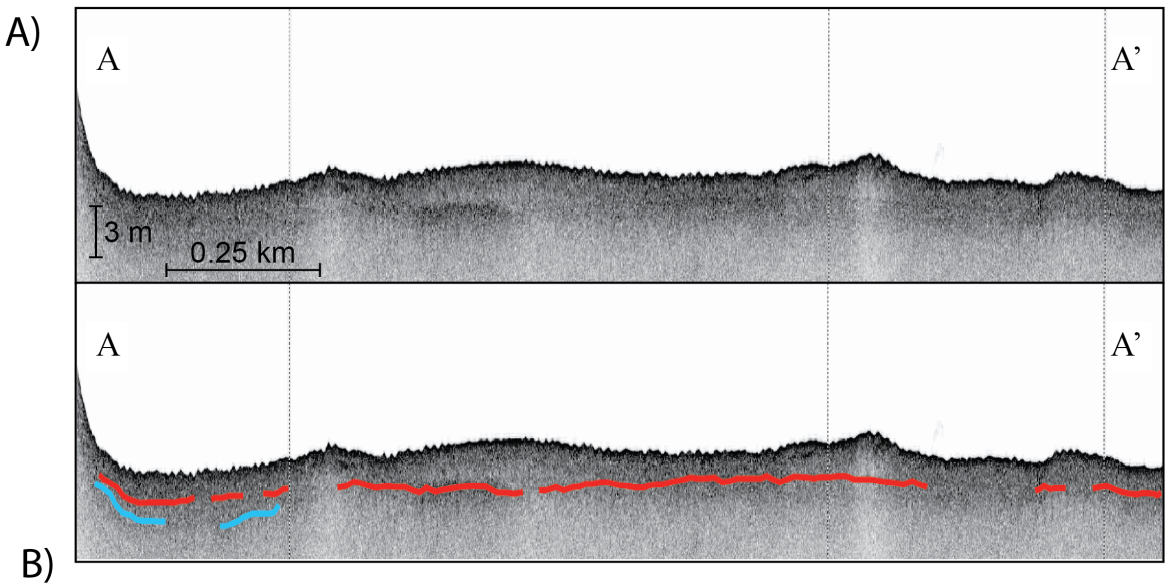
A)
A
A'
3 m
0.25 km
A
A'

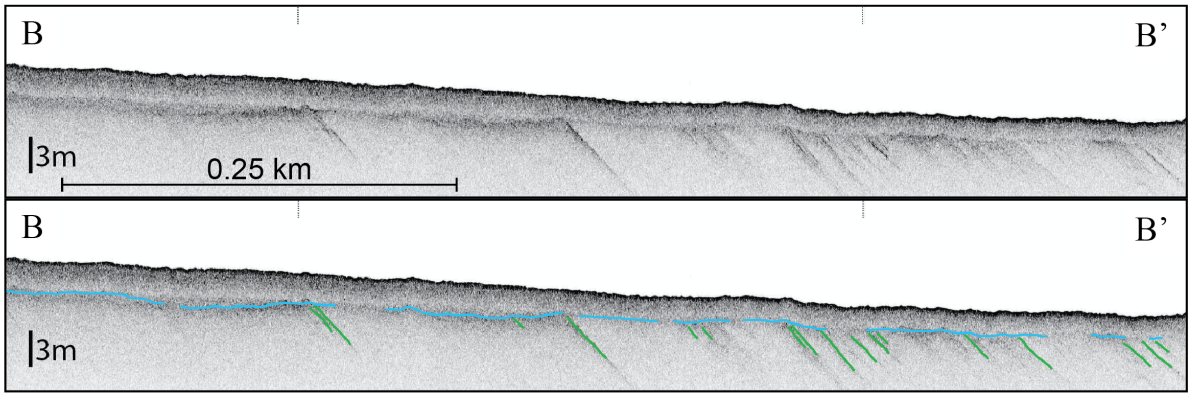
B)
B
B'
3m
0.25 km
B
B'
3m

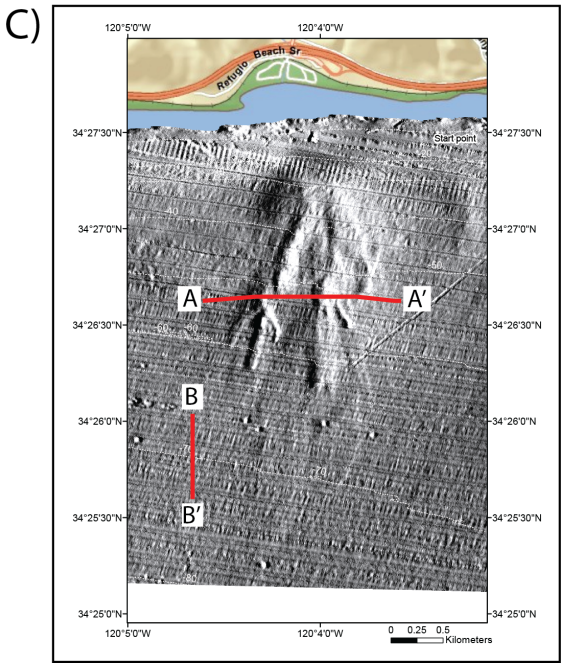
C)
120°5'0"W
120°4'0"W
Refugio Beach Sr
34°27'30"N
34°27'0"N
34°26'30"N
34°26'0"N
34°25'30"N
34°25'0"N
Start point
A
A'
B
B'
0 0.25 0.5
Kilometers

APPENDIX II – RADIOCARBON AGES FOR SANTA BARBARA CHANNEL HYPERPYCNITES

APPENDIX I. ALL RADIOCARBON AGES FROM THE TAJIGUAS FAN AND REFUGIO FAN

Lab ID	Core Name	Depth (cm)	Material	$\delta^{13}C$ (per mil)	^{14}C age ± 1σ (years BP)	Calibrated Age (Cal years BP)*
YAUT-007625	TG13-01	10	Bivalve	3.5	1215 ± 18	412 - 714
UCIAMS 186388[a]	TG13-01	23	Plant	-	1965 ± 20	1871 - 1984
UCIAMS 186389	TG13-01	43	Plant	-	1830 ± 20	1714 - 1820
UCIAMS 186390	TG13-01	68	Plant	-	2085 ± 20	1997 - 2118
UCIAMS 186391	TG13-01	114	Plant	-	3050 ± 20	3181 - 3344
UCIAMS 186392	TG13-01	124	Plant	-	4150 ± 20	4584 - 4822
UCIAMS 186393	TG13-01	143	Plant	-	5105 ± 25	5752 - 5917
UCIAMS 186394	TG13-02	17	Plant	-	4325 ± 20	4844 - 4960
D-AMS 008757	TG13-02	33	Plant	-29.1	6615 ± 35	7440 - 7568
D-AMS 008758	TG13-02	43	Plant	-14.3	7766 ± 36	8448 - 8603
D-AMS 008007	TG13-02	61	Plant	-28.4	4708 ± 29	5323 - 5579
D-AMS 008759	TG13-02	69	Plant	-17.0	4648 ± 33	5310 - 5467
UCIAMS 186395[b]	TG13-02	80	Plant	-	3270 ± 20	3452 - 3560
D-AMS 008008	TG13-02	87	Plant	-29.2	6739 ± 30	7568 - 7662
UCIAMS 186396[b]	TG13-02	113	Plant	-	3925 ± 15	4296 - 4422
D-AMS 008009	TG13-02	133	Plant	-23.7	7680 ± 36	8408 - 8542
UCIAMS 186397[a]	TG13-03	33	Plant	-	8960 ± 60	9910 - 10232
UCIAMS 186398[a]	TG13-03	51	Plant	-	1930 ± 20	1825 - 1924
D-AMS 008011	TG13-03	69	Plant	-26.7	427 ± 23	345 - 520
D-AMS 008010	TG13-03	122	Plant	-33.5	8619 ± 38	9529 - 9669
YAUT-007629	TG13-03	156	Bivalve	-0.23	9780 ± 29	10182 - 10617
D-AMS 008013	TG13-04	29	Plant	-10.3	2477 ± 30	2381 - 2721
UCIAMS 186399	TG13-04	60	Plant	-	8860 ± 40	9774 - 10164
UCIAMS 186400	TG13-04	116	Plant	-	11560 ± 700	11651 - 15693
D-AMS 008012	TG13-06	225	Plant	-11.9	10720 ± 43	12,590 - 12,728
YAUT-007630	RF13-01	81	Bivalve	4.66	5191 ± 22	4969 - 5507
YAUT-007631	RF13-01	160	Bivalve	1.64	5537 ± 22	5459 - 5876

*Bivalve ^{14}C ages were corrected using the Marine04 calibration curve and ΔR 252 ± 93 ^{14}C years (Hughen et al., 2004). Terrestrial ^{14}C ages were corrected using the IntCal04 calibration curve (Reimer et al., 2004). All dates were calibrated using Calib 7.0.7 (Stuiver and Reimer, 1993). Reported ages are 2σ values.

[a]Old ages are likely reworked material

[b]Ages are young and interpreted as contaminated samples because all other dates are in order if these are removed.

APPENDIX III – UNPUBLISHED CORE DESCRIPTIONS AND GRAIN SIZE FOR SANTA BARBARA CHANNEL HYPERPYCNITES

Cores descriptions and grain size measurements of TG13-05, TG13-06, and RF13-01 are presented below. Grain size was measured using a CILAS 1140 laser particle size analyzer. See Chapter 2 for methods and for core locations.

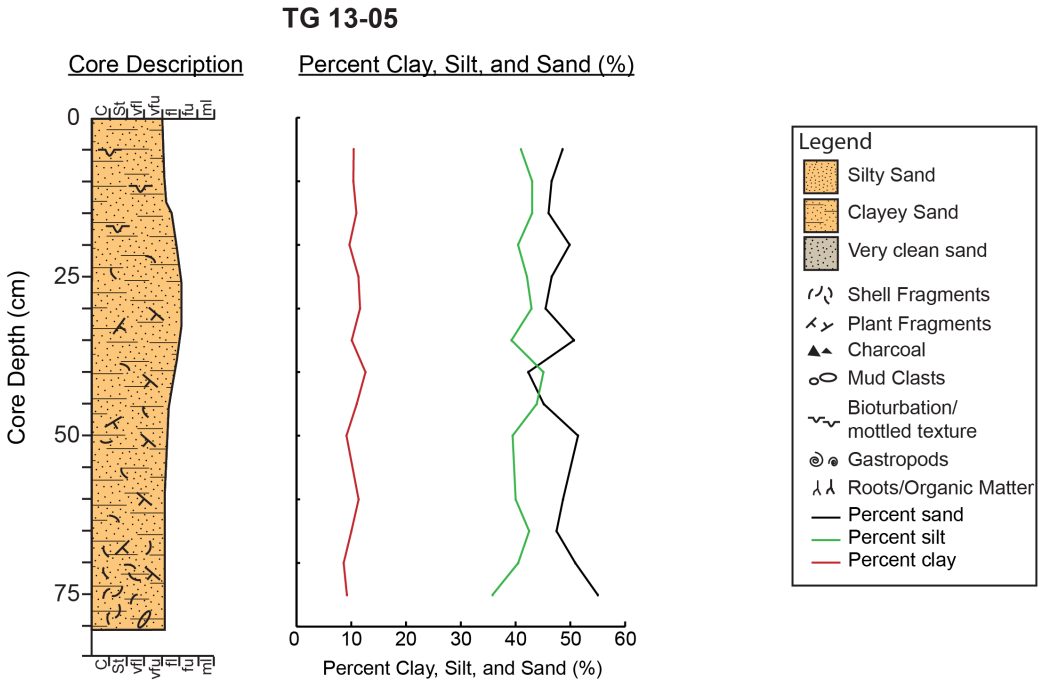

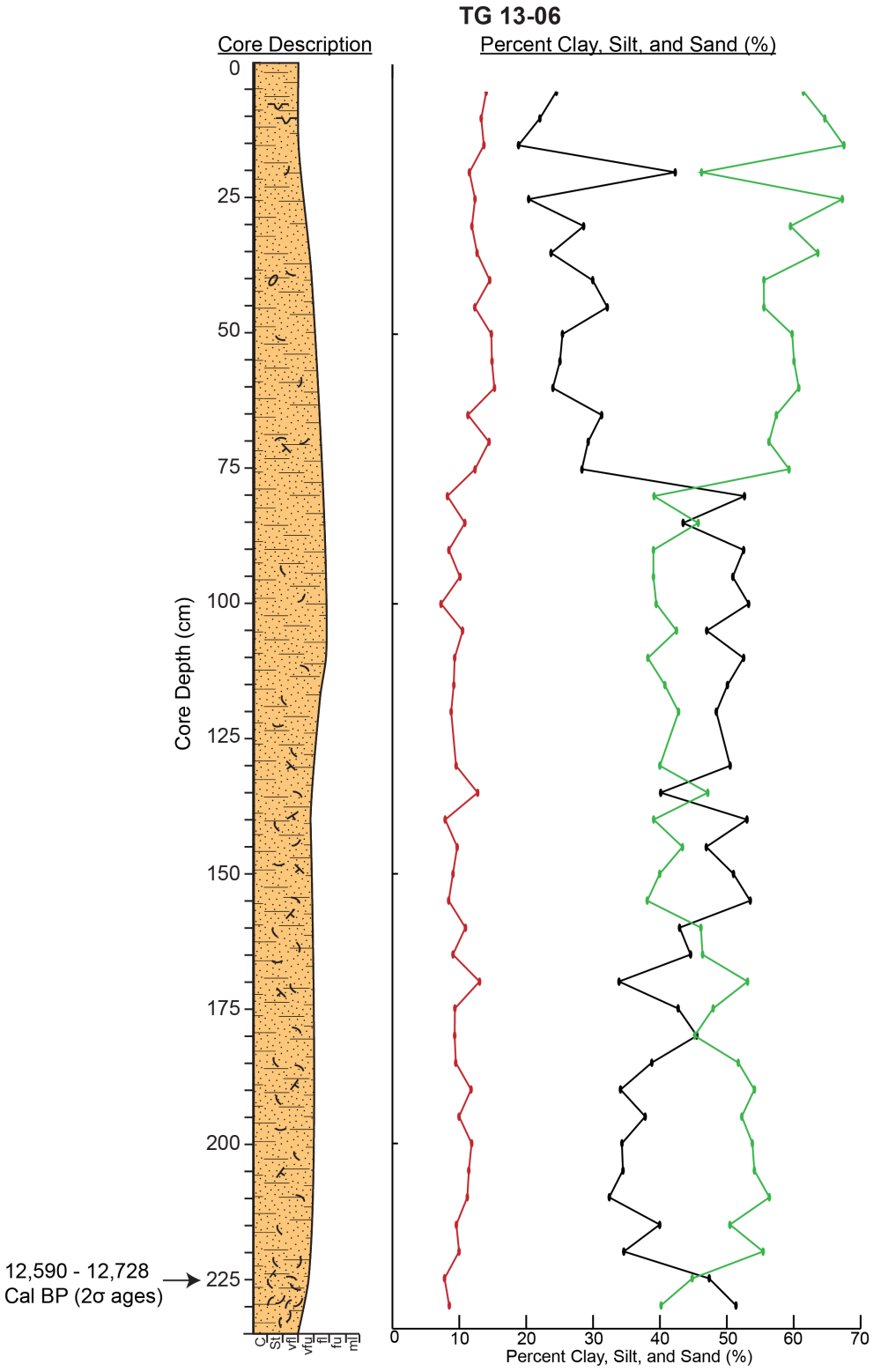
TG 13-06
Core Description
Percent Clay, Silt, and Sand (%)
Core Depth (cm)
0
25
50
75
100
125
150
175
200
225
12,590 - 12,728
Cal BP (2σ ages)
0
10
20
30
40
50
60
70
Percent Clay, Silt, and Sand (%)

RF 13-01

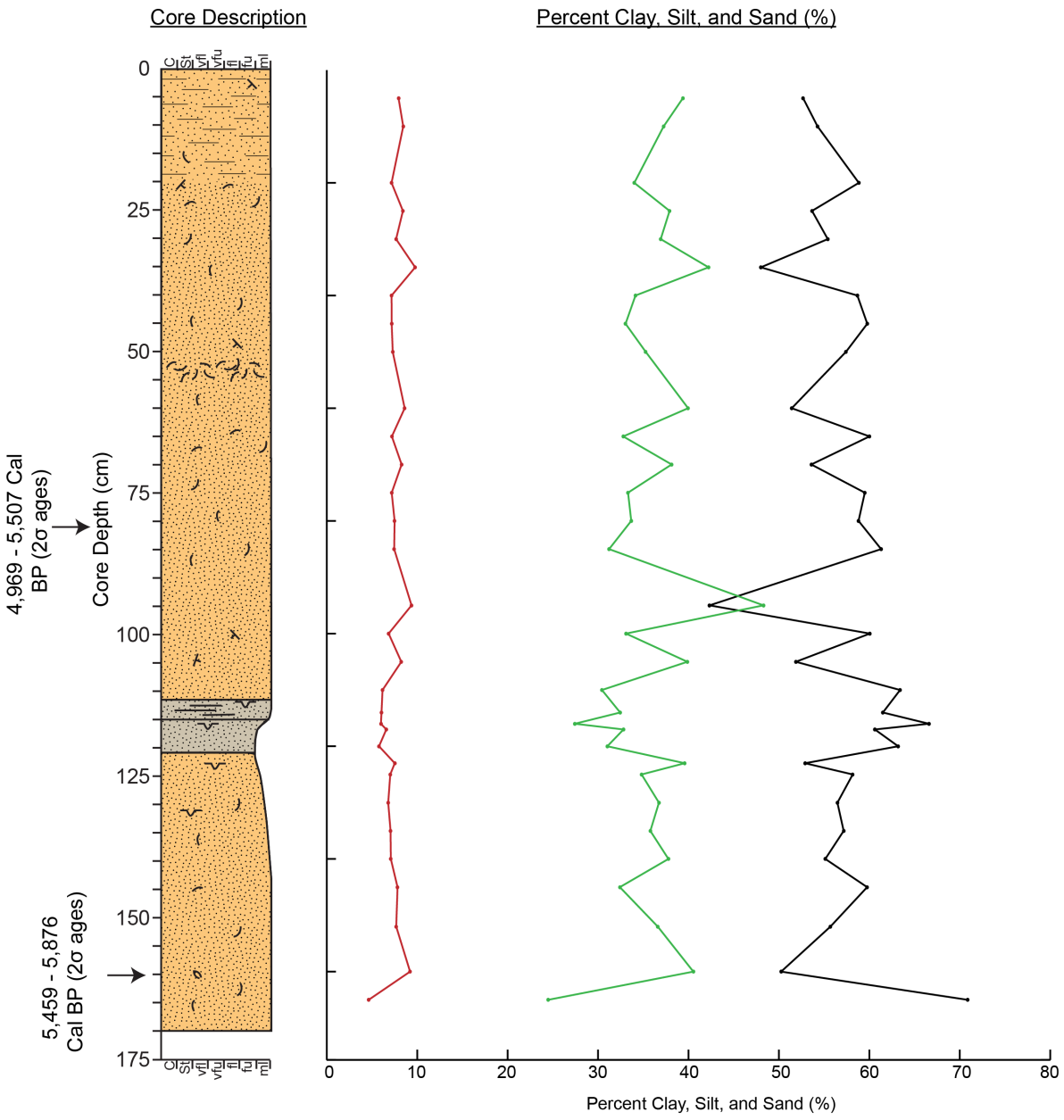
Core Description
Percent Clay, Silt, and Sand (%)
0
25
50
75
100
125
150
175
Core Depth (cm)
4,969 - 5,507 Cal BP (2σ ages)
5,459 - 5,876 Cal BP (2σ ages)
0
10
20
30
40
50
60
70
80
Percent Clay, Silt, and Sand (%)

APPENDIX IV – ADDITIONAL MEASURED SECTIONS FROM THE LA JARDINERA REGION, NEUQUÉN BASIN, ARGENTINA

The measured sections presented here were excluded from the large correlation diagram (Fig. 18) because they are not critical for understanding the outcrop geometry and the diagram is already very large. Locations of sections S1 and S2 are indicated by grey lines in Figure 17.

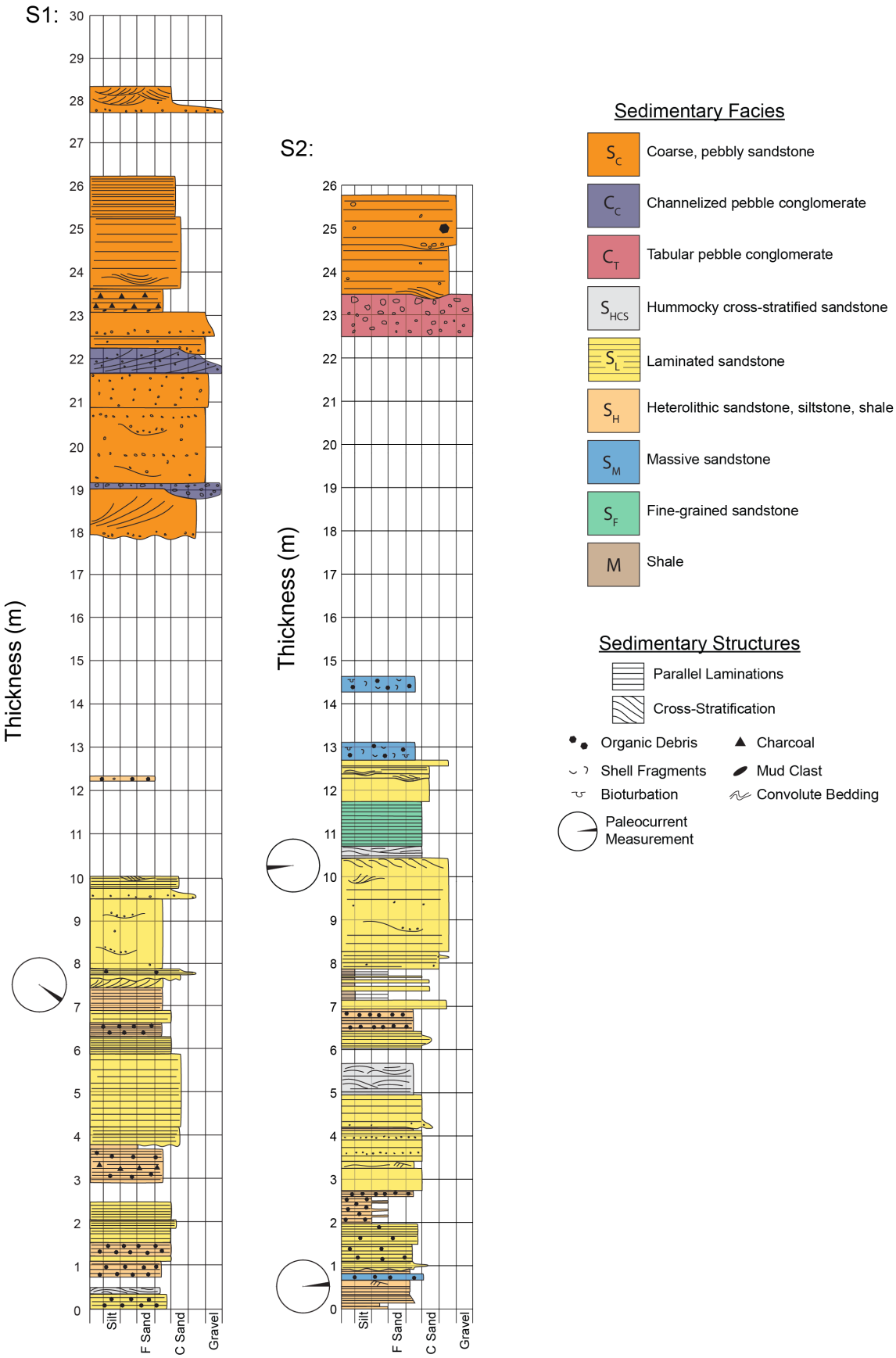
S1:
S2:
Thickness (m)
Thickness (m)
Silt
F Sand
C Sand
Gravel
Sedimentary Facies
Coarse, pebbly sandstone
Channelized pebble conglomerate
Tabular pebble conglomerate
Hummocky cross-stratified sandstone
Laminated sandstone
Heterolithic sandstone, siltstone, shale
Massive sandstone
Fine-grained sandstone
Shale
Sedimentary Structures
Parallel Laminations
Cross-Stratification
Organic Debris
Charcoal
Shell Fragments
Mud Clast
Bioturbation
Convolute Bedding
Paleocurrent Measurement